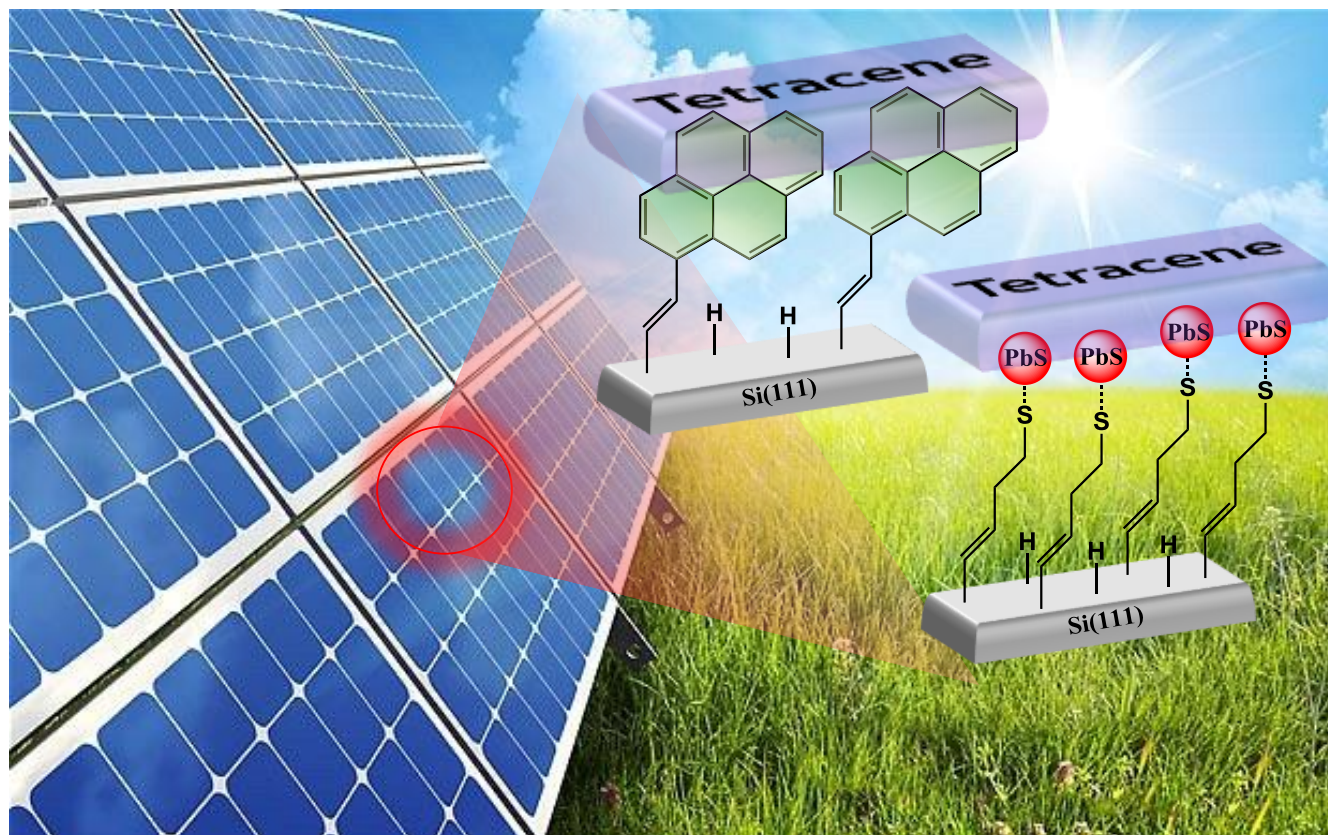# Nanomaterials for triplet exciton transfer into silicon

Steven Verboom
MSc Thesis February – September 2017



Supervised by Dr. Sidharam Pujari and Prof. Han Zuilhof
Laboratory of Organic Chemistry, Wageningen University

WAGENINGEN
UNIVERSITY & RESEARCH

FOM Institute
AMOLF

## Abstract

The unique combination of tetracene on silicon can greatly benefit the overall efficiency of silicon photovoltaic devices. Using singlet fission, the Shockley-Queisser of 33.7% can be surpassed to theoretical efficiencies of 44%; it is therefore of interest to further study the interaction of tetracene and silicon. In this thesis, several self-assembled monolayers on silicon were prepared and characterized to facilitate the energy transfer from tetracene into silicon. Two approaches were taken to mediate the energy transfer of tetracene into silicon: the first approach is using Dexter Energy Transfer between aromatic monolayers and tetracene bulk and the second approach, with Förster Resonance Energy Transfer, using Lead-Sulfide nanoparticles dynamically bound to thiol terminated monolayers.

Our findings suggest a significant interaction between silicon modified with 1-ethynyl pyrene and tetracene. Moreover, backfilling these surfaces with 1-pentyne greatly reduces the rate at which these surfaces oxidize. The surfaces with PbS NPs deposited on them show varying degrees of densities depending on the deprotection time of the thioacetate to the thiol monolayers as well as the duration of submergement in the PbS octane solution. Faster, denser and more homogeneous PbS NP surfaces were observed on hydrogen terminated silicon in contrast to the thiol terminated silicon surfaces. These results form a crucial stepping stone to further optimization of triplet energy transfer into silicon mediated by organic monolayers.

## Contents

## Introduction

Ever since the discovery of the photovoltaic effect by Alexandre-Edmond Becquerel in 1839 and the first solar cell in 1883 by Charles Fritts (1), the field of photovoltaics has seen an ever-increasing interest. Considering an increasing global energy demand and environmental concerns relating to our large carbon foot print, photovoltaics (PV) may be a practical and sustainable option to tackle this ever-growing demand. Especially, when one considers the decreasing production costs of PV has lowered the cost of PV-produced electricity to such a degree that it can now compete with a large portion of the consumer electricity prices across the world. In summary, the point of "grid parity" - when electricity generate by PV can be purchased for the same amount of money as electricity from conventional sources -  is almost upon us (1).

In 1961, William Shockley and Hans-Joachim Queisser formulated the so-called Shockley-Queisser (S-Q) limit by means of the S-Q detailed balance model. This model specifies that the maximum photovoltaic energy conversion efficiency for a single junction solar cell is 33.7% for an optimum semiconductor with a band gap of 1.34 eV (2). As research advances, solar cells are drawing closer to this S-Q limit; however, to this day not a single junction solar cell has surpassed the S-Q limit. The highest reported values, in literature, of single cell solar cells ranges between 25.0% -28.8% (3). The main contributors to not having met the S-Q limit is two-fold; namely, not
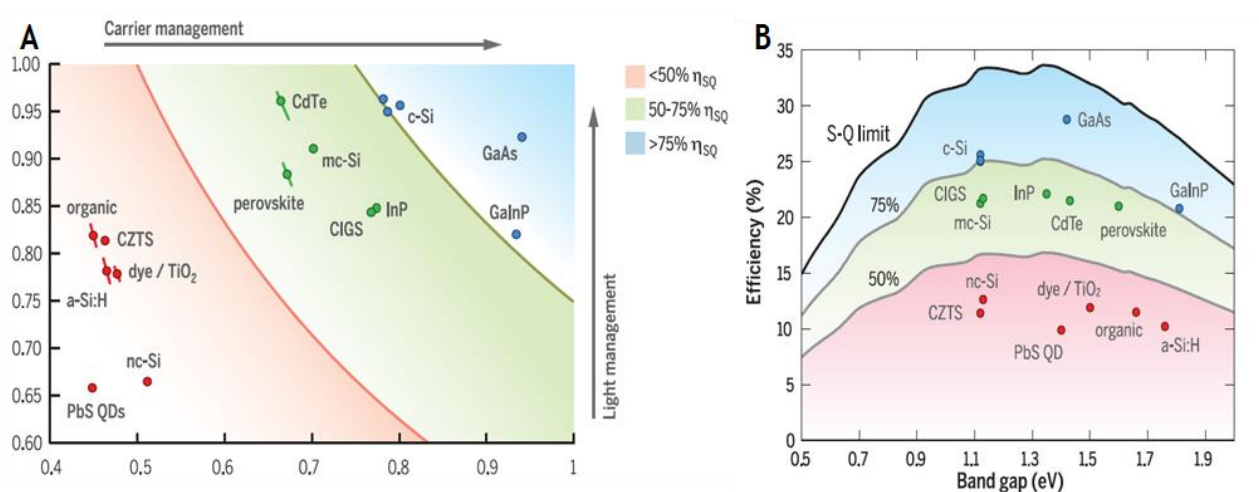


*Figure 1. A) an overview of the different solar cells materials plotted with respect to their light and carrier management. B) Theoretical Shockley-Queisser detailed-balance efficiency limit as a function of band gap (black line) and 75% and 50% of the limit (grey lines). Image were taken from Polman et al. 2016 (4).*

all incident light is absorbed into the active layers and not all generated carriers are collected **(Figure 1A)**.

Solar cells are made of various materials and all of them have different properties with respect to their light and carrier management. Polman *et al.* (2016)(4) compared the most recent developments of various photovoltaic systems and their respective efficiency per the S-Q limit (**Figure 1B**). As can be observed in **Figure 1B**; monocrystaline-Silicon (c-Si), thin-film single-crystalline Galium-Arsenide(GaAs) and Galium Indium Phospide (GaInP) currently fall within the upper bracket in terms of efficiency.  Note that although certain types of PV-systems fall below the 75% line, a lot of research is being done with respect to optimizing these systems. An excellent example is the case of perovskite; within 5 years this hybrid organic-inorganic solar cell has reached efficiencies above 20% (4).

The present study will cover the increasing the efficiency of crystalline silicon solar cells by means of using Singlet Fission (SF). Singlet Fission is a process in which an organic chromophore in an excited singlet state ($S_1$) shares its excitation energy with a neighbouring ground-state chromophore and both are then converted into triplet ($T_1$) excited states (5). The key is to then extract these generated triplet states from the chromophore into crystalline silicon and thereby one could, theoretically, reach an internal quantum efficiency (IQE) of 200%. As the exact mechanism and processes of Singlet Fission are beyond the scope of this work, the reader is referred to the following review and papers (5,6,7). Nonetheless, a conceptual explanation will be given in the Theory section below. Note, that because the quantum efficiency potentially exceeds 100%; the power conversion of single junction photovoltaic cells could rise above 40% (5,8) and thus circumventing the S-Q limited.

The phenomena of singlet fission has been observed in several materials such as polyacenes (5,9,10), several acene derivatives (5,9,11), isobenzofuran (5,12), carotenoids (5,13) and some polymers (5,14). It is important to realize that; in the process of SF, the excited triplets do not have to exactly match half of the initial singlet's energy (4). Therefore, one is restricted in the choice of SF-material dependent on the PV-systems band gap.  As previously stated, this research is based upon the transfer or excited triplets into silicon which has a band gap energy ($E_g$) of 1.12

eV (4). Tetracene, according to Tomkiewicz *et al.* (1971)(15), has an emission energy of $S_1 \rightarrow S_0$ at 2.32 eV and respectively an excitation from $S_0 \rightarrow T_1$ of 1.25 eV. This leaves 0.18 eV as activation energy and thus makes the process of SF in tetracene slightly endoergic. Above temperatures of -113 $^0$C it is argued that this energy barrier is overcome and that at room temperature SF is believed to be the sole fate of all singlet excitons (5). Contrary to the work of Smith, M. B., & Michl, J. (2010) (5), Wilson *et al.* (2013) (16) argues that the process of Singlet Fission is temperature independent. The transport of the generated triplet excitons into the silicon can then be performed by two different energy transfer processes: Dexter Energy Transfer (DET), and Förster resonance energy transfer (FRET). Further details of these energy transfer processes will be given in the Theory Section.

In the work of Piland *et al.* (2014) (17)**,** they observe no life-time change in the generated triplets in tetracene when deposited on bare silicon. This raises the question whether functionalized silicon may have a positive effect on the effectiveness of Dexter Energy Transfer into silicon. Additionally, when considering the work of Tabachnyk *et al.* (2014) (18) and David *et al.* (2015) (19), one could start hypothesizing about a solar cell covered in a tetracene film which generates triplets, that then transfers these triplets to the quantum dots[1] (QDs) and subsequently transferred from the QDs into the silicon by means of FRET. Yet prior to putting any of these hypotheses to the test, one first needs to make high quality monolayers and oxide-free silicon to facilitate the desired energy transfer process.

This research will therefore be assessing and manufacturing the quality of various self-assembled monolayers (SAMs): phenyl acetylene, 2-ethynyl-naphtalene, 1-ethynyl-pyrene, 1-butynyl-thioacetate and 1-butynyl-thiol on oxide-free silicon wafers. The assessment will be conducting various surface characterization methods amongst which are: ellipsometry, static contact angle measurements, atomic force measurements and x-ray photoelectron spectroscopy. Post modification the QDs and/or tetracene will be deposited to then be further analysed by AMOLF[2] for singlet life-time experiments to then asses the effect of the functionalized silicon on the

---

[1] Quantum Dots (QDs) and nanoparticles(NPs) are used interchangeably as they refer to the same particle
[2] AMOLF is one of the research laboratories of the Netherlands Organization for Scientific Research (NWO)

overall solar cell.  After which again a characterization will follow using ellipsometry, atomic force measurements and x-ray photoelectron spectroscopy.

## Theory

In this section a rudimental explanation of Singlet Fission, Dexter Energy Transfer, Förster Resonance Energy Transfer and an outline of silicon functionalization will be given. For a more detailed explanation of the various processes we refer the reader to the following works: Singlet Fission (5,6,7,20), Dexter Energy Transfer, Förster Energy Transfer (5,21) and silicon functionalization (22).

### Singlet Fission (SF)

Prior to talking about Singlet Fission, it is important to have an overview of the different quenching mechanisms that govern an excited singlet. **Figure 2** is a Jablonski diagram of the various relaxation processes that surround the phenomena of Singlet Fission.
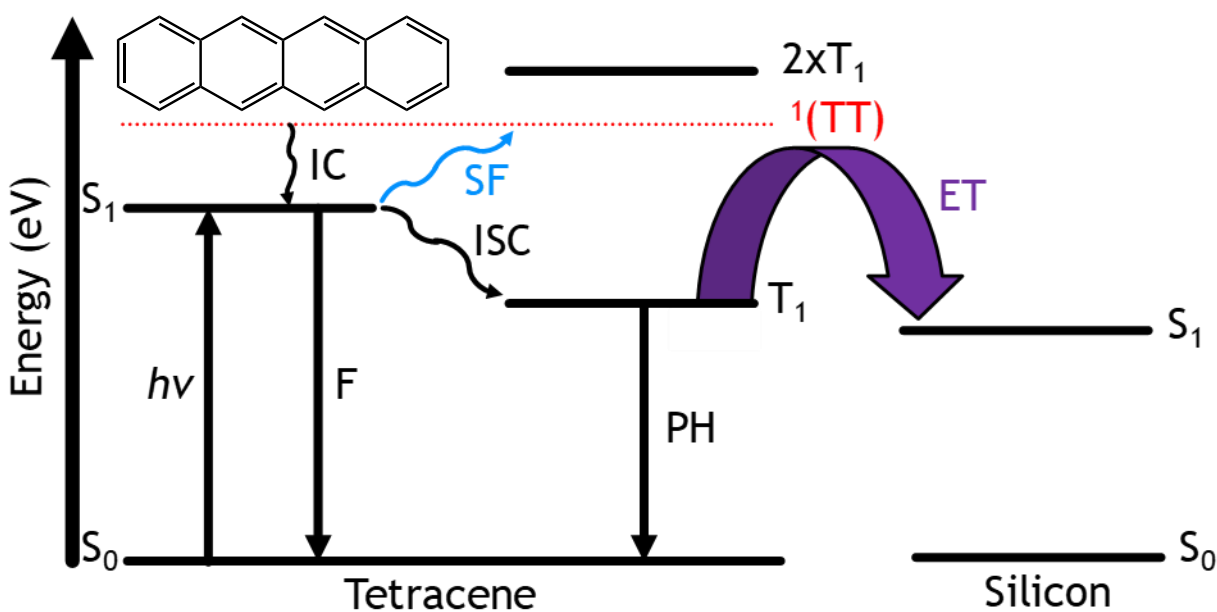


*Figure 2. Jablonski Diagram, of the various decay channels in tetracene including Singlet Fission. The radiative processes are given by the straight arrows and the non-radiative processes are curved arrows. After the absorbance of a photon (hv) a electron is excited to its singlet state at 2.32 eV; afterwards there are several ways in which this singlet can quench: Fluorescence (F), Inter-System Crossing (ISC), Singlet Fission (SF) and subsequent to either ISC or SF is either Energy Transfer (ET) from one chromophore to another or phosphorescence (PH).*

A general explanation of the interplay between photoluminescence and Singlet Fission would start with the absorbance of a photon (hv). This photon accordingly promotes an electron from

the ground state ($S_0$) to the first excited state ($S_1 = 2.32$ eV). However, the photon must exceed the band gap energy of at least first excited singlet state as otherwise the photon is not absorbed. Electrons can also be promoted to a higher singlet state ($S_2$ or higher) by means of absorbing higher energy photons. Note that after absorption an electron can rotate or vibrate down to its closest singlet excited state, which is called internal conversion (IC) a non-radiative process. Similarly, the de-excitation of a singlet back to its ground state ($S_0$) is referred to as fluorescence (F) as a photon of the according energy is emitted during this relaxation. Alternatively, instead of fluorescence a singlet exciton can first be converted into a bound triplet-triplet state $^1$(TT) which has an approximate energy of 2.35 eV, slightly above the tetracene singlet. This bound triplet state then dissociates into two separate triplet excitons ($T_1 = 1.25$) by means of singlet fission. Subsequently, these triplet excitons can: relax back to the ground state by means of phosphorescence (PH), recombine back to the $S_1$ through triplet annihilation or alternatively excite another electron by means of Energy Transfer (ET) processes such as Dexter Energy Transfer and Förster Resonance Energy Transfer; these processes will be further explained in a later paragraph.

To further elucidate the process of Singlet Fission one should realize that triplets are, theoretically, not the only product of singlet fission. Singlet fission has the potential to not only
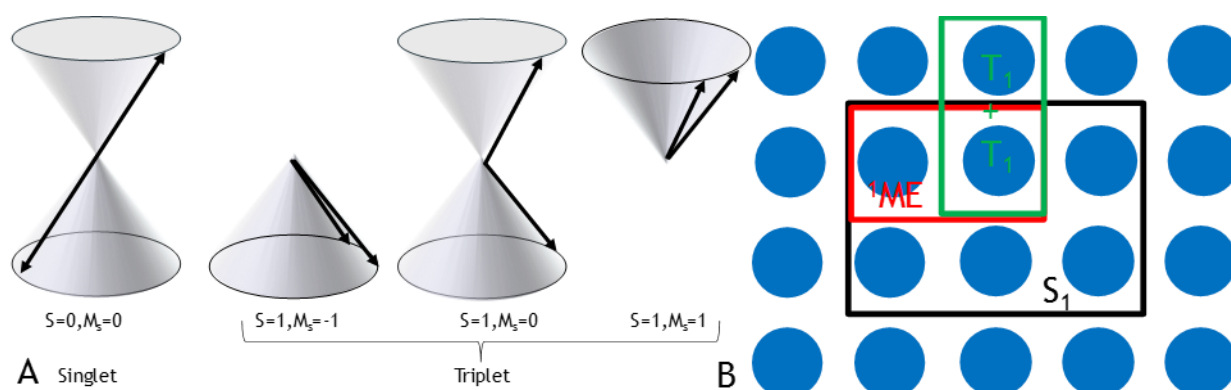


*Figure 3. A) a vector visualization of a two-electron system for both the Singlet and different Triplet states. The Singlet consists of two electrons one spin up and the other spin down which are out of phase therefore. The remaining two spins down, two spins up or one spin up and one spin down but in phase represent the different triplet states. B) A simplistic sketch of a crystal in which the several sub processes of Singlet Fission are outlined: the excitation of $S_1$ by means of the black rectangle, the multi-excitation generation ($^1$ME) in two adjacent chromophores in the red triangle and lastly triplet separation shown in the green triangle.*

create triplets but also so called quintets. However, these quintets have yet to be observed and are usually dismissed as too high energy states (5). An apt visualization of these different singlet and triplet states is given by Köhler, A., & Bässler, H. (2009) (7) in **Figure 3A**. The easiest way to think of these different states is to consider a two-spin system with spin and phase. Spin can be either up or down and phase can be either in or out of phase. This accordingly leads to four possible scenarios: one in which the spins and phases cancel out (S=0 and M=0), two in which the spins are both in the same direction be that either up or down (S=1 and M=1 or M=-1) and lastly where the spins are opposite but in phase and this resulting in a spin vector in the z-axis (S=1, M=0). These are the three different states that the triplet states refer to; however, we will now return to the topic of Singlet Fission and how to conceptualize this overall process.

To complete the conceptualization of Singlet Fission, it is useful to adopt the framework outlined by Kolomeisky *et al.*(2015) (20)  and summarized in **Figure 3B**. The black rectangle represents the delocalized excited singlet across several chromophores, next the red triangle depicts the multiexciton state, in which two triples have been formed but are still bound to each other. To separate these triplets from each other a certain binding energy ($E_b$) must be overcome; which, in the case of tetracene, is approximated to be 0.028 eV (20). This binding energy is readily overcome by means of entropic contributions if there are sufficient chromophores near the original bound triplet. Although this entropic contribution allows for the process to proceed it does significantly slow down the process, by approximately one order of magnitude, in comparison to the exoenergic Singlet Fission of pentacene (20). Lastly, in green, it shows the diffusion of one triplet to another chromophore either by means of Dexter Energy Transfer (20) or Förster Resonance energy transfer (23).

## Dexter Energy Transfer (DET) & Förster Resonance Energy Transfer (FRET)
DET and FRET and two non-radiative energy transfer processes in which either a triplet exciton is either passed on or excited respectively. DET is exponentially dependent on the distance between the two respective chromophores (Equation 1);

$$k_{dexter} = KJ \exp\left(\frac{-2R_{DA}}{L}\right) \qquad (1),$$

where $J$ is the normalized spectral overlap integral, $K$ is an experimental factor, $R_{DA}$ is the distance between the donor and acceptor and $L$ is the sum of van der Waals Radius (21). Whereas FRET has a sixth power dependence with respect to distance (Equation 2);

$$E = \frac{1}{1 + \left(\frac{r}{R_0}\right)^6} \qquad (2),$$

in which $r$ is the distance between donor (D) and acceptor (A) and $R_0$ is the characteristic distance (a.k.a the Förster radius) with a 50% transfer efficiency (21). Typical distances for DET are in the range 6- 20 Å and for FRET in the range of 30-100 Å. Therefore, DET and FRET are also referred to as short and long-range energy transfer processes respectively. The different distance dependencies can be attributed due to the different mechanisms that govern DET and FRET.

In sum, a rather crude simplification is that for Dexter Energy Transfer the chromophores have to be close enough that the orbitals of the electrons, that are to be exchanged, overlap. This accordingly allows for an excited electron, a singlet or a triplet, to "hop" to the other chromophore (**Figure 4A**). A simplified explanation of FRET is that due to Columbic interactions between the donor the de-excitation of a donor can cause an excitation in the acceptor; if and only if, the spectra overlap (**Figure 4B)** (21). In short, the key difference of FRET with DET, aside from the distance dependency, is that with FRET the energy is transferred through columbic interactions and with DET the energy transferred by means of transferring an electron.
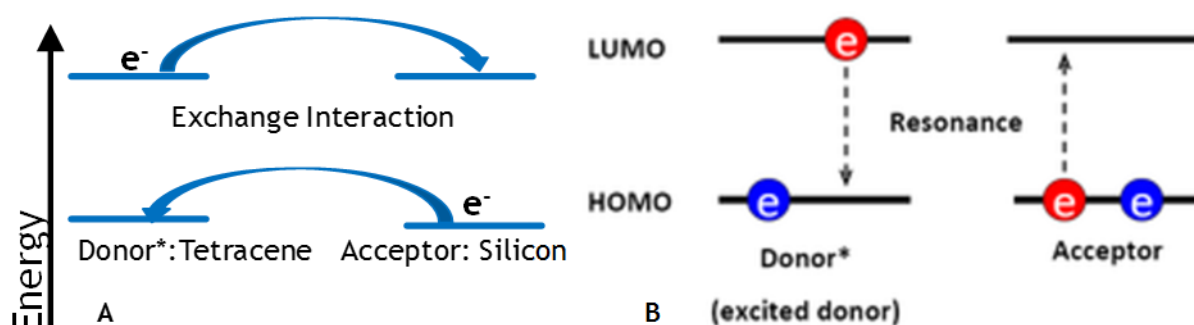


*Figure 4. A) a conceptualization of Dexter Energy Transfer (DET) from a donor tetracene to the acceptor silicon. B) Similarly, a conceptualization of Förster Energy Transfer (FRET) with again the donor being tetracene and the acceptor being silicon. Note that in the case of FRET no electron is exchanged whereas this is the fundamental concept of DET.*

## Silicon functionalization

Silicon, is the eight most common element in the universe by mass. In its elementally pure form, it has the ideal band gap, oxide surface chemistry and etching properties that make it the ideal material for the computer industry (24). Yet in the context of this research a non-oxide approach towards functionalizing silicon is required, because oxide functions as a passivizing layer in the process of electron transport. The field of functionalized silicon is hugely varied with it ranging from tribological properties (25), such as anti-fouling brushes, to the seemingly limitless possible chemistries and properties that are enabled by the chemically highly stable Si-C bond (26). Photovoltaic sensitization, using polyacenes has been previous reported by several researches (27,28) yet the functionalization of hydrogen terminated silicon with these polyacenes has only been reported by Garg *et al.* (2015) (29) and Locritani *et al.* (2015) (30) on surfaces and nanocrystals respectively.

Given the diversity of this field one would expect that the mechanism of its fundaments are well known and documented. Yet, as J. Buriak (2013) (22) puts it, there is an unexpected plurality of mechanisms for the functionalization of hydrogen terminated silicon. The mechanisms that are considered can be split into four categories of silicon functionalization by illumination: plasmons, photoemission, excitons and radicals. The exact differences of the mechanisms are outside of the scope of this research but for more details the review of J. Buriak (2013) (22) is very illuminating.

With the scope of this research in mind, one would ideally have a maximally packed monolayer which is stable under various conditions. In the work of Scheres *et al.* (2010) (31), they show that alkyne-derived monolayers are better than alkene-derived monolayers and therefor make alkyne-derived polyacenes an excellent candidate for this research as they would provide a stable monolayer on oxide-free silicon. Although 2-ethynyl tetracene would be the ideal compound to functionalize silicon with for this study, we will first focus on the monolayers formed by phenylacetylene,2-ethynyl naphthalene and 1-ethynyl pyrene for the aromatic part of this research and on 1-butynthiol for the Quantum Dots (QDs).

# Experimental Procedures

## Materials

Acetone (Sigma, HPLC grade), EtOH, $CH_2Cl_2$ and 40% ammonium fluoride solution (40% $NH_4F$) (Sigma/Honeywell, semiconductor grade) were used as received. For rinsing and contact angle measurements, deionized water (18.3 MΩ cm resistivity) was used.  1-Phenylacetylene (Sigma Aldrich, 98%) was distilled at $70^0C$ under reduced pressure (30mbar) before use, 2-ethynylnaphthalene (ABCR, 98%) and 1-ethynylpyrene (ABCR, 96%), were purified by recrystallization in mili-Q-water and DCM to attain a 99+% purity. 1-Butynol (ABCR, 97%) ,4-bromo-1-butyne (Sigma Aldrich, 97%) and potassium thioacetate (Alfa Aesar, 98%)  were used without any further purification. Silicon wafers were (111)-oriented single-side and single polished, 500-550 µm thick, N-type, phosphorus-doped samples, with a resistivity of 1.0-10.0 Ω cm and miss cut angle of $0.2^0$ (Siltronix,France).

## Equipment for Material Preparation

For sonication purposes a transonic 460/H Elma, with a Sonation Lab solutions cover around it, was used. Solvent evaporation under reduced pressure was performed with a BUCHI Rotavapor R-100, BUCHI Heating Bath B-100 and BUCHI Interface I-100. For bulb-to-bulb distillation a BUHCI Glass Oven B-585 was used in combination with a refrigerated Condensation Trap and a vacuum pump. Column Chromatography was performed using a Biotage Isolera One with Silicycle 120g Cartridges. NMR samples were measured in a Bruker Avance III 400MHz NMR operated by a Bruker TopSpin 3.5 pl 6 on Avance400 operating system. Analysis followed first order and the following abbreviations were used throughout: s = singlet,  d = doublet, t = triplet, td = triplet of doublet, tdd = triplet of doublet of doublet coupling constants (J) are given in Hertz (Hz).   Lastly, for GC-MS an Agilent GC-MS (Agilent 6890 + 5975C MSD + 6890 injector) with Column: HP-5MS (30m x 0.250mm x 0.25 um) and GC Chemstation Software was used.

## Synthesis of 1-butynylthioacetate

The following procedure is a modified procedure of that outlined by Horvath *et al.* (2014) (32). A 100 mL round bottom flask was charged with 70 mL acetonitrile. Subsequently, potassium thioacetate[3] (2.22g, 21.6 mmol) was added and stirred at 350 rpm for five minutes. Next, 4-

---

[3] Alternatively could be synthesized following the procedure of Juaristi, E., & Cruz-Sanchez, J. S. (1988) (33)

bromo-1-butyne (1mL,10.6mmol) was added to the solution in a dropwise manner and was then left stirring (500 rpm) overnight at room temperature. The salt was removed by filtration and afterwards the solvent was evaporated under reduced pressure resulting in a red-brown salt. Then the salt was washed with DCM and mili-Q-water and after separation the organic phase was washed, six times, with mili-Q-water to remove any residue salt or unreacted thioactetate. This resulted in (1.05 g, 7.7 mmol, 77% yield) 1-butynolthioacetate which was deoxygenated by means of three freeze-pump-thaw cycles before storing the solution in the glovebox. $^1$H NMR (400 MHz, Chloroform-*d*) δ 3.06 (td, *J* = 7.0, 1.3 Hz, 2H adjacent to thioacetate), 2.50 (tdd, *J* = 7.1, 2.7, 1.2 Hz, 2H adjacent to the alkyne ), 2.37 (t, *J* = 1.1 Hz, 3H of thioacetate alkane), 2.04 (td, *J* = 2.6, 0.8 Hz, 1H alkyne). $^{13}$C NMR (101 MHz, Chloroform-*d*) δ 195.21(C, carbonyl), 82.04(C, alkyne), 69.59(C, alkyne), 30.57(C, C-S), 28.12(C, alkane), 19.50(C, next to alkyne).

## Monolayer Formation

### Hydrogen Terminated Surface Preparation

1x1 cm pieces of n-Si (111) were consecutively sonicated for 10 minutes in: acetone, ethanol and DCM. Subsequently the wafers were dried by a stream of Argon and placed in Harrick Plasma Cleaner connected to a Harrick PlasmaFlo for plasma treatment. Followed by a purging of the chamber by Argon for 5 minutes. After 30 minutes of plasma treatment the samples were swiftly transported into a Nitrogen filled glovebox, where upon the samples were placed in an Argon saturated 40 % ammonium fluoride solution, to etch for 15 minutes. Next, the etched samples were rinsed with Argon saturated milli-Q-water and blown dry by a stream of Argon.

### Surface Modification Aromatics

The freshly etched and rinsed surfaces were then submerged in 2 mL neat (phenyl acetylene) or a 20% v/v mesitylene (in case of 2-ethtnyl naphthalene and 1-ethynyl-pyrene) solution of the desired monolayer which had been placed under high vacuum for at least 1h prior to submergement. The submerged samples were then kept at 80 $^0$C overnight as was described in previous surface modification literature (31,34) after which the surfaces were washed with DCM within the glovebox and prior to storage again sonicated for 10 min in DCM.

## Oxidation Study of Aromatic Surfaces

The stability of the modified surfaces with regards to their oxidation rate were assessed by exposing the modified surfaces to ambient circumstances. Two surfaces of silicon modified with: phenyl acetylene, 2-ethynyl-napthalene, 1-ethynyl pyrene and 1-ethynyl pyrene backfilled with pentyne were left in the fume hood for thirty days (humidity ~44% ±5% and Temperature 22 ± 5 °C). X-ray Photoelectron Spectroscopy measurements were made at 1, 2, 5, 10, 20 and 30 days.

## Surface Modification Thioacetate

The freshly etched and rinsed surfaces were then submerged in 2 mL solution 20% v/v of 1-butynylthioacetate in freshly distilled mesitylene. Alike to the modification of surfaces with aromatic alkynes, the surfaces were kept submerged at 80 $^0$C overnight with argon overflow. Next, the surfaces were washed with DCM within the glovebox and prior to storage again sonicated for 10 min in DCM.

## Deprotection of Thioacetate Modified Surfaces

For the deprotection of thioacetate modified surfaces a modified procedure of previous thioacetate deprotection was used (35). A thioacetate modified surface was submerged and swirled in a mixture of potassium carbonate (0.69 g, 5 mmol) and methanol (5 mL) for 5 min. Afterwards, the surfaces were rinsed with copious amounts of Milli-Q-water, ethanol and sonicated in DCM for a minimum of 5 minutes. Subsequently, the samples were blown dry with a stream of Argon and placed in a glovebox, for storage, until further use.

Additionally, the deprotection time was varied to also investigate the effects of the deprotection time on the density of the Lead-Sulfide nanoparticles. The times that the surfaces were left in the potassium carbonate in methanol mixture were: 1, 3, 5 and 15 minutes.

## Deposition of Lead-Sulfide Nanoparticles (PbS NPs)

Surfaces which had Lead-Sulfide nanoparticles deposited on them, were submerged in a solution of the PbS NPs dispersed in octane at a concentration of 50mg/mL for 24 hours under a nitrogen atmosphere. Afterwards the samples were repeatedly dipped in octane and were then sonicated in octane and DCM for 5 minutes.

Also, the period that the samples were left submerged in the PbS NP solution was varied to similarly investigate the effects on the density of the PbS NPs. The deposition periods that were investigated were: 1,2.5,5,16 and 24 hours.

## Pentyne-backfilling

Surfaces that were backfilled with pentyne were treated as described above with the exception that instead of storing them they were placed once more in a nitrogen atmosphere glovebox. The samples were now placed in a pressure proof thick glass vial filled with 1-2 mL (samples must be submerged) of neat pentyne solution. The flask and samples were then placed in a beaker filled with molecular sieves and were heated up to 80°C and left overnight. Subsequently the samples were again washed with DCM inside the glovebox, and once more sonicated for 10 min in DCM prior to storage and or characterization.

## Monolayer Characterization

### Static Contact Angle (SCA)

Static water angle measurements were made with an automated Krüss DSA 100 goniometer. Depending on the size of the modified surfaces 2-3 droplets were dispensed on the surface and the contact angles were determined using a Tangent 2 fitting model. The standard error in the determined contact angles is approximately 1°.

### Ellipsometry

The elipsometric thicknesses of the samples were assessed d by using a rotating Sentech Instruments 9Type SE-400) ellipsometer, operating at 623.8 nm (He-Ne laser), and an angle of incidence of 70°. The optical constants of a freshly etched hydrogen terminated Si(111) surface were taken as n=3.821 and k=0.05 as was reported previously by Scheres and coworkers (30). The reported values are the result of a planar three layered (ambient, monolayer, substrate) model with the assumed refractive indices of 1.00 and 1.46 for the ambient and monolayer respectively. All the reported values are averages of at least 10 measurements and the error is approximately 0.2 nm.

### X-ray Photoelectron Spectroscopy (XPS)

X-ray photoelectron spectroscopy (XPS) spectra were attained on a JPS-9200 photoelectron spectrometer (JEOL,Japan). The analysis was performed under ultra-high vacuum conditions

using a monochromatic Al Kα X-rays (hv = 1486.7 eV) at 12kV and 20 mA and an analyzer pass energy of 10 eV. A take-off angle $\varphi$ of 80° was used. All the XPS spectra were processed with Casa XPS software (2.3.18) and the binding energies were calibrated on the hydrocarbon ($CH_2$) peak with a binding energy of 285.0 eV.

## Atomic Force Microscopy (AFM)

Atomic Force Microscopy measurements were obtained by means of an Asylum MFP-3D Atomic Force Microscope which was equipped with a 100-micron closed-loop XY-stage which allows for AFM imaging as well as precise sample positioning. A minimum of two scans per modified surface at 20 x  20, 5 x 5 and 1 x 1 µm were made in standard ACAirTopography mode. After the measurements, a height and roughness profile was produced using the AFM Analysis tool in Igor Pro 6 with a third order flattening.

## Auger Electron Spectroscopy  (AES)

AES measurements were performed at room temperature with a scanning Auger electron spectroscope (JEOL Ltd. JAMP-9500F field emission scanning Auger microprobe) system. AES spectra were acquired with a primary beam of 10 keV. The takeoff angle of the instrument was 0°. We used the differential energy spectrum to subtract background from the direct Auger spectrum for calculating the peak-to-peak intensity. The first differential $d(N(E))/d(E)$ Auger spectra were obtained by numerical derivation of the direct N(E) integrated Auger data displaying an absolute scale with counts/second units by a universal Savitzky–Golay (SG) Quadratic differential filter using seven points and used to calculate the peak-to-peak intensity of Auger electrons and derive the elemental compositions. The differential spectrum is simply the differential of the direct spectrum with respect to energy. Line profiles were measured horizontally across the sample and the relative concentrations of the specified elements were plotted.

## Computational procedures

In Materials Studio software (version 6.0) unit cells were constructed and expanded to supercells of 12 × 12, 10 × 15 or 12 x 15 units with various degrees of coverage (25%, 33%, 40%, 50%, 60%, 67%, 75% and 83%), following literature procedures (35) **Figure 5** shows an example of a Pyrene covered Si(111) surface with a coverage of 40%. The geometries were optimized using the
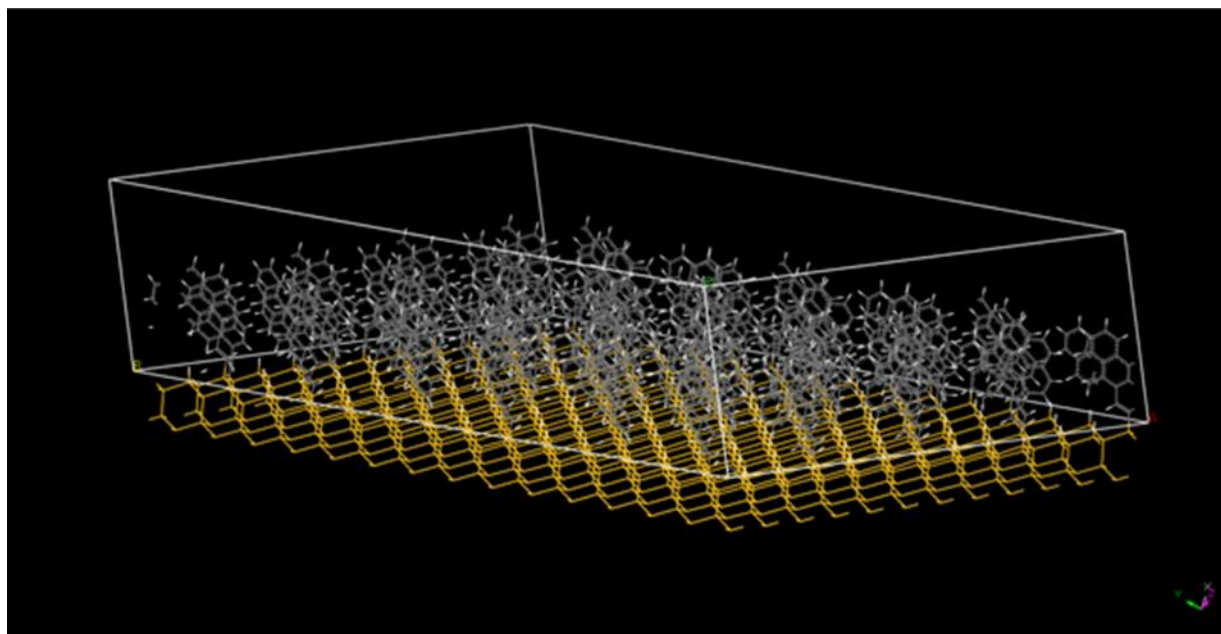
**Figure 5**. *Example of a 40% substituted Si-Pyr cell in Material Studios.*

polymer consistent force field (PCFF).  The exact patterns that were used can be found in the supporting information (**Figure S.1.**).

Two scripts were written in Matlab (version 2016B) to facilitate the analysis and data presentation of the Material Studio results and the stability study of the aromatically functionalized surfaces. The script for the Material Studio analysis exports the data from the designated excel sheet and accordingly plots and fits the data points to a second order polynomial. The script for the stability study similarly exports the data from an excel sheet and subsequently plots all the spectra within one figure. For both scripts please see the supporting information (**Section P**).

## Time-Correlated Single Photon Counting (TCSPC)

Time-correlated single photon counting (TCSPC) measurements were performed with a home-built setup equipped with PicoQuant PDL 828 "Sepia II" and a PicoQuant HydraHarp 400 multichannel picosecond event timer and TCSPC module. A 485 nm pulsed laser (PicoQuant LDH-D-C-485) with a repetition rate of 0.7 MHz and a power of 2mW was used as source of excitation and focused using a Nikon Plan APO VC 60x A 1.2 WI lens. The samples were encapsulated between two cover slides, inside the $N_2$ glovebox. A single-photon avalanche diode (SPAD) detector (Micro Photon Devices, MPD-5CTD) was used for the detection of the photoemission. A

Chroma ET500LP long-pass filter and a Chroma ZET488NF notch-filter was used to remove the excitation laser. Dwell time per pixel was between 25ms and 50ms, depending on the sample.

## Results & Discussion

In this section we will be further discussing the obtained results of the various SAMs on Si(111). First, are the polyacene like monolayers also referred to as the aromatic surfaces. Note that Singlet Fission has not been reported in any of these compounds, but the interest is whether these aromatic systems may facilitate triplet energy transfer into crystalline silicon. Prior to any photonics related measurements, one has to first asses the quality and stability of the desired monolayer and this is for the majority what will be discussed below. Second, are the silicon wafers sensitized by means of using Lead-Sulfide (PbS) quantum dots (supplied by AMOLF).
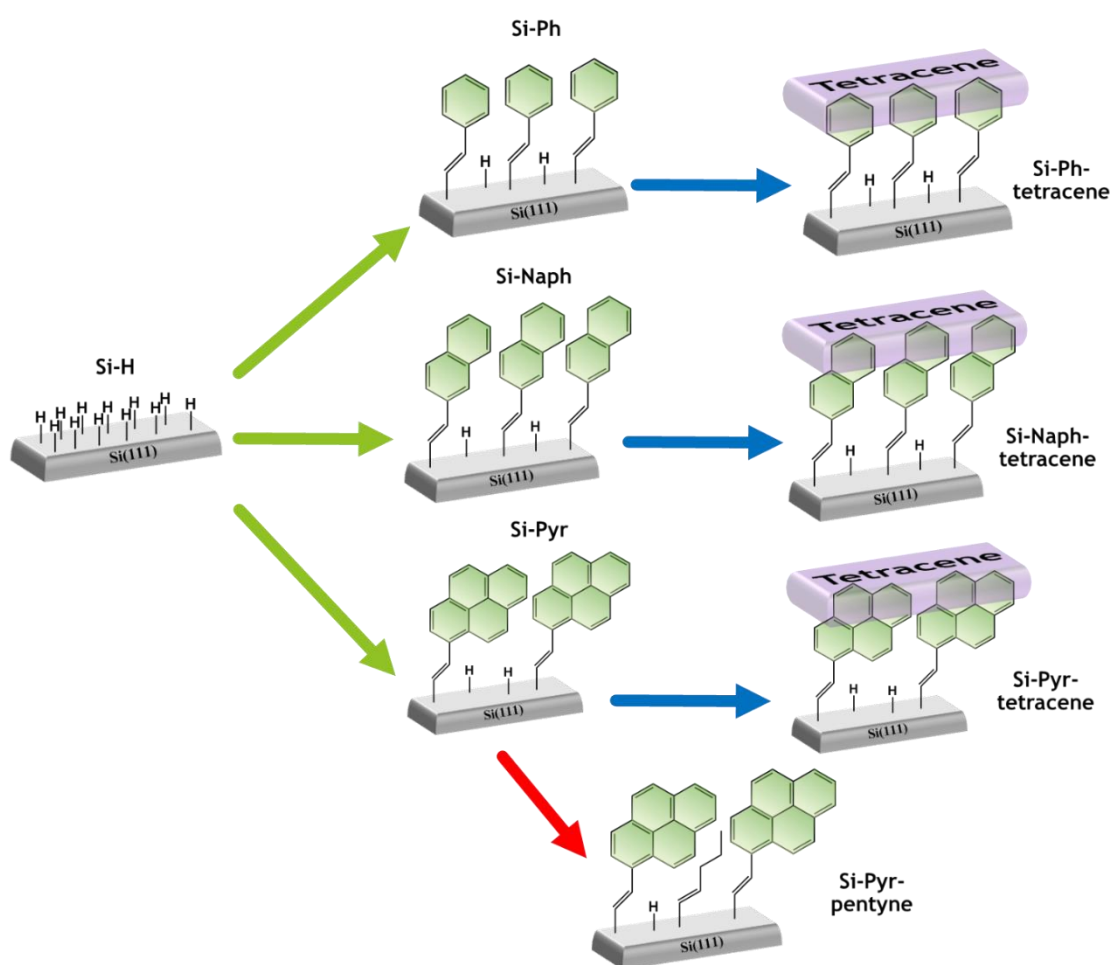


**Figure 6.** *Overview of the different modifications of the various aromatic surfaces. First Si-H is modified with different SAMs to either Si-Ph, Si-Naph or Si-Pyr. These surfaces then have 4-40 nm tetracene deposited onto them (done by AMOLF) resulting in Si-Ph-tetracene,Si-Naph-tetracene and Si-Pyr-tetracene. Alternatively, to prevent the rapid oxidation of Si-Pyr one can backfill surfaces with pentyne to counteract immediate oxidation resulting in Si-Pyr-pentyne for example.*

## Silicon functionalized with aromatic surfaces

All the aromatic functionalized surfaces summarized in **Figure 6**: silicon modified with phenylacetylene (Si-Ph) and silicon modified with 2-ethynyl-napthalene(Si-Naph), silicon modified with 1-ethynyl pyrene (Si-Pyr), silicon modified with 1-ethynyl pyrene and backfilled with 1-pentyne and respectively all three aromatic surfaces covered with a layer of tetracene (Si-Ar-tetracene) are all functionalized with two aims in mind. First, to prevent the oxidation of hydrogen terminated silicon and second to enable or enhance the previously explained Dexter energy transfer into the silicon bulk. The following paragraphs will further elaborate as to how these aromatic monolayers were characterized, performed in a stability study and life-time experiments of the generate singlets.

## Characterization of the aromatic surfaces

After the aforementioned sample preparation and modification and prior to any characterization; two samples of each batch were measured by ellipsometry for a first indication of the quality of the desired monolayer. The theoretical length of the monomer was assessed by using a model of the completely stretched out monomer in Chem3D. This would give an adequate upper-limit to what a completely sterile modified surface would look like. **Table 1** accordingly summarizes the findings across several batches and several surfaces, note that the reported values are averages of all the measurements. Additionally, the thickness of the layer was also calculated by means of using the carbon: silicon ratio supplied by the XPS wide scans and the following equation (25):

$$Th_{xps} = \lambda_{ML}^{Si} \sin(\varphi) \ln\left(1 + \frac{C}{Si}\right) \; with \; \lambda_{ML}^{Si} = 39.5 \text{ Å and } \varphi = 80^0 \qquad (3),$$

where $Th_{xps}$ represents the thickness found by using the C:Si ratio found by the XPS wide-scan, $\lambda_{ML}^{Si}$ being the attenuation length of the Si 2p photoelectron and with $\varphi$ respresting the angle between the surface and plane and the detector.

*Table 1* *summarizes the different heights per surface. The theoretical column is found measuring the differences of the top and bottom carbon in Chem3D, the measured column represents the averages of ellipsometry measurements, the C:Si ratio is obtained by the XPS wide scans and lastly the calculated column logically follows from using the previously found C:Si ratio in Equation 3.*

| Monolayer | Theoretical (Chem 3D, Å) | Measured (Ellip, Å) (±2 Å) | C:Si (XPS, %) (±2 %) | Calculated (XPS, Å) (±2 Å) |
|---|---|---|---|---|
| Phenyl acetylene | 6.5 | 10 | 23.3:75.5 | 9.2 |
| 2-ethynylnaphtalene | 8.5 | 14 | 25.9:68.0 | 11.0 |
| 1-ethynylpyrene | 10.6 | 16 | 39.0:53.6 | 18.7 |

Interestingly, both the measured and calculated heights of the functionalized surfaces exceed the theoretical upper limit of the completely stretched out molecule. The differences between the measured and theoretical values may be due to the uncertainty associated with the ellipsometry measurements (index of refraction, cleanliness of the silicon etc.) (37); however, Jakubowicz et al. (2005) (38) have similar ellipsometric data when comparing *p*-nitrobenzenethiol monolayers on gold surfaces. The ellipsometry data here can only serve as a qualitative support of the "monolayer" nature of the adsorbed film and thus the interpretation should be regarded with some degree of reservation until more evidence is available. Nonetheless, several nanometer differences by ellipsometry and an overestimation based on the carbon to silicon ratio by XPS; would also seem to point that there is some physio-absorption. To counter this the
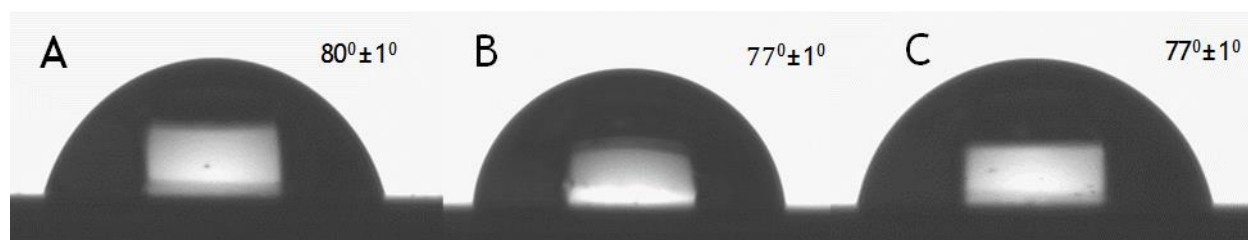


**Figure 7.** *A) Snapshot of Si-Ph surface with a Mili-Q-water droplet with an SCA angle of 80⁰. B) A picture of Si-Naph with a Mili-Q-water droplet with an accordingly SCA of 77⁰ and lastly C) is the same as A and B but now with a Si-Pyr surface also with a SCA of 77⁰.*

surfaces post modification are sonicated in DCM and toluene but the heights still exceed the upper limit found by Chem3D.

After checking the initial quality of the batch several other experiments were conducted to further assess the quality of the aromatic surfaces. Amongst these tests is the static water contact angle. On every surface a minimum of three drops were placed and for all three surfaces a minimum of two different batches were measured. Comparing the SCA findings (**Figure 7**) to those previously reported (39) for Si-Ph; it becomes apparent that the found static contact angles are smaller than reported by Kondo *et al.* (2010) (39). This difference could be either be attributed to local impurities or a not perfectly homogeneous monolayer. Additionally, the
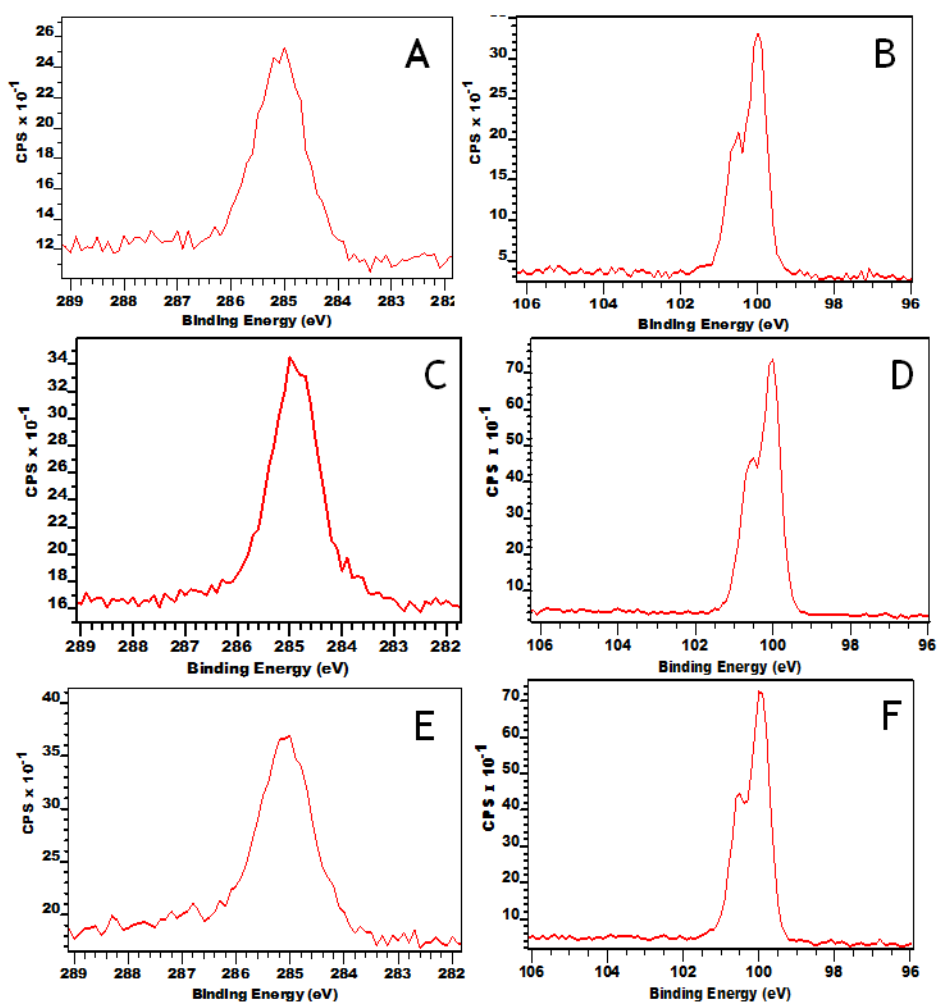


*Figure 8. A) the carbon narrow scan of a Si-Ph surface, B) the silicon narrow scan of a Si-Ph surface. C) the carbon narrow scan of a Si-Naph surface, D) the silicon narrow scan of a Si-Naph surface. E) and F) are also carbon and silicon narrow scans respective but of a Si-Pyr surface.*

difference in SCA between Si-Ph, Si-Naph and Si-Pyr is hypothesized to be due to the lower density of these SAMs. These surfaces would more readily oxidize and therefor also show lower SCA values.

Having completed a first assessment of the various aromatic functionalized silicon surfaces, to either deem a batch successful or not, two samples were submitted for further XPS analysis. **Figure 8** gives an overview of the carbon and silicon narrow scans of Si-Ph, Si-Naph and Si-Pyr. In the Si narrow scans the emission peaks of 99.5 eV and 100.1 eV correspond to the $Si2p_{3/2}$ and $Si2p_{1/2}$ respectively (see **Figure 8 B, D** and **F**). More importantly a flat baseline around 103 eV is present in all surfaces; this is indicative of the absence of a silicon oxide (SiOx) layer. This is of vital importance to the overall functioning of the proposed cascade outlined in the theory section as the oxide would act as a pacifying layer and thus the absence of it is key. Additionally, the absence of any other distinguishable peaks aside from the characteristic C-C peak (285 eV) in the carbon narrow scan is a good indication that no carbons are bound to other heterogeneous elements (see **Figure 8 A, C** and **E**).

Lastly, AFM measurements were made of a minimum of two surfaces at (at least) two different spots on the respective surface. **Figure 9** shows the 5 µm areas of the Si-Ph, Si-Naph and the Si-Pyr modified surfaces, below each respective surface are profile plots to give an indication of the
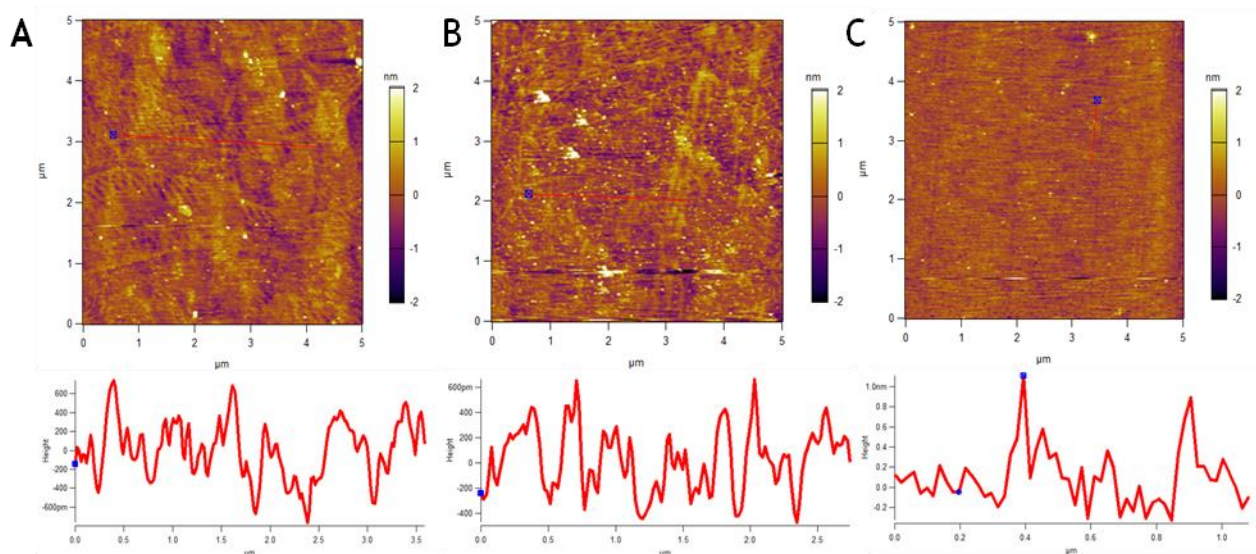


**Figure 9.** *AFM and height profiles of Si-Ph (RMS = 0.4 $\pm$0.2 nm), Si-Naph (RMS= 0.5 $\pm$0.2 nm ) and Si-Pyr (RMS= 0.3 $\pm$0.2 nm )*

roughness of the surface. In the case of Si-Ph the upper and lower limit vary between -400 to 600 pm; approximately 1 nm. Similarly, for Si-Naph the upper and lower limit are between -300 to 600 pm, and lastly with Si-Pyr the limits range from approximately -0.1 nm till 1 nm. The respective RMS values are 0.4 ,0.5,0.3 $\pm$0.2 nm for Si-Ph, Si-Naph and Si-Pyr respectively; this would suggest that the surfaces are   In sum three aromatic surfaces have a varying height profile of approximately 1 nm which agrees with their respective heights summarized in **Table 1.**

In sum, the acquired data suggests that various aromatic surfaces were modified successfully and are oxygen free. The thicknesses range from 9-16 Å which is within the typical Dexter Energy transfer range of 6-20 Å. Similar results were obtained by Garg *et al.* (2015) (29) especially with respect to the SCA, ellipsomtery and 1 x 1 μm AFM measurements. The key difference is that in their research were modifying hydrogen termintaed silicon with longer alkyl chains whereas in this research exlcusively ethynyl substituted polyacenes were used.

## Molecular Dynamics Study

It was suggested by the static contact angle measurements that as the aromatic sizes increase the density of the respective monolayer would decrease. To test this Material Studios was employed for a theoretical assessment of this claim by following the procedure outlined by Scheres *et al.* (2011) (36). By using the equation supplied in their work:

$$E_{packing} = \frac{E_{chains}}{n} - E_{relaxed\ chain} \qquad (4),$$

one can make a plot of the different packing energies dependent on a variety of monolayer densities. To get a representative model of the actual monolayer two or three different monolayer geometries were averaged, the geometries that were used can be found in the Supporting Information (**FIGURE S.1**). Having calculated the different packing energies of the different monolayers and fitting them to a second-degree polynomial and overlaying the Si-Ph, Si-Naph and Si-Pyr results with each other results in **Figure 10**. In this figure, one can clearly distinguish that Si-Pyr has a lower optimal packing density (40% -16 kcal/mol), according to the fit, in comparison to that of Si-Naph( 49%, -12 kcal/mol) and Si-Ph (50%,- 4 kcal/mol). These theoretical results would suggest that that a Si-Pyr surface would have approximately 10% more unreacted Si-H sites left than Si-Ph; which in turn could more readily oxidize.
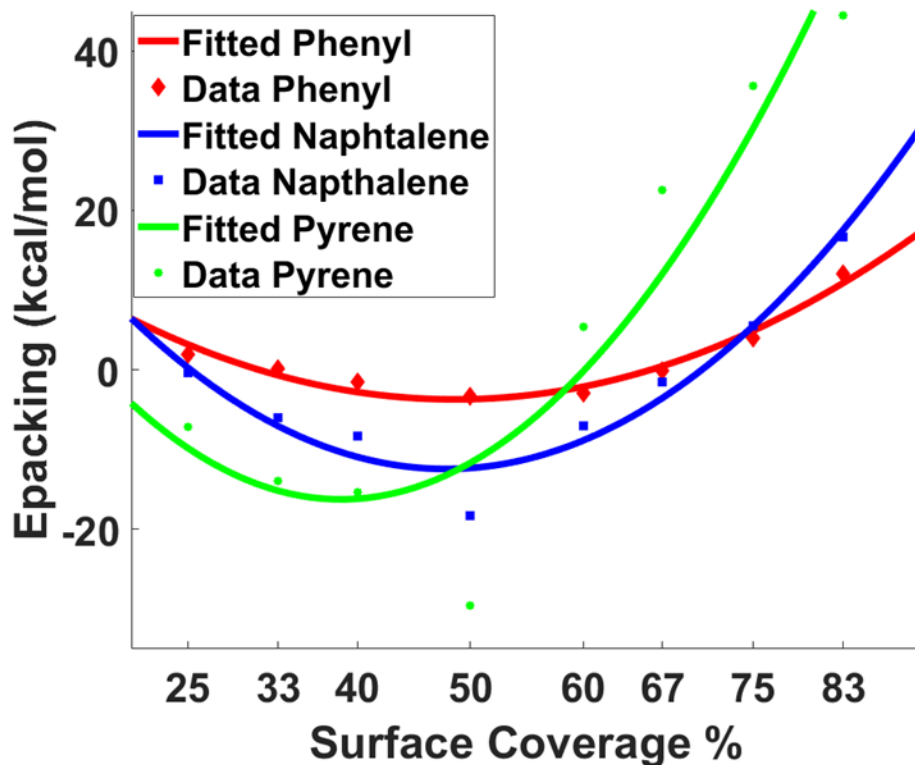
*Figure 10*. *Overlay of the different fits of Si(111) functionalized with Phenylacetylene,2-ethynyl naphtalene and 1-ethynyl pyrene.*
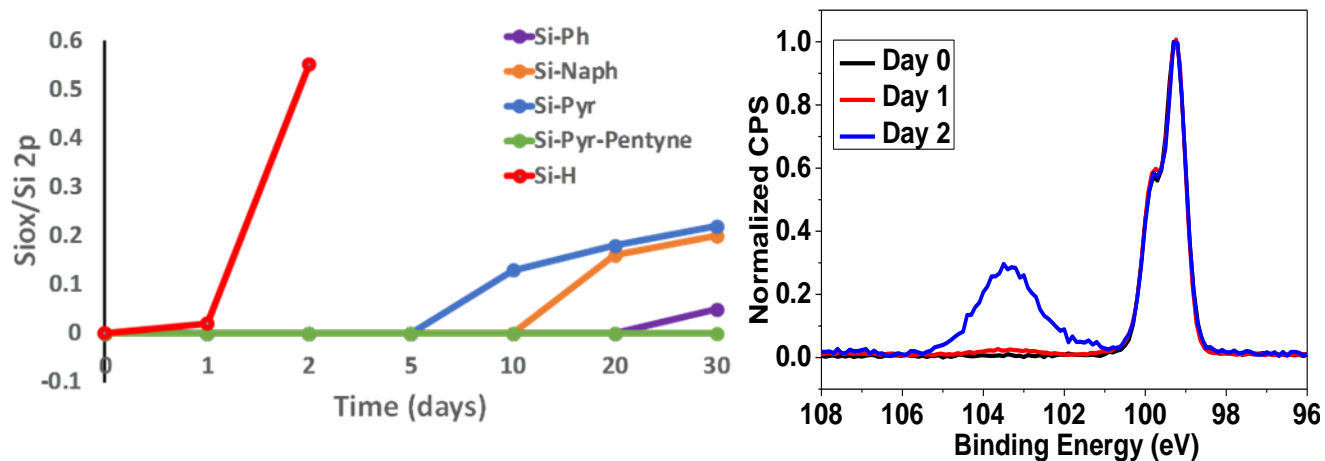
### Stability Study

To test the postulated hypothesis on a more practical basis four different aromatic surfaces were prepared: Si-Ph, Si-Naph, Si-Pyr and Si-Pyr backfilled with pentyne. These were then left at room temperature at atmospheric circumstances and silicon narrow scans were made at day 0,2,5,10,20 & 30 days. **Figure 11** shows the overlaid silicon narrow scans per functionalized surface and **Figure 12** summarizes the exact $Si_{ox}/Si_{2p}$ ratios over the course of the stability study. The exact values of **Figure 12** are given below in **Table 2**:
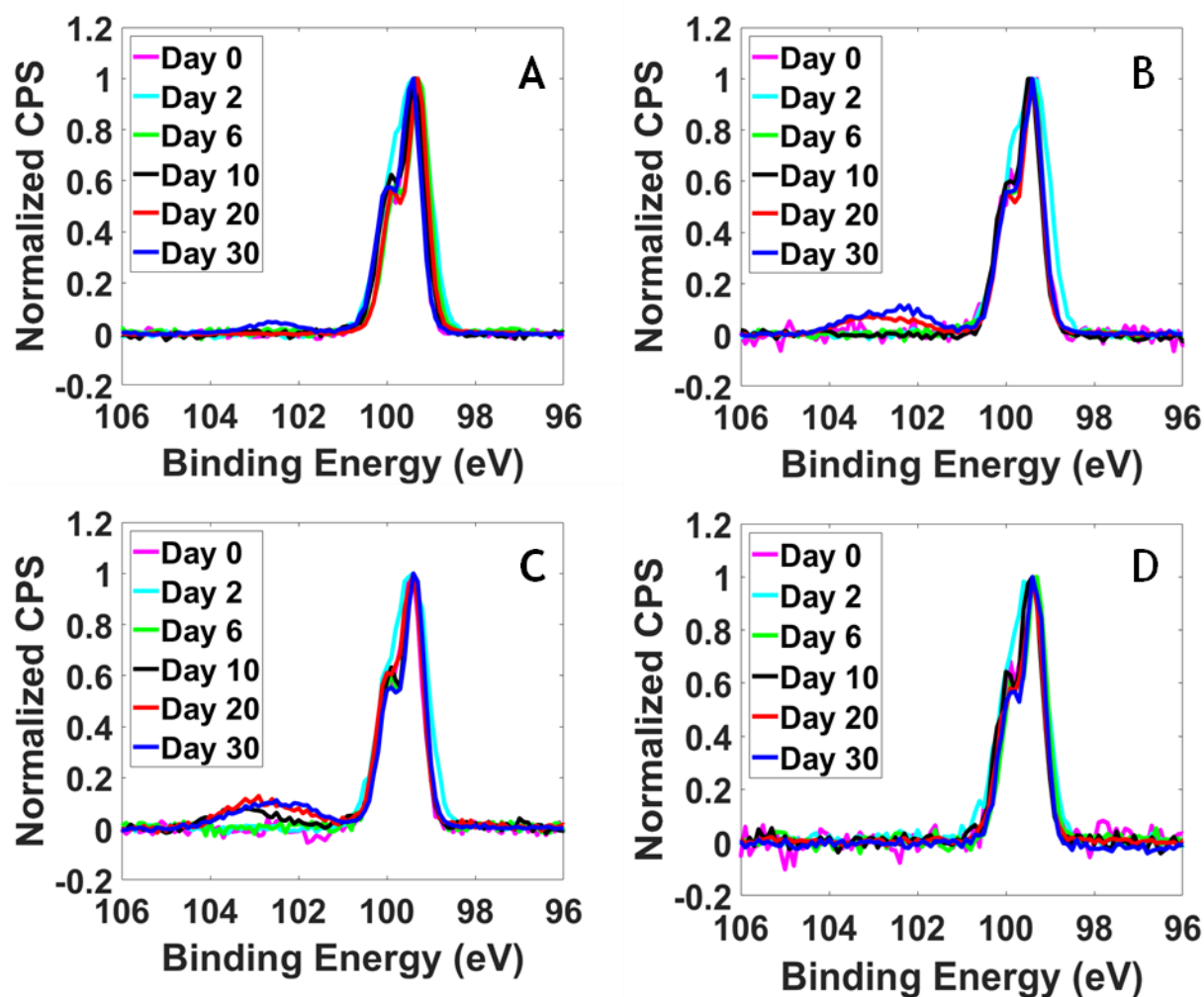
**Figure 11.** *Normalized overlaid silicon narrow scans of Si-Ph (A), Si-Naph (B), Si-Pyr (C) and Si-Pyr-Pentyne (D) of the stability study from 0 to 30 days.*

**Table 2**. *Averaged $Si_{ox}/Si_{2p}$ ratio of Si-Ph,Si-Naph,Si-Pyr, Si-Pyr-pentyne and Si-H measured over a 30 day period. -[a] signifies that no silicon oxide was identified and -[b] signifies that no measurements were conducted for this data point.*

| Surface | day 0 | day 1 | day 2 | day 5 | day 10 | day 20 | day 30 |
|---|---|---|---|---|---|---|---|
| Si-Ph | -[a] | -[a] | -[a] | -[a] | -[a] | -[a] | 0.05 |
| Si-Naph | -[a] | -[a] | -[a] | -[a] | -[a] | 0.16 | 0.20 |
| Si-Pyr | -[a] | -[a] | -[a] | -[a] | 0.13 | 0.18 | 0.22 |
| Si-Pyr-pentyne | -[a] | -[a] | -[a] | -[a] | -[a] | -[a] | -[a] |
| Si-H | -[a] | 0.02 | 0.55 | -[b] | -[b] | -[b] | -[b] |

*Figure 12*. *Graph that summarizes the oxide growth, based on the data of **Table 2**, in the different aromatic monolayers and hydrogen terminated silicon. Surfaces were left in the laboratory exposed to air for the duration of this stability study(Left). Stability of freshly etched Si-H surface exposed to air, a huge SiOx signal can be observed at 103.3 eV from Day 2 (Right).*

The data of the stability study agrees with the previously suggest hypothesis; that SAMs with larger aromatic groups have a lower overall density and are therefore more readily oxidized than other aromatic SAMs. The Si-Pyr surfaces showed the first signs of oxidation on day 12 whereas the Si-Ph surfaces only started minimally oxidizing by the 30th day. Additionally, **Table 2** would suggest that after initial oxidation the oxide growth per day seems to slowly decay. This could be attributed to a decreasing amount of available Si-H sites; and as oxygen has to diffuse to these sites a decay of the rate at which oxidation happens could be expected. This is most clearly illustrated in the case of Si-Pyr but can also be observed in Si-Naph. Lastly, the option of countering oxidation of these larger aromatic monolayers, by means of pentyne backfilling, are according to the results very effective. The Si-Pyr-pentyne surfaces do not show any indication of silicon oxide after 30 days of exposing them to air; which could greatly benefit the application of such monolayers as it significantly increases the ease of handling when these surfaces can be kept outside of a glovebox without any immediate consequences.

## Tetracene covered aromatic SAMs

After having characterized the various SAMs to be of sufficient quality, the surfaces were studied at AMOLF for tetracene deposition and TCSPC measurements. Subsequently, the samples were

send back to be re-analyzed by ellipsometry, AFM and XPS (AFM and XPS measurements are included in the Supplementary Information **Figures S.2** to **S.6**).

Similarly, to the ellipsometry measurements (**Table 3**) pre-tetracene deposition the expected upper limit is that of the out stretched molecules plus the indicated tetracene thickness, based on the tetracene evaporation rate. The large discrepancy between the expected thicknesses and the measured thicknesses measured by ellipsometry can be reasoned as follows. Prior to the tetracene deposition the surfaces were exposed to air for an extended period of time; this could explain part of the difference due to physio-absorption but the difference is too large to be solely be explained by physio-absorption. A more feasible explanation may be that the deposition rate of tetracene is not constant at all times and that therefore results in a higher than anticipated tetracene layer/ islands.

*Table 3.* *summarizes the theoretical, measured thicknesses of the Si-Ph-tetracene, Si-Naph-tetracene and Si-Pyr-tetracene surfaces with both the 4 and 35 nm island thicknesses.*

| Monolayer | Expected (Chem3D, nm) | Measured (Ellip, nm) (±2 nm) |
|---|---|---|
| **Phenyl acetylene 4nm** | 4.6 | 10.8 |
| **Phenyl acetylene 35nm** | 35.6 | 64.1 |
| **2-ethynylnaphtalene 4nm** | 4.8 | 17.4 |
| **2-ethynylnaphtalene 35nm** | 35.8 | 65.1 |
| **1-ethynylpyrene 4nm** | 5.6 | 19.9 |
| **1-ethynylpyrene 35nm** | 36.6 | 69.7 |

From the singlet-life time measurement data (**Figure 13**), was concluded that no clear life-time differences could be observed in Si-Ox, Si-H, Si-Ph or Si-Naph. It was noted that Si-H does seem to have a slightly lower average life time than the Si-Ph or Si-Naph surfaces. This lower average life time could also possibly hint towards energy transfer or other quenching mechanisms. This conclusion would conflict with the findings of Piland (2014) (17) and coworkers which had

observed no decrease of triplet life times in thin films of tetracene on hydrogen terminated silicon. The essential difference between this research and the one conducted by Piland *et al.* (2014)(17)  is that in this research tetracene islands were deposited onto Si-H rather than thin films. On the contrary, Si-Pyr did show some encouraging results with the overall observed singlet life time ranging from 4-6 ns whereas the observed delayed singlet life time varies from 100-200 ns to 300-500 ns varying from island to island. The fact that some islands having a different life-time than others could be an indication that triplet energy transfer may be happening. Yet, these preliminary measurements are only an indication as these life-time differences could also be explained by other mechanisms such as triplet annihilation.

Moreover, when looking at triplet life-time (tau 1) as a function of tetracene thickness (**Figure S.7** in the Supporting Information) it is rather remarkable that the highest life-time is observed at a thickness of 4nm and lower values at higher thicknesses. More data is required to make any concrete conclusions but initial measurements are encouraging for further investigation.

In sum, when comparing the various surfaces, one can conclude that Si-Pyr-tertracene is the most promising surface when it comes to signs of successful triplet energy transfer into silicon. In the case of Si-H,Si-Ph and Si-Naph the results are insufficient to draw any conclusions; the life-times of Si-Naph do change from island to island are but within an error of 1.5 with respect to eachother. Additionally, with Si-H and Si-Ph the faster overall life time suggests that something is at play which could either hint at energy transfer but could also be explained by other quenching mechanisms. Si-Ox shows an overall slower decay when compared to the other surfaces and seems to be most constant with respect to the observed life-times. This is to be expected as oxygen was thought to act as a passivating layer between the sensitizing tetracene and the silicon.
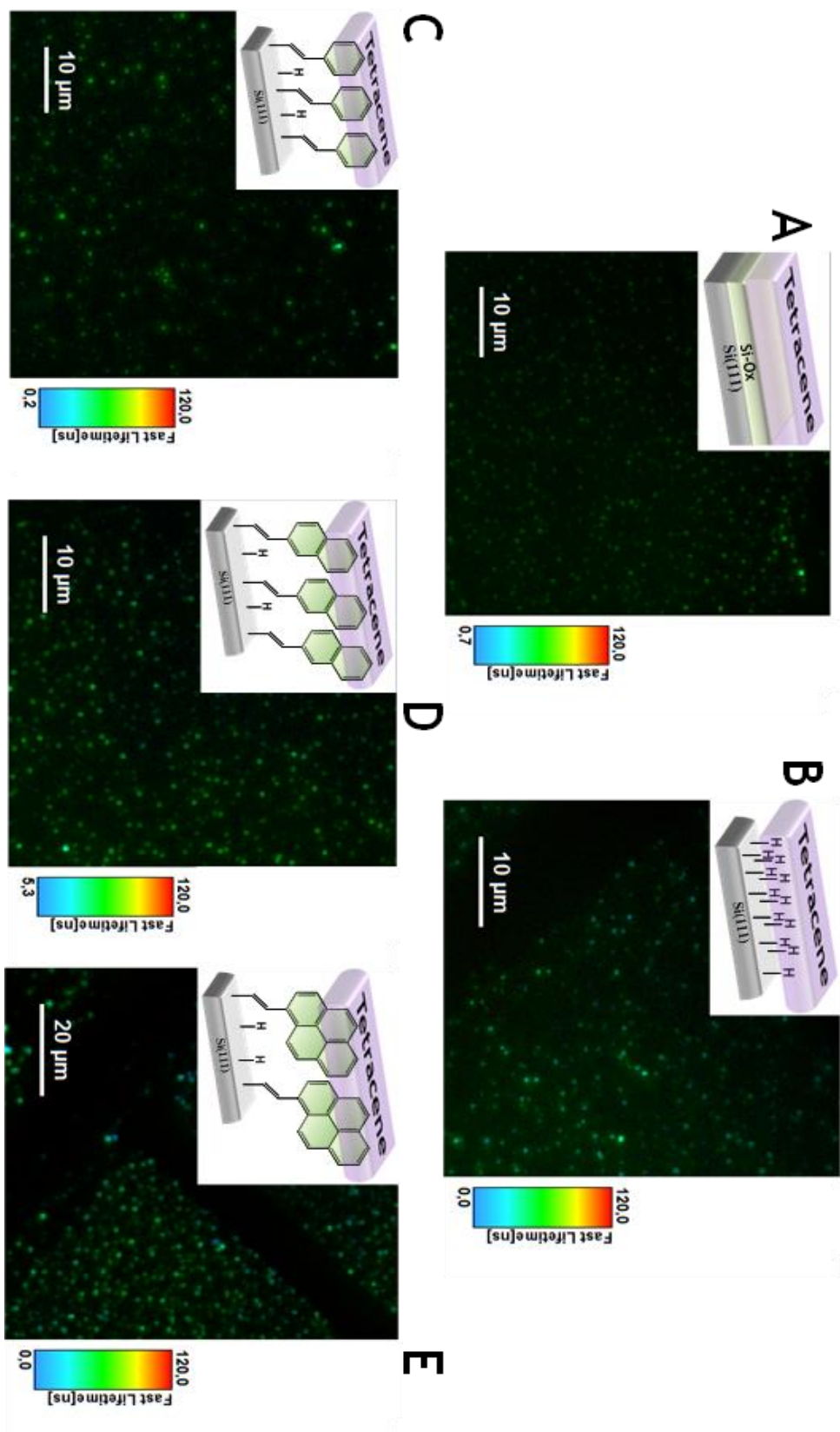
*Figure 13.* *TCSPC measurements, of Si-Ox (A), Si-H (B), Si-Ph(C), Si-Naph (D) and Si-Pyr(E) with tetracene islands deposited onto them. The different colors signify a different life-time in which green signifies longer life times than the blue spots which resemble shorter life-times.*

## Silicon functionalized with thiol

Similarly, to the aromatic functionalized surfaces, the thiol functionalized surfaces are modified to: prevent oxidation and to facilitate energy transfer from the tetracene layer to the silicon bulk. In contrary to the aromatic surfaces this energy transfer does not happen by means of Dexter Energy Transfer but rather by means of Förster Resonance energy transfer. **Figure 14** summarizes the different steps that were taken to produce a silicon functionalized surface that may dynamically bond Lead-Sulfide (PbS) nanoparticles (NPs) (also referred to as quantum dots(QDs)). These steps include: the modification of etched silicon with 1-butynylthioacetate, the deprotection of these thioacetates to their respective thiols and lastly the deposition of the PbS NPs onto these thiols.
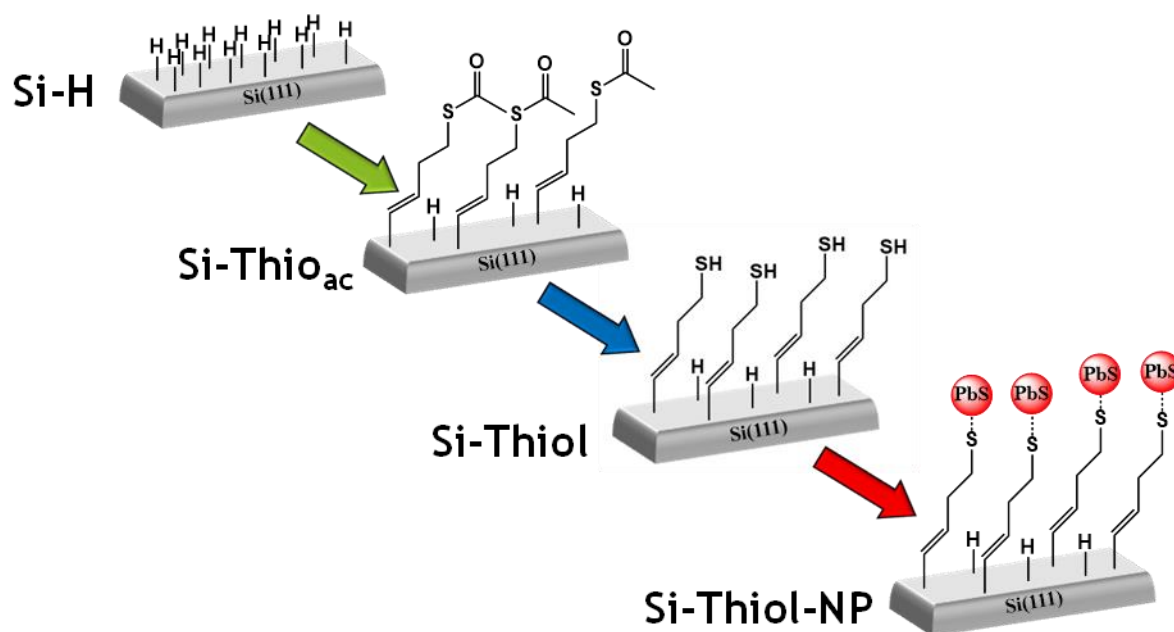


*Figure 14. An overview of the different modifications involved with the silicon functionalized with thiol surfaces. First the modification with 1-butynylthioacetate (green arrow) at 80 ⁰C. Second the deprotection of the thioacetate, by submerging the samples in saturated potassium (0.66 g in 5 mL) in methanol for 5 minutes, to the thiol (blue arrow). Third the lead-sulfide (PbS) nanoparticle deposition which was dispersed in an octane solution (red arrow).*

Like the silicon functionalized with aromatic surfaces, the next paragraphs will further discuss: the synthesis of 1-butynylthioacetate, the characterization of the Si(111) functionalized surfaces with 1-butynylthioacetate and 1-butynylthiol,the characterization of the silicon thiol functionalized surfaces with PbS NPs deposited onto them, an experiment varying the deprotection times  of these thioacetates to thiols and lastly another experiment focusing on the different deposition times of the PbS NPs onto the Si-Thiol.
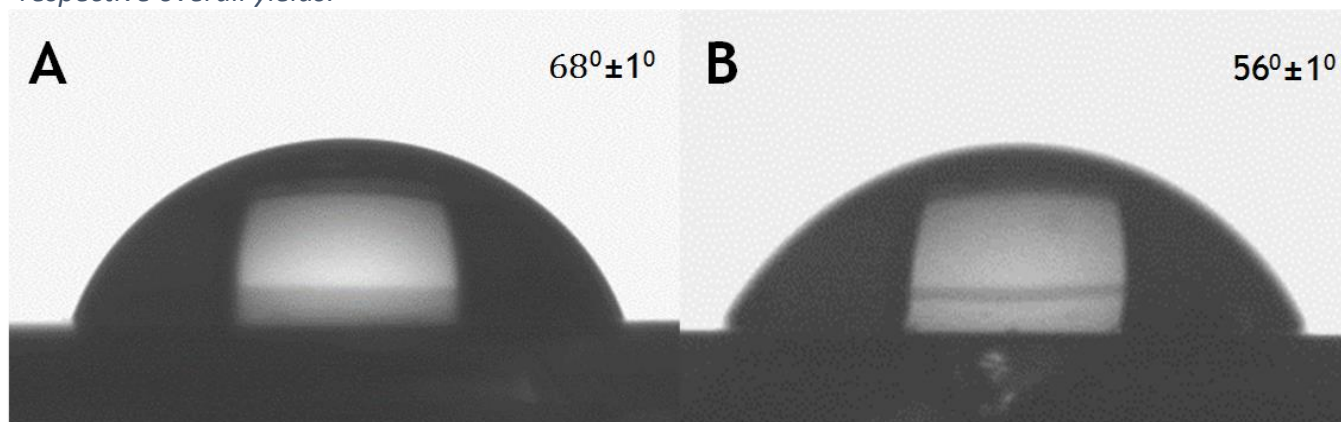
## Synthesis of 1-butynylthioacetate

In this thesis two different synthetic routes were employed for the synthesis of 1-butynylthioacetate (**Figure 15**). The first route be means of activating 1-butynol with mesylate-chloride to then form 1-butynylthioacetate. The second route by means of substituting the bromide for the thioacetate. **Figure 15**, is a schematic depiction of these two different routes. The main difference in yields is thought to be due to the fact that the activated alkyne (first route) does not need to be separated. Even though literature (40) suggests that the first step should be feasible with a 100% yield, personal experiences with this reaction do not exceed yields of 50%. The subsequent second step is also reported by Iannazzo *et al.* (2016) (40) to have lower yields. The exact synthetic procedures starting for 1-butynol are given in the Supporting Information, but due to the synthetically easier reaction and the higher yield I would recommend using the (second route) synthesis for all purposes (given in the Methods section).

## 1-Butynyl-Thioacetate & 1-Butynyl-Thiol Modified Surfaces (Si-Thio$_{ac}$ & Si-Thiol)

Likewise, to the characterization of the aromatic silicon surfaces, prior to any further steps two samples of each batch were measured. **Table 4** summarizes these findings; once more the ellipsometry measurements exceed the theoretical limit of the outstretched monomer. Considering this and the roughly 2 Å extra when calculating the height based on Equation 3 would indicate that these surfaces are not complete clean. However, keeping surfaces complete clean is extremely difficult as this can only be achieved in highly controlled systems like a glovebox; yet as the measuring equipment tends to be outside of these systems on always allows for some physio-absorption to occur.
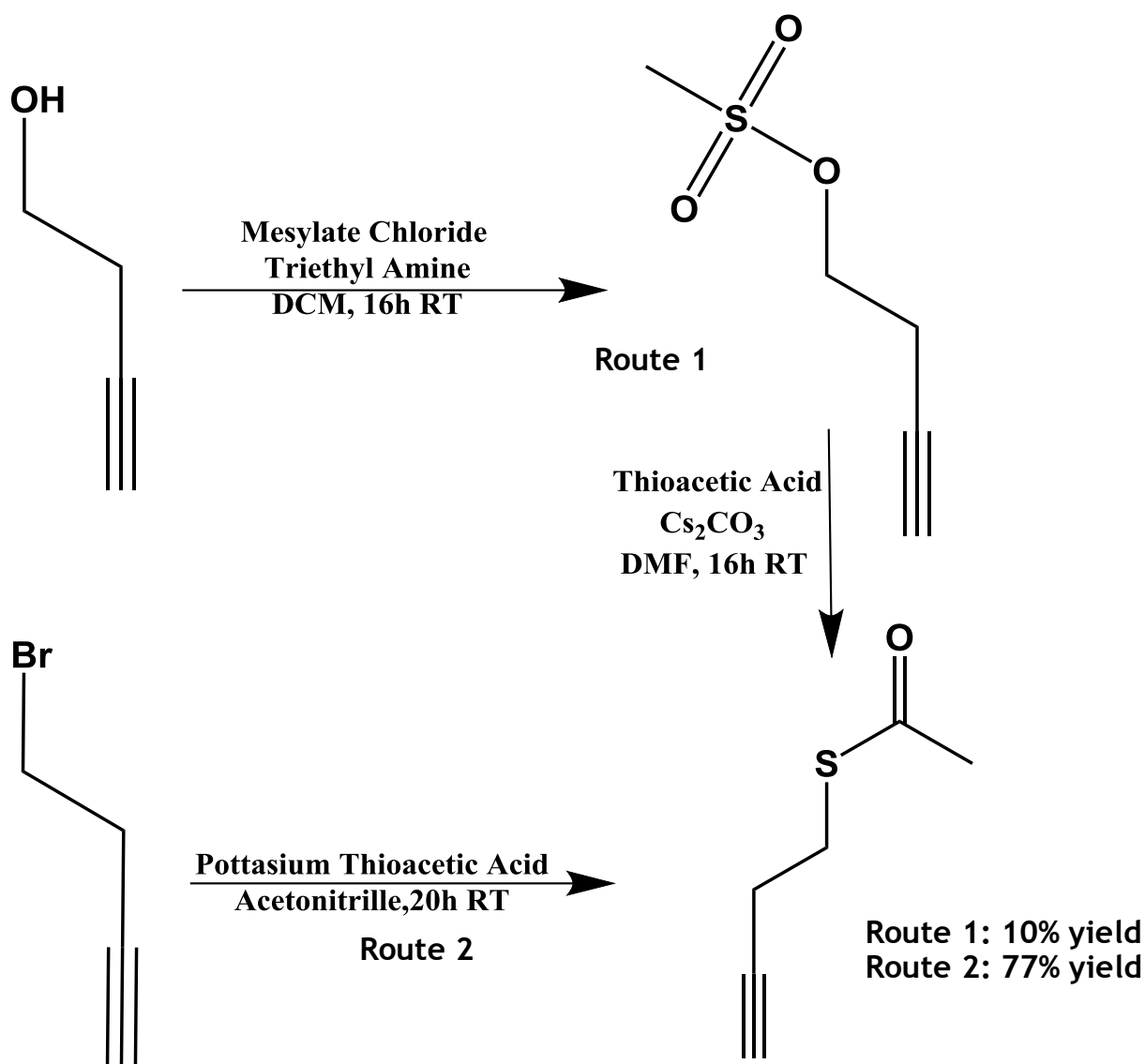
**Figure 15.** *Overview of the two different synthetic routers towards 1-butnylthioacetate with their respective overall yields.*



**Figure 16.** *SCA images of Si-Thio$_{ac}$ (A) and Si-Thiol(B) with their found SCA measurements.*

*Table 4. Overview of the different thicknesses of 1-butynylthioacetate and 1-butynylthiol by means of ellipsometry and XPS. Alike to Table 2 the theoretical column was determined by the use of Chem3D, the measured column by means of averaging the various ellipsometry measurements, the C:Si ratio by using the XPS wide-scan and lastly the calculated column by using these ratios in combination with Equation 3.*

| Monolayer | Theoretical (Chem 3D, Å) | Measured (Ellip, Å) (±2 Å) | C:Si (XPS, %) (±1-2 %) | Calculated (XPS, Å) (±2 Å) |
|---|---|---|---|---|
| 1-butynylthioacetate | 9.1 | 9.6 | 27.8 : 72.2 | 11.4 |
| 1-butynylthiol | 6.5 | 12.4 | 33.2 : 66.8 | 13.8 |

Next was the assessment of the Si-Thio$_{asc}$ or Si-Thiol by means of SCA, the results are summarized in **Figure 16**. Previous work (41) reported a SCA of $55^0$ of butanethiol on a gold surface, the observed results of $56^0 \pm 1^0$ for the Si-Thiol surface are in agreement with these findings and would suggest a successful deprotection from Si-Thio$_{ac}$ to Si-Thiol.

The XPS data of **Figure 17**, was acquired to check three things: the successful modification of Si-Thio$_{ac}$ and Si-Thiol, the degree to which the functionalized surfaces are silicon oxide free and lastly to verify the presence of the sulfur group of the thioacetate and thiol. **Figure 17A** shows the respective ratios of the C-C, C-S and C=O bonds. Theoretically these values ought to be in the ratio of 4:1:1 and this is approximately in line with the ratio suggested by **17A** which is 4.6 : 1 : 0.7 (C-C : C-S : C=O). The slightly higher C-C area suggests that there may be some minor impurities or contamination on the surface. On the other hand, **Figure 17B** is a strong indication that no silicon oxide is present and **Figure 17C** shows the presence of the sulfur of the attached thioacetate group.

The key difference between **Figures 17A** and **17D** is the decrease/absence of the previously found carbonyl peak around 289.0 eV. From the significant decrease of this carbonyl bump one can assume that the conversion of the Si-Thio$_{ac}$ surfaces to the Si-Thiol surfaces was successful. Moreover, from **Figure 17E** one can conclude that these surfaces are still silicon-oxide free which

is crucial for the subsequent energy transport mechanism. Additionally, when comparing Figure **17C** with **17E** one can observe that there has been barely any change with respect to the sulfur signal which is good sign as we do not desire to remove the thiol group.

Comparing the carbon, silicon and sulfur narrow scans of the Si-Thiol-NP surfaces (**Figure 17G, H, I**). It is utmost importance that the surfaces remain oxide-free. Moreover, the carbon signal of **Figure 17G** is similar to that of **Figure 17D** which is a good indication that no oxidation of the sulfur has occurred. This is also supported by the lack of a peak near 232 eV in the S 2s narrow scan as this according to Mostegel *et al.* (2015) (42) would correspond to oxidized sulfur. Note that the sulfur narrow scans of S 2s was chosen over the more commonly used S 2p narrow scan as the satellite peak of the silicon caused too much uncertainty with respect to what can or
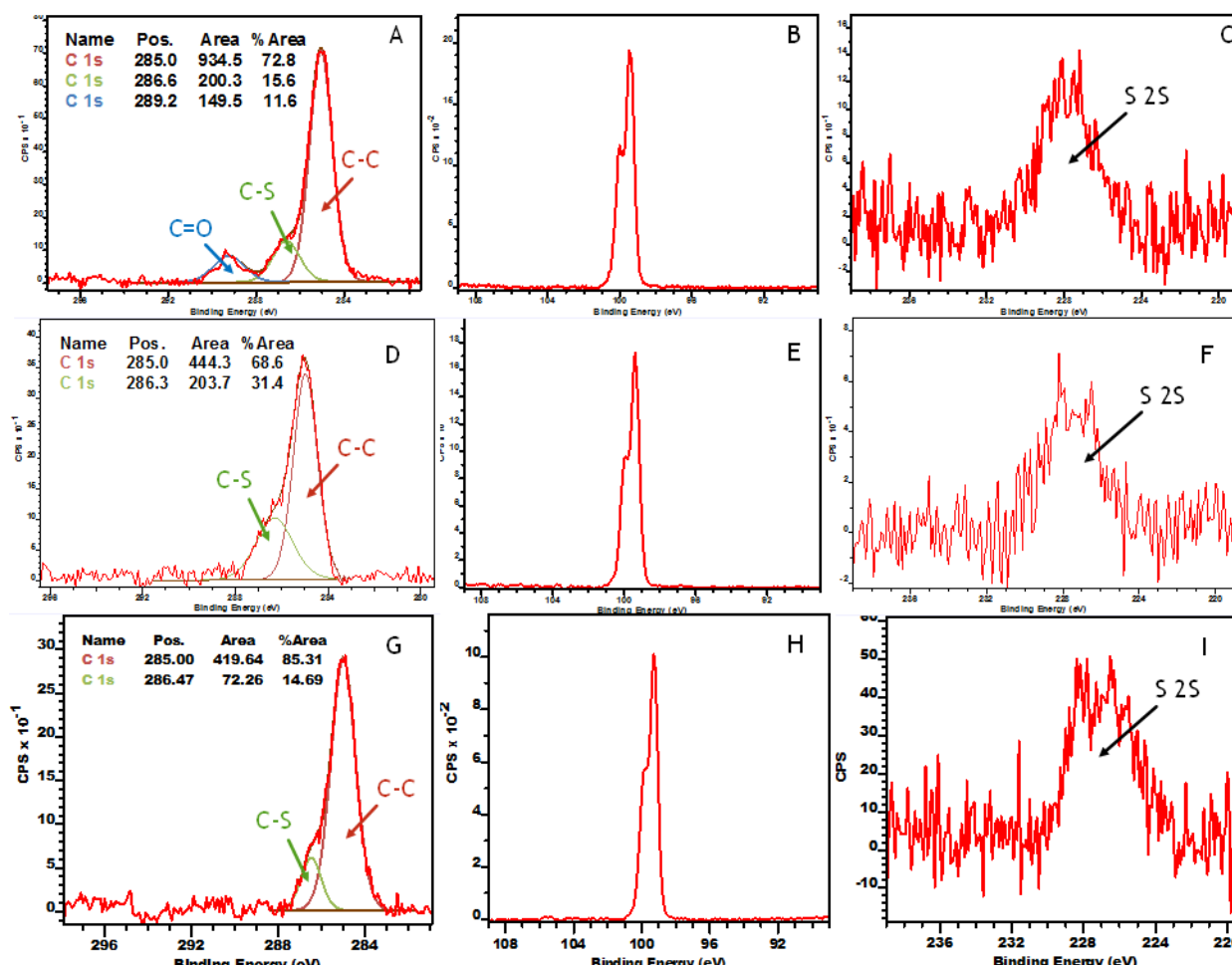


**Figure 17.** *From left to right are the carbon, silicon and sulfur narrow scans respectively. The three rows are these narrow scans of the following surfaces: Si-Thio$_{ac}$ (first row), Si-Thiol (second row) and Si-Thiol-NP (third row).*

cannot be considered a peak. The Pb narrow scan of the Si-Thiol-NP surface is supplied in the Appendix (**Figure S.8**).

For the last characterization method of the thiol modified surfaces, we turn to **Figure 18** which are the respective AFM images and height profiles of the different steps within the process of creating a Si-Thiol-NP surface. The results shown in **Figure 18**, show a clear difference between the Si-Thio$_{ac}$ and Si-Thiol surfaces when compared to the Si-Thiol-NP surfaces. This was to be expected as the expected size of the deposited NPs is around 10nm; this also reinforced by the height of the Si-Thiol-NP surfaces. On the contrary, if the particles are 10 nm one would expect to see a multitude of dots with also a width of approximately 10 nm. Yet, as can be observed from **Figure 18**, this is clearly not the case; one could explain this phenomenon by the clustering of NPs thereby forming islands of a respective height of 10nm but of a larger overall width. It is hypothesized that in the absence of available thiol groups to dynamically bond the NPs, the NPs instead cluster together thus forming the observed islands with a larger than 10nm width but with a height that matches the given average size of the NPs. Also, considering the relative flatness of Si-Thio$_{ac}$ (RMS= 0.5 $\pm$ 0.2nm) and Si-Thiol (RMS= 0.3 $\pm$ 0.2nm) prior to the NP deposition is a good indication that the observed dots are indeed the desired PbS nanoparticles; since the RMS increases to 5.3 $\pm$ 0.2nm for the Si-Thiol-NP.
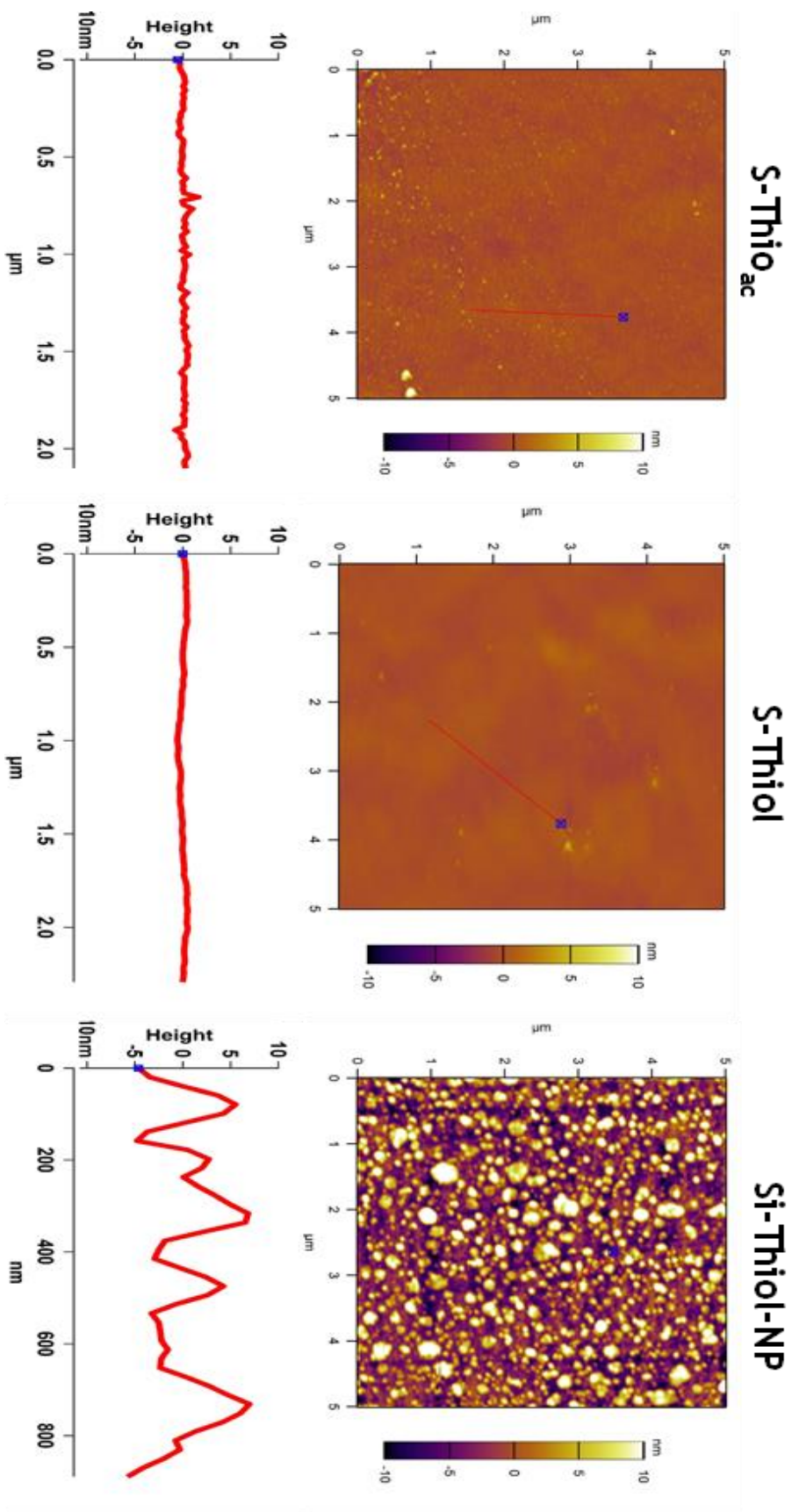
**Figure 18.** *AFM measurements of Si-Thio$_{ac}$ (RMS= 0.5 ± 0.2nm), Si-Thiol (RMS= 0.3 ± 0.2nm) and Si-Thiol-NP (RMS= 5.3 ± 0.2nm) with their according height profiles.*

## Deprotection study of Si-Thioac to Si-Thiol

Following the characterization of the Si-Thio$_{ac}$, Si-Thiol and Si-Thiol-NP surfaces, further optimization of this process was desired. The first step was to study the effect of shorter and longer deprotection times of the Si-Thio$_{ac}$ to the Si-Thiol. **Figure 19**, summarizes the findings of deprotecting a Si-Thio$_{ac}$ surface at various time scales in a saturated $K_2CO_3$ solution in methanol; after deprotection the Si-Thiol surfaces were dipped in the supplied PbS solution for 24 hours to maximize the density of the NPs on the thiols. One can observe that even after 1 minute of deprotecting the surfaces has been able to dynamically bond some PbS NPs. Contrarily, after leaving the Si-Thio$_{ac}$ surfaces in a deprotecting solution for 15 minutes or longer the SAMs are significantly damaged. This result agrees with previous work (26) stating that alkyne monolayers are the least stable in basic solutions opposed to either neutral or acidic solutions. These results would indicate that an optimal deprotection time is somewhere between 3 to 5 minutes: as prior to 3 minutes one can still observe larger islands whereas one could argue that in the 5 minute measurements the surface starts to show signs of damaging. Nonetheless, the 5-minute measurement is by far the densest and homogeneously dispersed surface, this is even further supported by **Figure 20** which is an AFM measurement of the same surfaces but then on a 1 x 1 μm area. It is thought that in the absence of an available thiol group the NPs cluster together around one dynamically bound NP. Thus, one would then observe multiple NPs stacked together forming an island; this is observed in both the 1 and 3-minute case of Figure 21 whereas Si-Thiol-NP surfaces that have been deprotected for 5 minutes do not show these islands.

## Deposition time study of NP solution on Si-Thiol

Aside from optimizing the deprotection period, one can also study the different times that the surfaces are submerged in the PbS solution. To form a common analysis basis all surfaces were deprotected for a period of 5 minutes after which they were immediately submerged for the allotted time: 1, 2.5, 5, 16 and 24 hours. After the samples, have been submerged for their respective times, they were washed with octane and then subsequently sonicated in octane and DCM for 5 minutes prior to any measurements.  **Figure 21** summarizes the AFM measurements of the various surfaces at their respective deposition times. Note that these measurements, in contrast to the previous AFM measurements are of an area of 1x1 μm. This is because at the 5x5
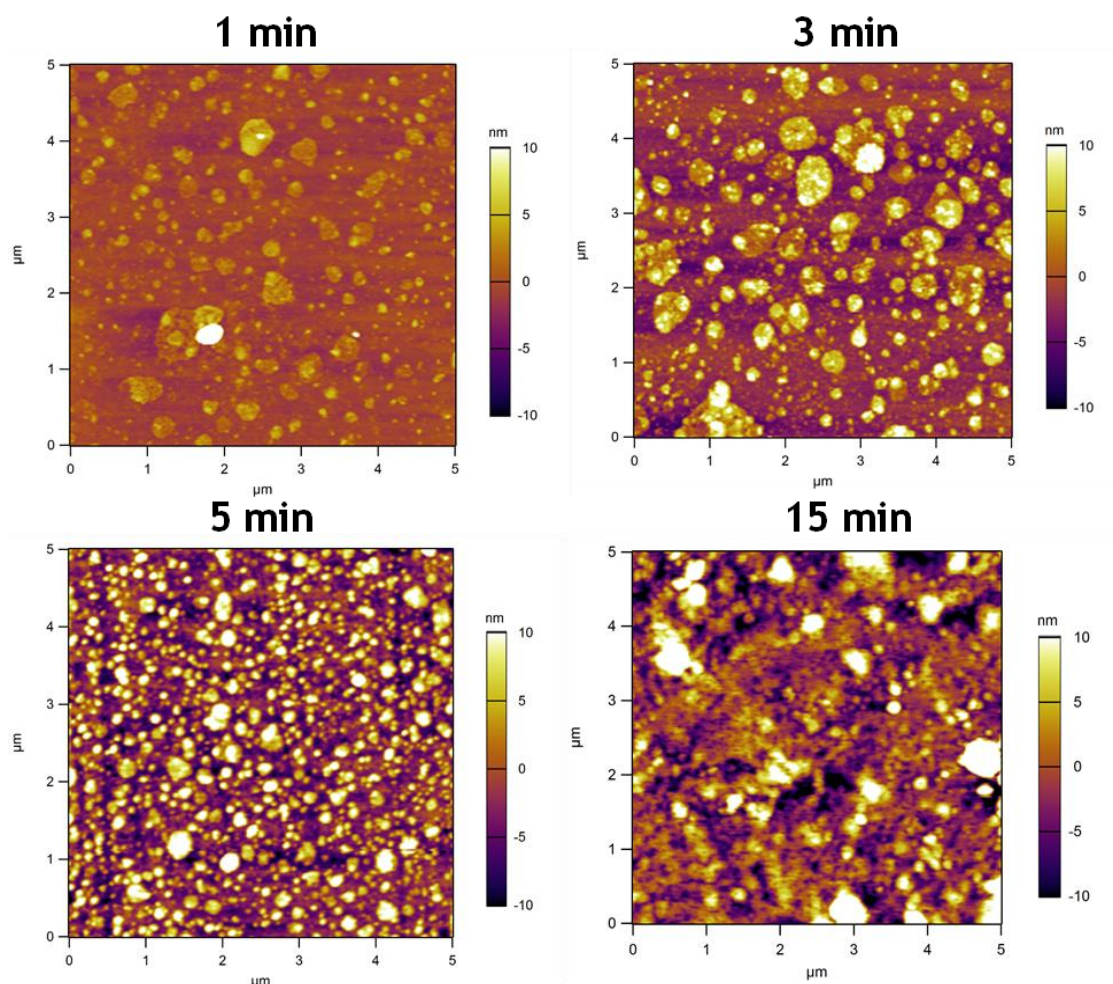
***Figure 19***. *AFM images of Si-Thiol-NPs at different deprotection times: 1 minute (RMS= 3.4 $\pm$ 0.2nm), 3 minutes (RMS= 3.6 $\pm$ 0.2nm), 5 minutes (RMS= 5.3 $\pm$ 0.2nm) and 15 minutes (RMS= 5.9 $\pm$ 0.2nm) in $K_2 CO_3$ dissolved in methanol.*
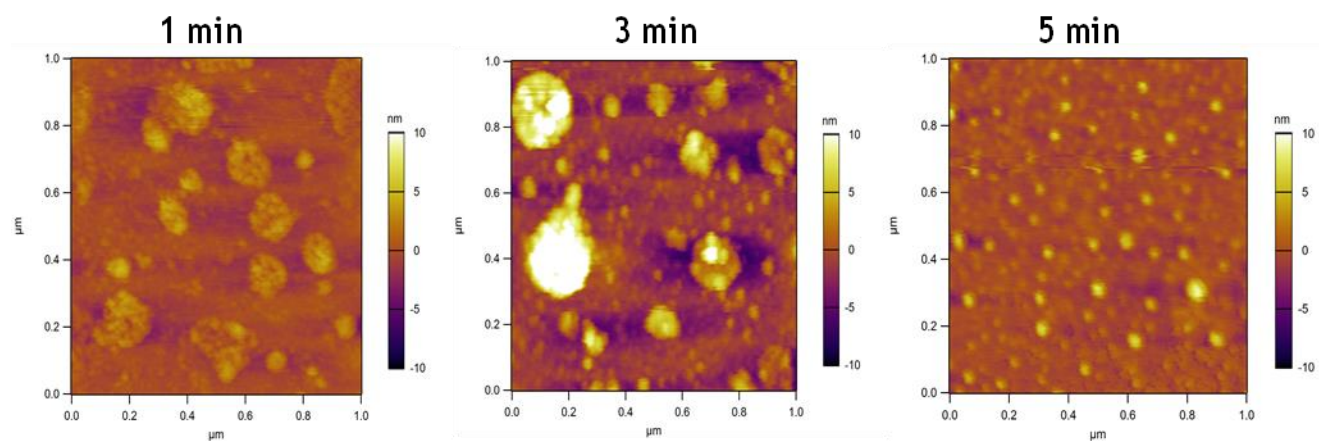


***Figure 20.*** *AFM images of 1x1 um of the various deprotected time scales of Si-Thioac: 1min (RMS= 1.2 $\pm$ 0.2nm) , 3min (RMS= 3.1 $\pm$ 0.2nm) and 5 min (RMS= 1.1 $\pm$ 0.2nm)*

µm scale one could not clearly distinguish between the 2.5, 5h, 16h and 24 h surfaces. In **Figure 21**, a submerging time of 1h is clearly insufficient for a homogeneous packing of the NPs on the thiol surface. Surprisingly, after only 2.5 hours one can already clearly see the first NPs having dynamically bound to the Si-Thiol surface; although the differences between the 2.5h and the 5 and 16h surfaces are rather slim one can observe a slight increase of number of particles. The surfaces that were left in the PbS solution for 24h are significantly denser than any of the previous surfaces. It would be interesting to compare these results to that of for example of 36 or 48 hours deposition times but due to time constraints these surfaces were not prepared

In sum, numerous Si-Thiol-NP have been prepared and for the densest possible NP distribution the surfaces that have been deprotected in a saturated potassium carbonate methanol solution for 5 minutes and then left submerged in the PbS solution for 24 hours.
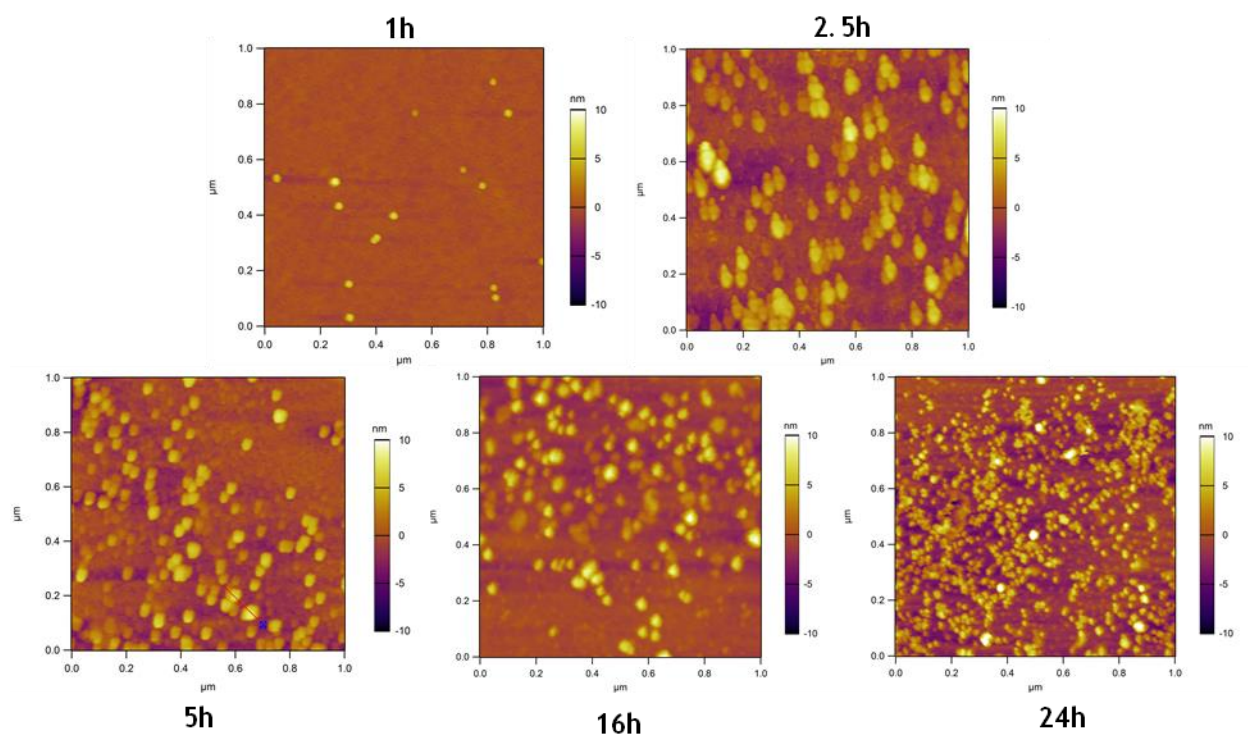


***Figure 21.*** *Si-Thiol-NP surfaces after 5 minutes of deprotection and various deposition times: 1h(RMS= 0.5 ± 0.2nm),2.5h (RMS= 2.9 ± 0.2nm),5h(RMS= 1.8 ± 0.2nm),16h (RMS= 1.7 ± 0.2nm) and 24h (RMS= 2.5 ± 0.2nm)*

## Si-H vs Si-Thiol

Preparing blancs are crucial to any experiement; they provide essential information whether the chosen treatement was effective or not. Yet, when modifying surfaces one has to consider two kinds of blancs, namely: Silicon-Oxide (Si-Ox) and hydrogen terminated silicon (Si-H). There are intermediates like hydroxy terminated silicon (Si-OH) but these will not be discussed in this research. **Figure 22** is a schematic representation of the deposition of PbS NPs onto a Si-H surface.

Initially, it was expected that the NPs would not bind to either the Si-Ox or the Si-H as it was thought that the PbS NP exclusively interact with Si-Thiol surfaces. Surprisingly, this expectation was proven to be wrong as the AFM results of the Si-Ox-NP, Si-Thiol-NP and Si-H-NP surfaces are summarized in **Figure 23**. Curiously it seems that the Si-H-NP surface when submerged for an identical time as the Si-Thiol-NP surface yields a more densly and homogenously spread coverage of PbS NPs. Please note that after the PbS NP deposition all surfaces were sonicated in octane and DCM for 5 minutes prior to any measurements. Initial findings were even sonicated several times in various solvents such as acetone, ethanol, toluene and hexane as the observed dots were
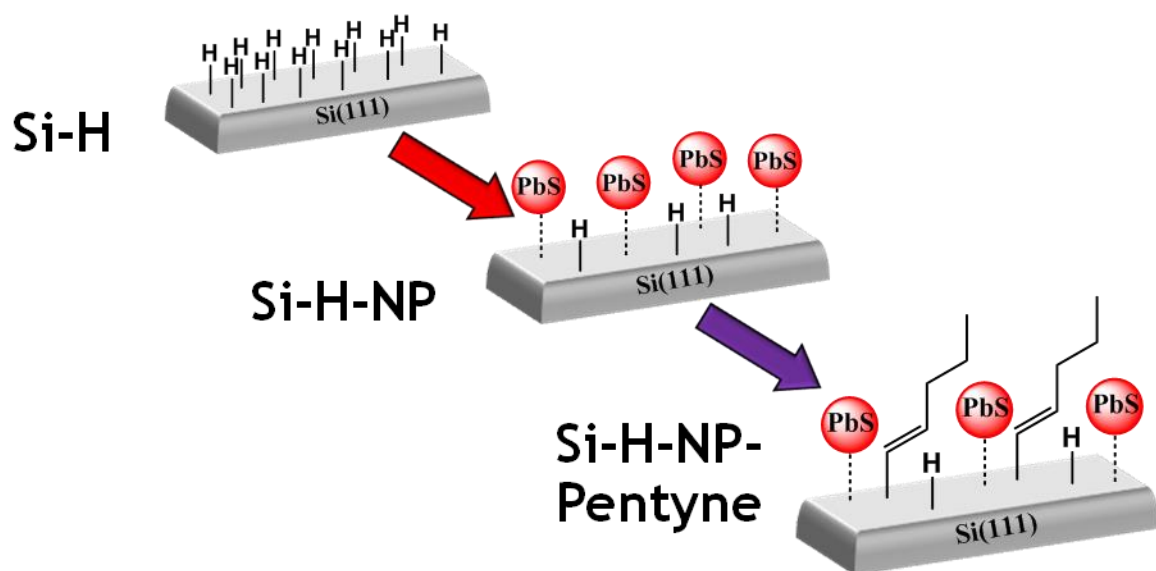


***Figure 223.*** *Schematic overview of the modification process of Si-H-NP-Pentyne. A freshly etched Si-H surface is dipped in a PbS solution for a minimum of 150 minutes after which one can optionally backfill with pentyne to prevent the oxidation of the unreacted Si-H sites.*
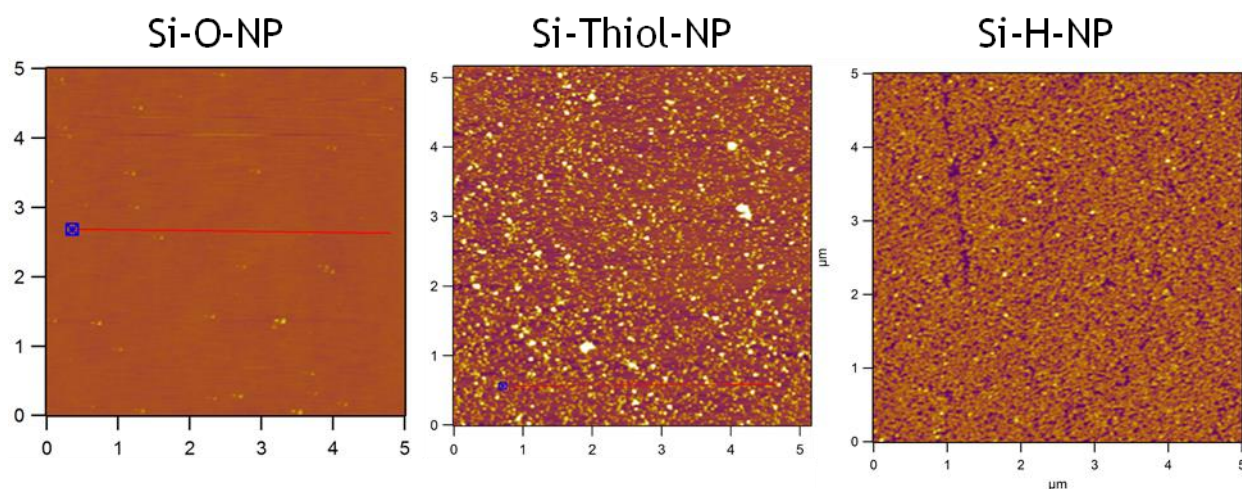
**Figure 23**. *Comparison of Si-Ox-NP (RMS= 0.2 ± 0.2nm), Si-Thiol-NP (RMS= 0.3 ± 0.2nm) and Si-H-NP (RMS= 2.0 ± 0.2nm) modifications after 5 minutes of sonication in octane and 5 minutes sonication in DCM.*
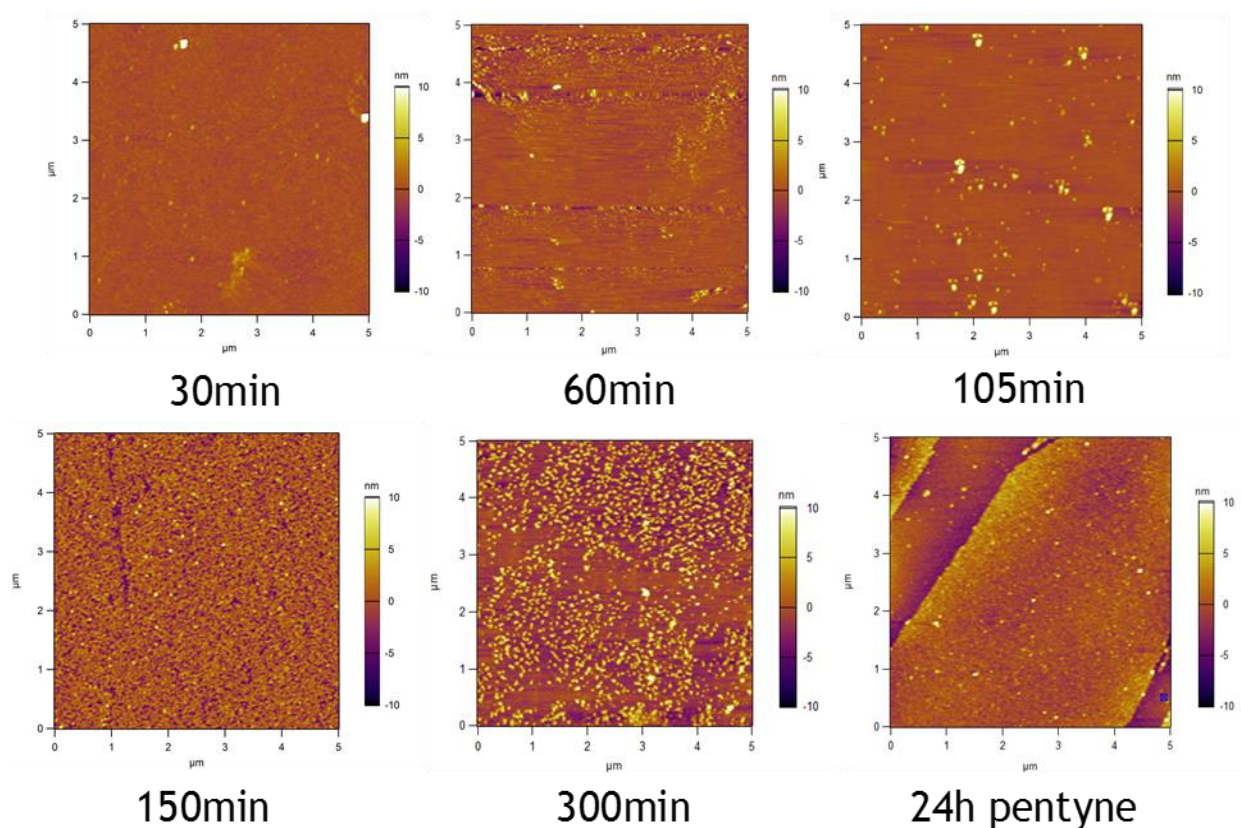


**Figure 24.** *Results of different deposition study; where hydrogen terminated silicon has been submerged in a PbS NP solution for various time intervals: 30 min (RMS= 0.9 ± 0.2nm), 60 min, (RMS= 3.2 ± 0.2nm), 105 min (RMS= 1.0 ± 0.2nm), 150 min (RMS= 2.0 ± 0.2nm), 300 min (RMS= 2.9 ± 0.2nm) and 24 hours (RMS= 1.6 ± 0.2nm) which were subsequently backfilled with pentyne.*

thought to be physoabsorbed particles. The mechanism or the interaction between the Si-H and the PbS particle remain unknown and were not further investigated due to the limited time of this project. However it is hypothesized that the sulfide in the PbS nanoparticles interacts with the hydrogen terminated silicon in some way. Recently, Buriak and coworkers (2016) (43) have proposed several reaction mechanisms for formation of Si-S bond, driven by either UV irradation or thermally driven homolytic silicon hydrogen and silicon-silicon bond cleavage, that may explain the formation of the ≡Si–S bond on hydrogen terminated silicon.

After these initial results, another deposition study was conducted but now with freshly etched Si-H surfaces and the results of this study are sumarized in **Figure 24**. It is clear that after atleast 2.5h of submerging Si-H surfaces in the PbS NP solution that the remarkable homogeneity and
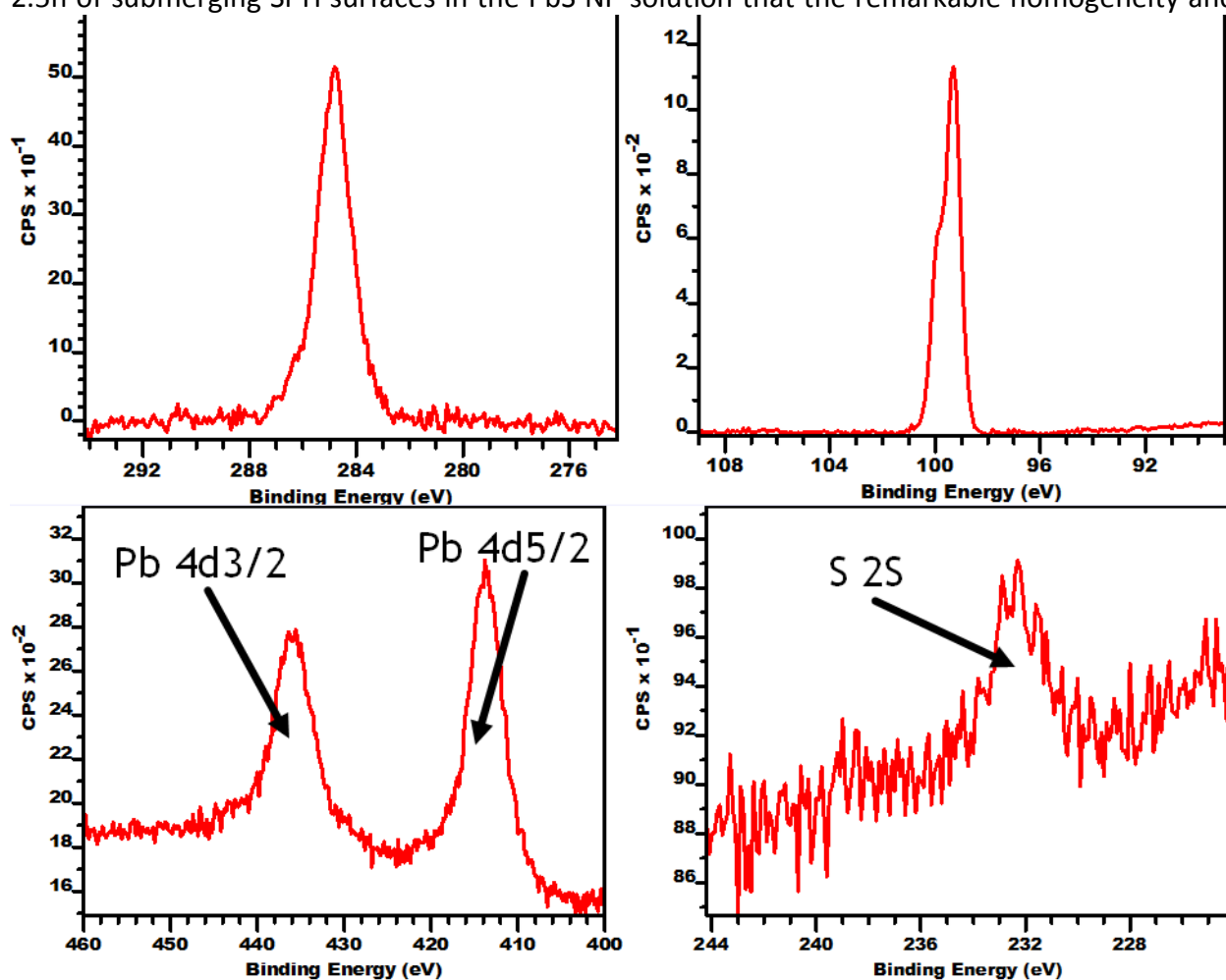


*Figure 25. XPS narrow scans of the Si-H-NP-pentyne surface. Top right is the carbon narrow scan, the top left is the silicon narrow scan. Bottom Left shows the 4d orbitals of Lead and bottom right shows the S 2S peak of presumable the PbS NPs.*

density can be observed. The observed differences in density between the 150 minutes and 300 minutes surfaces are negligible as at a larger scale (20 x 20 µm) the surfaces look equally dense. To prevent any possible oxidation of unreacted Si-H sites on the 24h surfaces, these were also backfilled with pentyne at $80^0$ C in a neat pentyne solution; as was previously outlined in the Experimental Procedures section in the subsection Monolayer formation.  Interesting to note is that the 24h pentyne surface seems to be even more densely packed than the 150 minutes or 300 minutes surfaces; it is unclear whether the elevated temperatures may have an additional effect which would explain these observations. Nonetheless, the results would indicate that a minimum time of 150 minutes is required to get a densely packed PbS NP coverage on a Si-H surface; which is remarkably shorter than the 24 hours required for the Si-Thiol surface (not to mention the previously required modification and deprotection steps).

Subsequently, to ensure that the observed particles are PbS nanoparticles; XPS (**Figure 25**) and Auger electron spectroscopy (AES) (**Figure 26** & **Figure 27**) measurements were made of the 24h pentyne backfilled Si-H-NP surfaces to determine the elemental composition of these modified surfaces.

First, the narrow scans of both the carbon and silicon indicate a successful modification with respect to the silicon being oxygen free and no other carbon signals being distinguishable apart from the C-C bonds and the underlying C=C bond. With respect to the lead and sulphur these regions were chosen as the traditional regions of Pb 4f and S 2p overlapped with the satellite peak of Si (as previously explained with the XPS measurements of the Si-Thiol-NP surfaces).

Second it is important to distinguish between the S 2s spectra shown in the bottom right of **Figure 25** and those shown of the Si-Thiol-NP in **Figure 17I**. There is a notable shift from 228 eV in the Si-Thiol-NP S 2s spectra to 232 eV in the Si-H-NP spectra; literature (40) suggests that this 232 eV could correspond to oxidized thiol SAMs. This is in contradiction with the silicon narrow scan spectra as this shows no sign of oxidation; however, as the NPs consist of several sulphur sites that may still be exposed to air on the topside there still is a possibility that these sites may have been oxidized. Nonetheless, one would still expect to see a similar peak around 228 eV as not all the sulphur sites would have been oxidized so readily. This would suggest that either the

observed shift can be attributed to the unknown interaction between the PbS and the hydrogen terminated surface. Regardless, further investigation on the exact mechanism and the bond character of the PbS NPs and the Si-H surface would provide crucial insight into these findings.

Third, are the $1^{st}$ derivate AES spectra (**Figure 26**) of the two different spots; at spot 1 (in red) one can clearly observe a higher silicon signal than at spot 2 (in blue). On the other hand, at spot two the Pb and S signals are higher than at spot 1; this in combination with the clearly distinguishable dots in the SEM image strongly suggest that the observed particles are PbS NPs. The differences in Si, Pb and S signal intensities are most clearly observed in the figure below the SEM image where the two spectra are overlapped. Additionally, the differences have also been quantified and summarized in the table below. Lastly, the spatial AES measurements of the indicated line in **Figure 27** clearly shows the presence of Pb and S at the dots and a higher Si signal in the absence of them. Moreover, in the Supporting Information (**FIGURE S.9**), the separate SEM images are overlaid with different colours to indicate the respective element intensity. Combining the results of **Figures 26** and **27**, we can conclude that Si-H-NP-pentyne surfaces are extremely densely packed and that the observed nanoparticles are composed of lead and sulfide.

In sum, Si-H-NP surfaces in comparison to Si-Thiol-NP are prepared more readily, result in denser and homogenous PbS NP depositions. The absence of having to prepare 1-butnylthioacetate and its respective deprotection does not only safe time but is also financially more favourable as no chemicals have to be purchased. The combination of a faster process, a shorter minimal deposition time and a resulting denser and evenly spread PbS NPs on the surface could therefore be considered for larger scale productions.
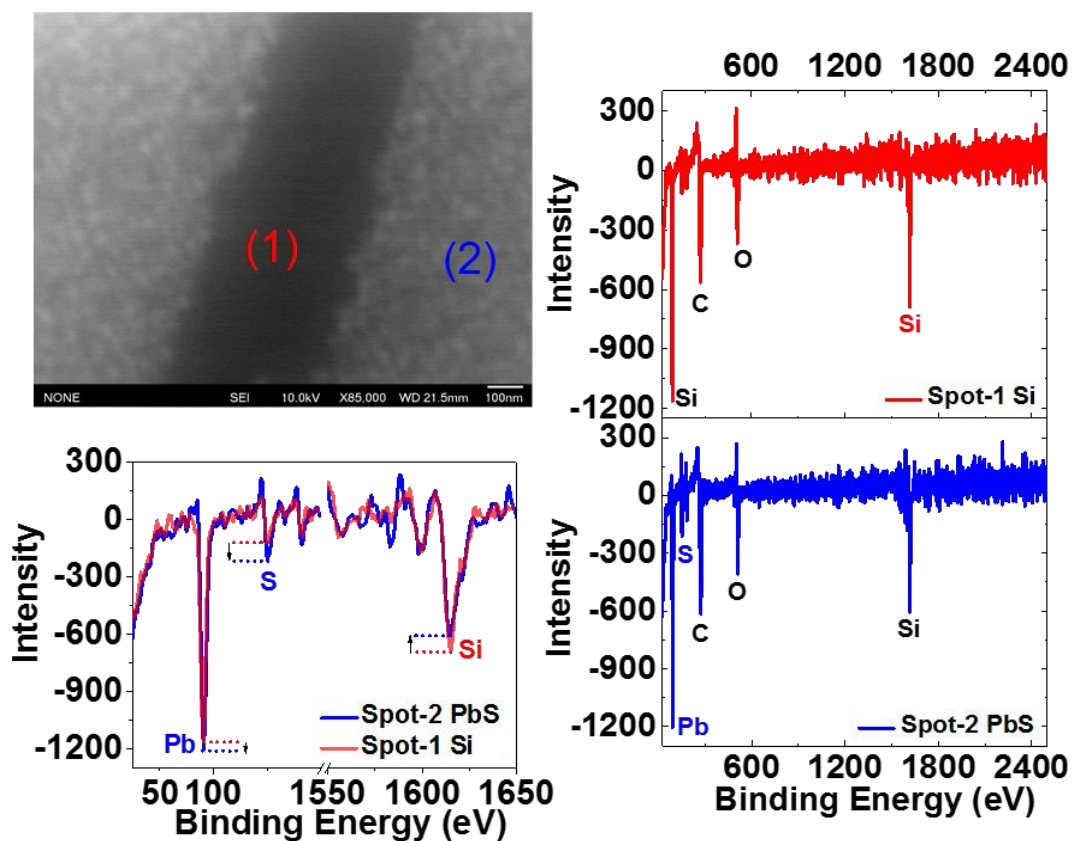
**Figure 26.** *Top left, SEM image of the Si-H-NP-pentyne surface. The other figures are the first derivative AES spectra in which the signature peaks for Pb, S, C, O and Si have been indicated.*
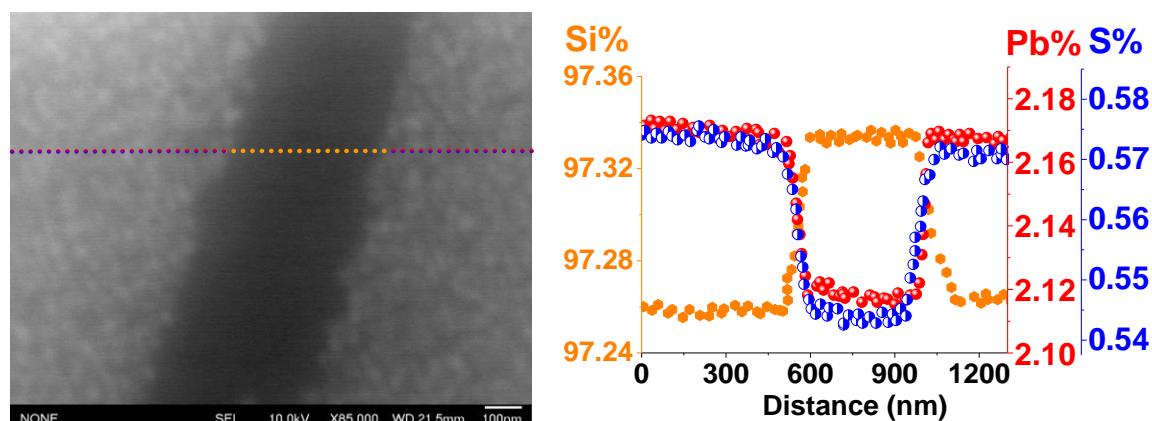


**Figure 27**. *SEM and Auger plot of the elements mapped across the indicated line.*

## Conclusions

The aim of this research was to modify and characterize various functionalized silicon surfaces with the aim to further improve the efficiency of silicon based photovoltaic cells by means of using Singlet Fission. Two routes were employed the facilitate the energy transfer of the sensitized tetracene into the photovoltaic material silicon: Dexter Energy Transfer and Förster Resonance Energy Transfer. The surfaces targeted for Dexter Energy Transfer were modified with phenylacetylene (Si-Ph), 2-ethynl naphthalene (Si-Naph) and 1-ethynyl pyrene (Si-Pyr). The surfaces that were theorized to facilitate Förster Resonance Energy Transfer were surfaces modified with 1-butynyl thioacetate (Si-Thioac) which were then deprotected to thiol surfaces (Si-Thiol) which then had PbS NPs deposited onto them.

Various surface modifications have been performed and characterized successfully, including: Si-Ph, Si-Naph, Si-Pyr, Si-Thio$_{ac}$, Si-Thiol, Si-Thiol-NP and Si-H-NP. Additionally, tetracene islands of 4 and 35 nm thickness were deposited on the Si-Ph, Si-Naph and Si-Pyr surfaces and characterized accordingly with their respective photonic properties.

With respect to the silicon functionalized with the polyacenes (Si-Ph, Si-Naph and Si-Pyr), the Si-Pyr surfaces showed the most encouraging results with significant life time differences varying from island to island. The first results of the Si-Ph and Si-Naph TCSPC measurements showed no indications of successful energy transfer or any change in life time. Additionally, backfilling Si-Pyr with pentyne has successfully prevented the most readily oxidizing surface to remain oxide free under atmospheric circumstances for up to at least thirty days.

The surfaces functionalized with thiols were also characterized by means of ellipsometry, SCA, XPS and AFM. Deprotecting the Si-Thio$_{ac}$ surfaces for 5 minutes with saturated $K_2CO_3$ in methanol and subsequently submerging them for 24 hours in the PbS nanoparticle solution led to the most dense and reproducible Si-Thiol-NP surfaces. Deprotecting for shorter periods could lead to NP clustering on the surface and deprotecting for longer periods can damage the SAM. A minimum of 2.5 hours is required for the nanoparticles to dynamically bound to the Si-Thiol surface but keeping the samples in the PbS NP solution for a longer period of time will result in more homogeneous and denser spread of the PbS NPs on Si-Thiol.

Lastly, hydrogen terminated silicon has also been found to interact with the supplied PbS NP solution. The surfaces only need to be submerged for 2.5h to get reproducible and a denser NP coverage than with any of the Si-Thiol-NP surfaces. AFM, XPS and AES confirm these particles to be PbS NPs, that seem to be bound in some way, given the fact that removal by sonication in numerous solvents was not observed. It is unclear whether the pentyne backfilling of these Si-H-NP surfaces influences their respective density and therefor further investigation is required. Yet the Si-H-NP-pentyne surfaces display unparalleled density and further research is recommended.

## Future Research

Every research, every paper, every thesis are only steps in the journey towards a better understanding and or exploitation of the world around us. Similarly, with this thesis there are several avenues that could be further explored and in the following paragraphs I would like to further explain which investigations, in my opinion, would be most worthwhile.

The silicon surfaces modified with several aromatic alkynes are still missing one important polyacene and that is tetracene. The synthesis of 5-ethynyl tetracene has been attempted but this synthesis was not completed successfully (See supporting information **Section K** for the full procedure). It would be of great value to see both the AFM and TCSPC measurements of a silicon surface modified with 5-ethynyl tetracene as one would expect that this would have results like the Si-Pyr surfaces. Additionally, one could consider attempting the synthesis of 2-ethynyl-tetracene; although synthetically more challenging the different position may result in a different configuration of the tetracene units in the monolayer and thereby having a different effect on both the tetracene island formation and the anticipated energy transfer. The synthesis of 2-bromotetracene is outlined in the work of Kitamura & Kawase (2013) (44) and the subsequent reaction from the 2-bromo-tetracene to the 2-ethynyl-tetracene is identical to the procedure of 5-ethynyl tetracene (45) (See **Figure S.10** in the supporting information for the reaction scheme). Additionally, it would be interesting to investigate whether the different life-times that are being observed are the result of actual triplet energy transfer into the silicon or whether another competing quenching mechanism is at play. In short, a good next step in the process of using polyacenes would be to modify a surface with either 5 or 2-ethynyl tetracene and accordingly study the photonic properties of this configuration.

Next are the silicon surfaces covered with PbS nanoparticles, for the sake of convenience the Si-Thiol-NP and Si-H-NP surfaces are lumped together as no tetracene has been deposited on these surfaces. These TCSPC measurements would be extremely interesting especially when comparing them to the TCSPC measurements of Si-Pyr and perhaps the silicon functionalized with 5-ethynyl tetracene.  Lastly, it would be interesting to explore the option of using more environmental friendly nanoparticles as lead is rather toxic. Silicon nanoparticles (SiNP) ,like PbS NP, have size-dependent bandgap energies(46) one could theorize that a SiNP of the right size would also be

able to perform Förster Resonance Energy Transfer and accordingly attribute to a more environmental friendly photovoltaic cell.

The question remains whether Dexter Energy Transfer or Förster Resonance Energy Transfer will lead to the next generation of photovoltaic cells. With this thesis, the first steps have been made on promoting the exciton transfer from tetracene islands into silicon bulk by means of using functionalized silicon and the results strongly encourage further investigation of the interplay between the tetracene and silicon functionalized surfaces.

## Acknowledgements

# References

1) Palz, W. (Ed.). (2010). *Power for the world: the emergence of electricity from the sun*. Pan Stanford Publishing.

2) Shockley, W., & Queisser, H. J. (1961). Detailed balance limit of efficiency of p-n junction solar cells. Journal of applied physics, 32(3), 510-519.

3) Green, M. A., Emery, K., Hishikawa, Y., Warta, W., & Dunlop, E. D. (2015). Solar cell efficiency tables (Version 45). *Progress in photovoltaics: research and applications*, *23*(1), 1-9.

4) Polman, A., Knight, M., Garnett, E. C., Ehrler, B., & Sinke, W. C. (2016). Photovoltaic materials: Present efficiencies and future challenges. *Science*, *352*(6283), aad4424.

5) Smith, M. B., & Michl, J. (2010). Singlet fission. *Chemical reviews*, *110*(11), 6891-6936.

6) Mikhnenko, O. V. (2012). Dynamics of Singlet and Triplet Excitons in Organic Semiconductors.

7) Köhler, A., & Bässler, H. (2009). Triplet states in organic semiconductors. *Materials Science and Engineering: R: Reports*, *66*(4), 71-109.

8) Hanna, M. C., & Nozik, A. J. (2006). Solar conversion efficiency of photovoltaic and photoelectrolysis cells with carrier multiplication absorbers. Journal of Applied Physics, 100(7), 074510.

9) Yost, S. R., Lee, J., Wilson, M. W., Wu, T., McMahon, D. P., Parkhurst, R. R., ... & Sfeir, M. Y. (2014). A transferable model for singlet-fission kinetics. *Nature chemistry*, *6*(6), 492.

10) Lee, J., Bruzek, M. J., Thompson, N. J., Sfeir, M. Y., Anthony, J. E., & Baldo, M. A. (2013). Singlet exciton fission in a hexacene derivative. *Advanced Materials*, *25*(10), 1445-1448.

11) Yang, L., Tabachnyk, M., Bayliss, S. L., Böhm, M. L., Broch, K., Greenham, N. C., ... & Ehrler, B. (2014). Solution-processable singlet fission photovoltaic devices. *Nano letters*, *15*(1), 354-358.

12) Johnson, J. C., Nozik, A. J., & Michl, J. (2010). High triplet yield from singlet fission in a thin film of 1, 3-diphenylisobenzofuran. *Journal of the American Chemical Society*, *132*(46), 16302-16303.

13) Gradinaru, C. C., Kennis, J. T., Papagiannakis, E., van Stokkum, I. H., Cogdell, R. J., Fleming, G. R., ... & van Grondelle, R. (2001). An unusual pathway of excitation energy deactivation in carotenoids: singlet-to-triplet conversion on an ultrafast timescale in a photosynthetic antenna. *Proceedings of the National Academy of Sciences*, *98*(5), 2364-2369.

14) Dennler, G., Sariciftci, N. S., & Brabec, C. J. (2006). Conjugated polymer-based organic solar cells. *Technology*, *11*, 2.

15) Tomkiewicz, Y., Groff, R. P., & Avakian, P. (1971). Spectroscopic approach to energetics of exciton fission and fusion in tetracene crystals. *The Journal of Chemical Physics*, *54*(10), 4504-4507.

16) Wilson, M. W., Rao, A., Johnson, K., Gélinas, S., Di Pietro, R., Clark, J., & Friend, R. H. (2013). Temperature-independent singlet exciton fission in tetracene. *Journal of the American Chemical Society*, *135*(44), 16680-16688.

17) Piland, G. B., Burdett, J. J., Hung, T. Y., Chen, P. H., Lin, C. F., Chiu, T. L., ... & Bardeen, C. J. (2014). Dynamics of molecular excitons near a semiconductor surface studied by fluorescence quenching of polycrystalline tetracene on silicon. *Chemical Physics Letters*, *601*, 33-38.

18) Tabachnyk, M., Ehrler, B., Gélinas, S., Böhm, M. L., Walker, B. J., Musselman, K. P., ... & Rao, A. (2014). Resonant energy transfer of triplet excitons from pentacene to PbSe nanocrystals. *Nature materials*, *13*(11), 1033.

19) Davis, N. J., Böhm, M. L., Tabachnyk, M., Wisnivesky-Rocca-Rivarola, F., Jellicoe, T. C., Ducati, C., ... & Greenham, N. C. (2015). Multiple-exciton generation in lead selenide nanorod solar cells with external quantum efficiencies exceeding 120%. *Nature communications*, *6*.

20) Kolomeisky, A. B., Feng, X., & Krylov, A. I. (2014). A simple kinetic model for singlet fission: A role of electronic and entropic contributions to macroscopic rates. *The Journal of Physical Chemistry C*, *118*(10), 5188-5195.

21) Mikhnenko, O. (2006). Light Harvesting and Energy Transfer.

22) Buriak, J. M. (2013). Illuminating silicon surface hydrosilylation: an unexpected plurality of mechanisms. *Chemistry of Materials*, *26*(1), 763-772.

23) Roberts, S. T., McAnally, R. E., Mastron, J. N., Webber, D. H., Whited, M. T., Brutchey, R. L., ... & Bradforth, S. E. (2012). Efficient singlet fission discovered in a disordered acene film. *Journal of the American Chemical Society*, *134*(14), 6388-6400.

24) Keyes, R. W. (2005). Physical limits of silicon transistors and circuits. *Reports on Progress in Physics*, *68*(12), 2701.

25) Pujari, S. P. (2013). *Covalently bound fluorine-containing monolayers on silicon and oxides: formation, stability and tribology*.

26) Puniredd, S. R., Assad, O., & Haick, H. (2008). Highly stable organic modification of Si (111) surfaces: towards reacting Si with further functionalities while preserving the desirable chemical properties of full Si– C atop site terminations. *Journal of the American Chemical Society*, *130*(29), 9184-9185.

27) Wilson, M. W., Rao, A., Ehrler, B., & Friend, R. H. (2013). Singlet exciton fission in polycrystalline pentacene: from photophysics toward devices. *Accounts of chemical research*, *46*(6), 1330-1338.

28) Wilson, M. W., Rao, A., Clark, J., Kumar, R. S. S., Brida, D., Cerullo, G., & Friend, R. H. (2011). Ultrafast dynamics of exciton fission in polycrystalline pentacene. *Journal of the American Chemical Society*, *133*(31), 11830-11833.

29) Garg, K., Majumder, C., Nayak, S. K., Aswal, D. K., Gupta, S. K., & Chattopadhyay, S. (2015). Silicon-pyrene/perylene hybrids as molecular rectifiers. *Physical Chemistry Chemical Physics*, *17*(3), 1891-1899.

30) Locritani, M., Yu, Y., Bergamini, G., Baroncini, M., Molloy, J. K., Korgel, B. A., & Ceroni, P. (2014). Silicon nanocrystals functionalized with pyrene units: efficient light-harvesting antennae with bright near-infrared emission. *The journal of physical chemistry letters*, *5*(19), 3325-3329.

31) Scheres, L., Giesbers, M., & Zuilhof, H. (2010). Organic monolayers onto oxide-free silicon with improved surface coverage: alkynes versus alkenes. *Langmuir*, *26*(7), 4790-4795.

32) Horvath, P., Šebej, P., Solomek, T., & Klan, P. (2014). Small-molecule fluorophores with large stokes shifts: 9-iminopyronin analogues as clickable tags. *The Journal of organic chemistry*, *80*(3), 1299-1311.

33) Juaristi, E., & Cruz-Sanchez, J. S. (1988). Synthesis and Conformation of 4, 4, 5, 5-Tetramethyl-1, 2-dithiane Mono-S-oxide. *The Journal of Organic Chemistry*, *53*(14), 3334-3338.

34) Alexander B. Sieval,Vincent Vleeming,Han Zuilhof,* & Ernst J. R. Sudhölter*,† (1999) An Improved Method for the Preparation of Organic Monolayers of 1-Alkenes on Hydrogen-Terminated Silicon Surfaces. Langmuir 1999, 8288-8291. DOI: 10.1021/la9904962

35) Journet, M., Rouillard, A., Cai, D., & Larsen, R. D. (1997). Double radical cyclization/β-fragmentation of acyclic ω-yne vinyl sulfides. synthesis of 3-vinyldihydrothiophene and dihydrothiopyran derivatives. a new example of a 5-endo-trig radical cyclization. The Journal of Organic Chemistry, 62(25), 8630-8631.

36) Scheres, L., Rijksen, B., Giesbers, M., & Zuilhof, H. (2011). Molecular modeling of alkyl and alkenyl monolayers on hydrogen-terminated Si (111). Langmuir, 27(3), 972-980.

37) Tao, Y. T., Wu, C. C., Eu, J. Y., Lin, W. L., Wu, K. C., & Chen, C. H. (1997). Structure evolution of aromatic-derivatized thiol monolayers on evaporated gold. *Langmuir*, *13*(15), 4018-4023.

38) Jakubowicz, A., Jia, H., Wallace, R. M., & Gnade, B. E. (2005). Adsorption kinetics of p-nitrobenzenethiol self-assembled monolayers on a gold surface. *Langmuir*, *21*(3), 950-955.

39) Kondo, M., Mates, T. E., Fischer, D. A., Wudl, F., & Kramer, E. J. (2010). Bonding structure of phenylacetylene on hydrogen-terminated Si (111) and Si (100): surface photoelectron spectroscopy analysis and ab initio calculations. *Langmuir*, *26*(22), 17000-17012.

40) Iannazzo, L., Soroka, D., Triboulet, S., Fonvielle, M., Compain, F., Dubée, V., ... & Etheve-Quelquejeu, M. (2016). Routes of Synthesis of Carbapenems for Optimizing Both the Inactivation of l, d-Transpeptidase LdtMt1 of Mycobacterium tuberculosis and the Stability toward

41) Engelkes, V. B., Beebe, J. M., & Frisbie, C. D. (2004). Length-dependent transport in molecular junctions based on SAMs of alkanethiols and alkanedithiols: effect of metal work function and applied bias on tunneling efficiency and contact resistance. *Journal of the American Chemical Society*, *126*(43), 14287-14296.

42) Mostegel, F. H., Ducker, R. E., Rieger, P. H., El Zubir, O., Xia, S., Radl, S. V., ... & Griesser, T. (2015). Versatile thiol-based reactions for micrometer-and nanometer-scale photopatterning of polymers and biomolecules. *Journal of Materials Chemistry B*, *3*(21), 4431-4438.

43) Hu, M., Liu, F., & Buriak, J. M. (2016). Expanding the Repertoire of Molecular Linkages to Silicon: Si–S, Si–Se, and Si–Te Bonds. ACS applied materials & interfaces, 8(17), 11091-11099.

44) Kitamura, C., Taka, N., & Kawase, T. (2013). Synthesis of 8-bromo-5, 12-tetracenequinone and 2-bromotetracene derivatives. *Research on Chemical Intermediates*, *39*(1), 139-146.

45) Müller, A. M., Avlasevich, Y. S., Schoeller, W. W., Müllen, K., & Bardeen, C. J. (2007). Exciton fission and fusion in bis (tetracene) molecules with different covalent linker structures. *Journal of the American Chemical Society*, *129*(46), 14240-14250.

46) Ruizendaal, L., Pujari, S. P., Gevaerts, V., Paulusse, J. M., & Zuilhof, H. (2011). Biofunctional Silicon Nanoparticles by Means of Thiol-Ene Click Chemistry. Chemistry–An Asian Journal, 6(10), 2776-2786.

# Supporting Information

## Figure S.1 Material Studio (A)
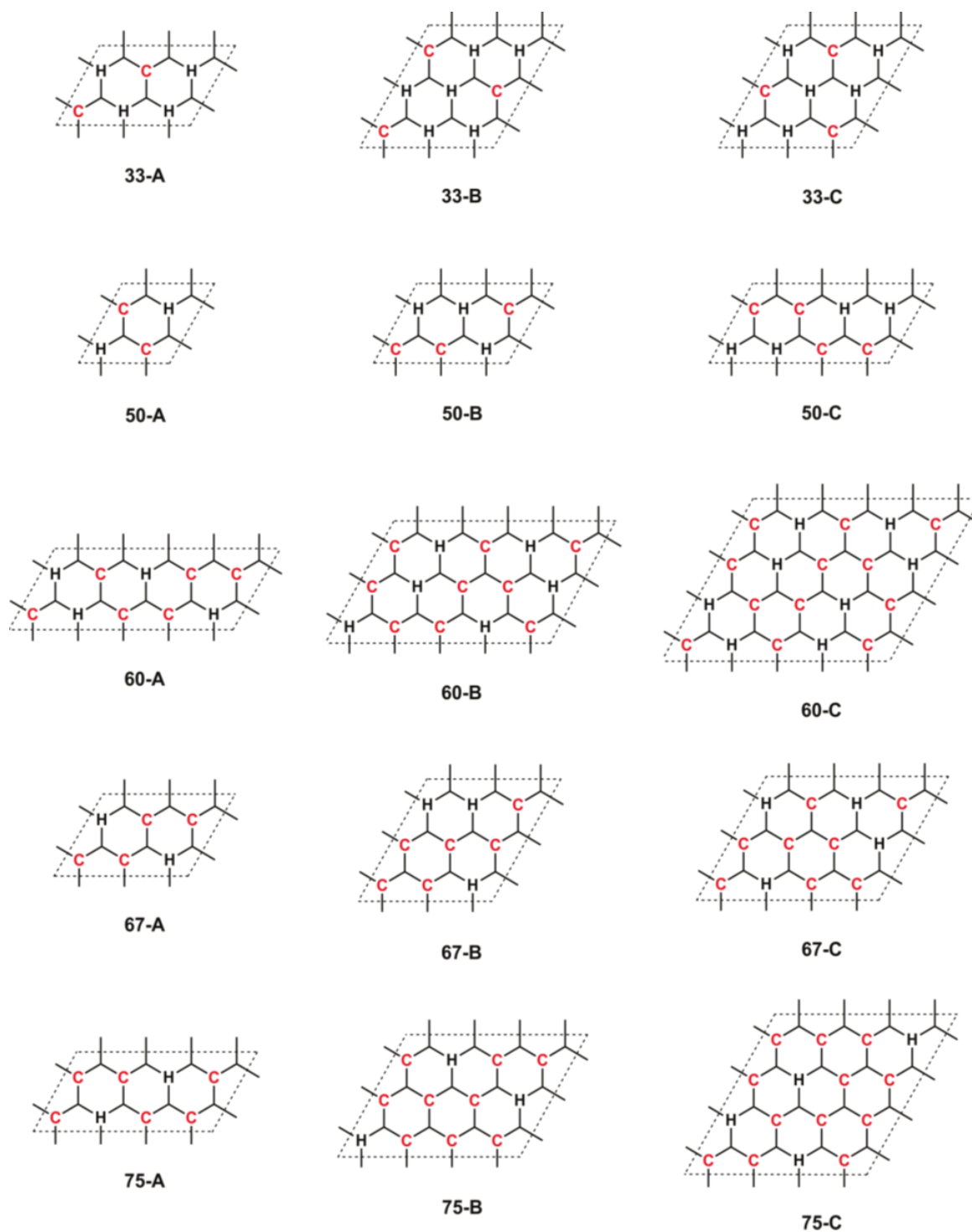


**Figure S. 1**. *The different substitution patterns used in Material Studios to find the most energetically favorable surface coverage.*

## Figure S.2 Atomic Force Measurement Aromatics (B)
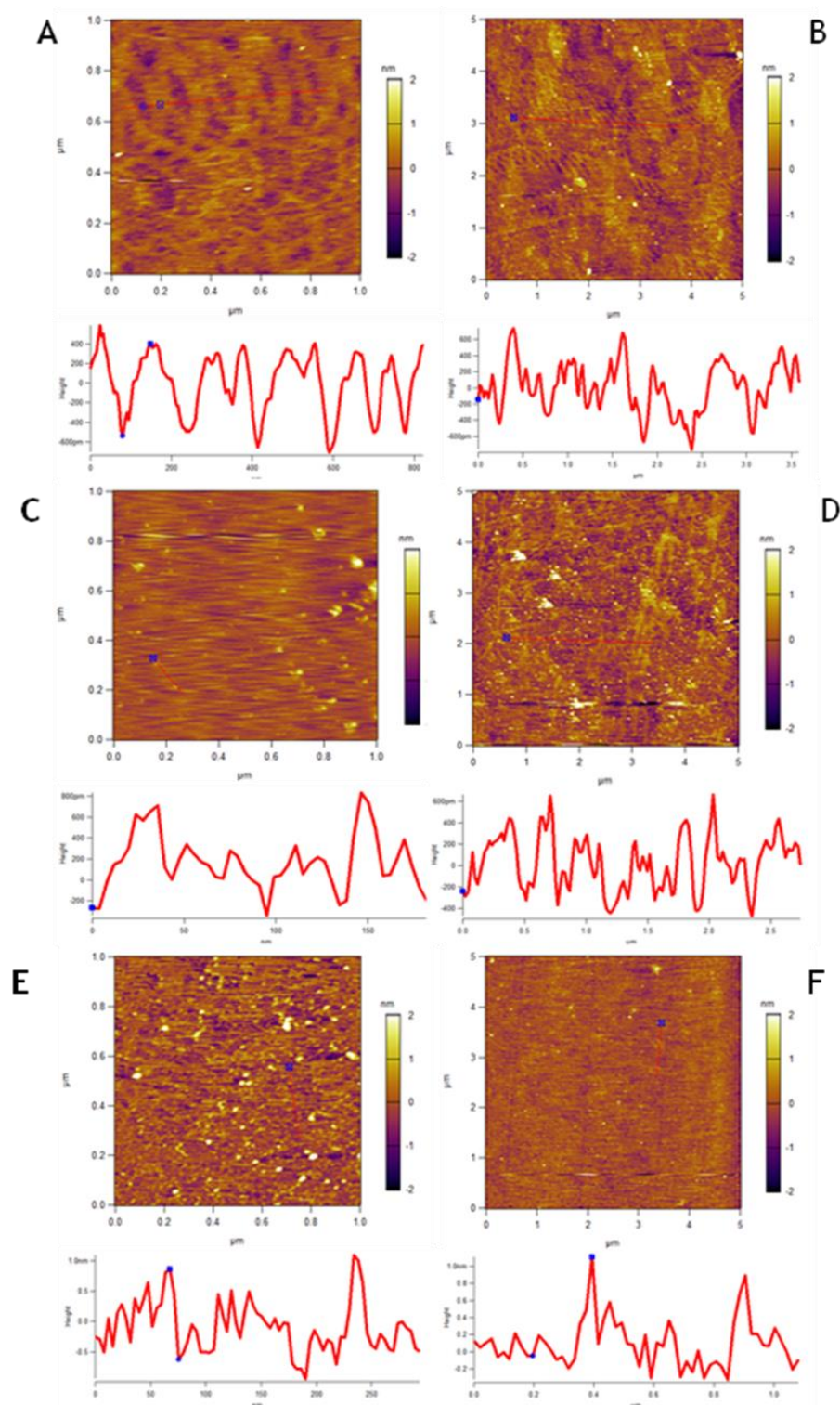


***Figure S. 2*** *A&B) the 1x1 and 5x5 um AFM measurements and height profiles of Si-Ph. C&D) Also the 1x1 and 5x5 um AFM and height profiles of Si-Naph. E&F) AFM measurements and height profiles of Si-Pyr.*

## Figure S.3 Atomic Force Measurement Aromatics – Tetracene (C)
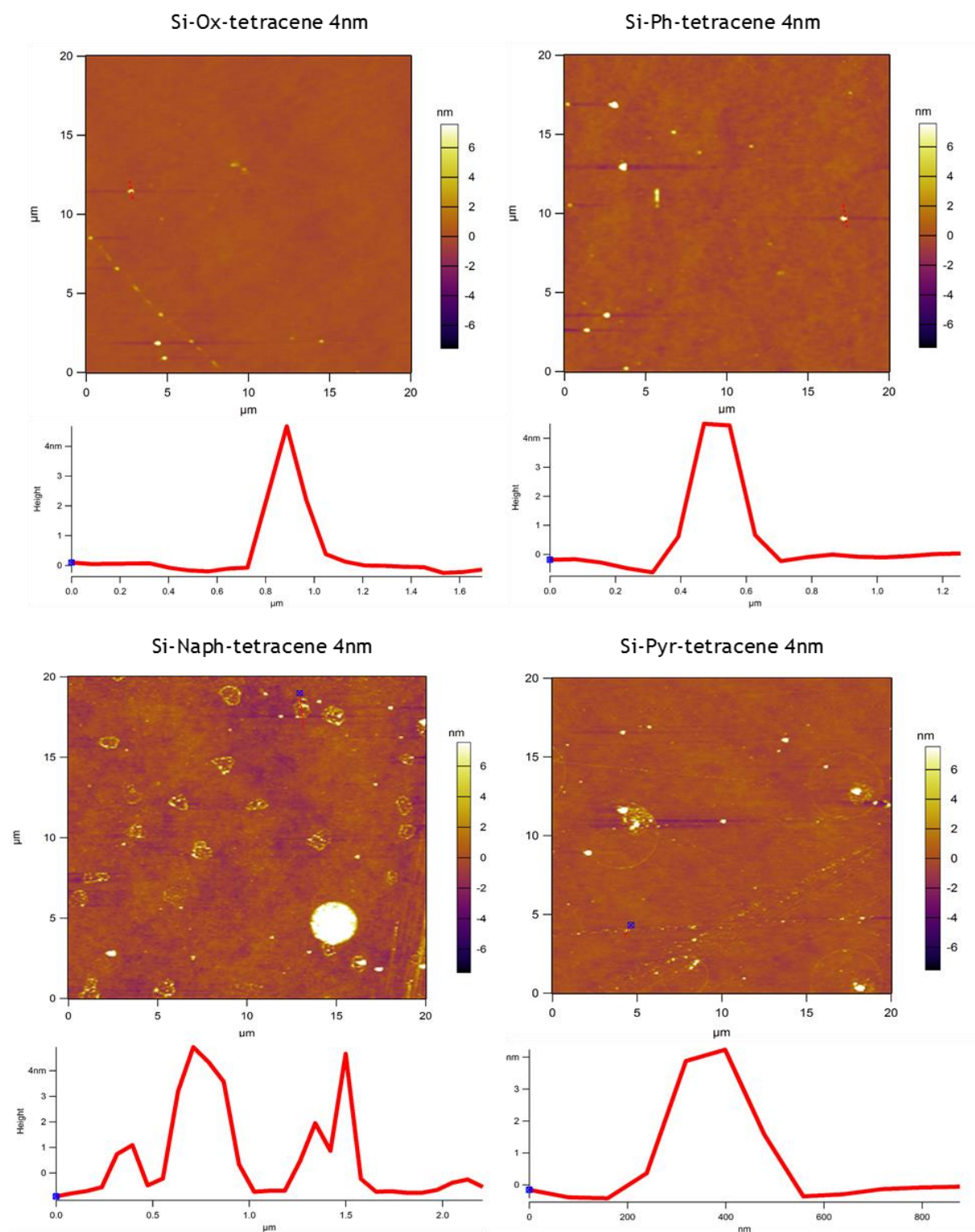


**Figure S. 3.** *20x20 um AFM images of Si-Ox-Tetracene, Si-Ph-Tetracene, Si-Naph-tetracene and Si-Pyr-tetracene. Included are theyr respective height profiles which indicate a thickness of 4 nm which corresponds to the expected island height.*

Figure S.4. XPS Si-Ph-Tetracene (D)
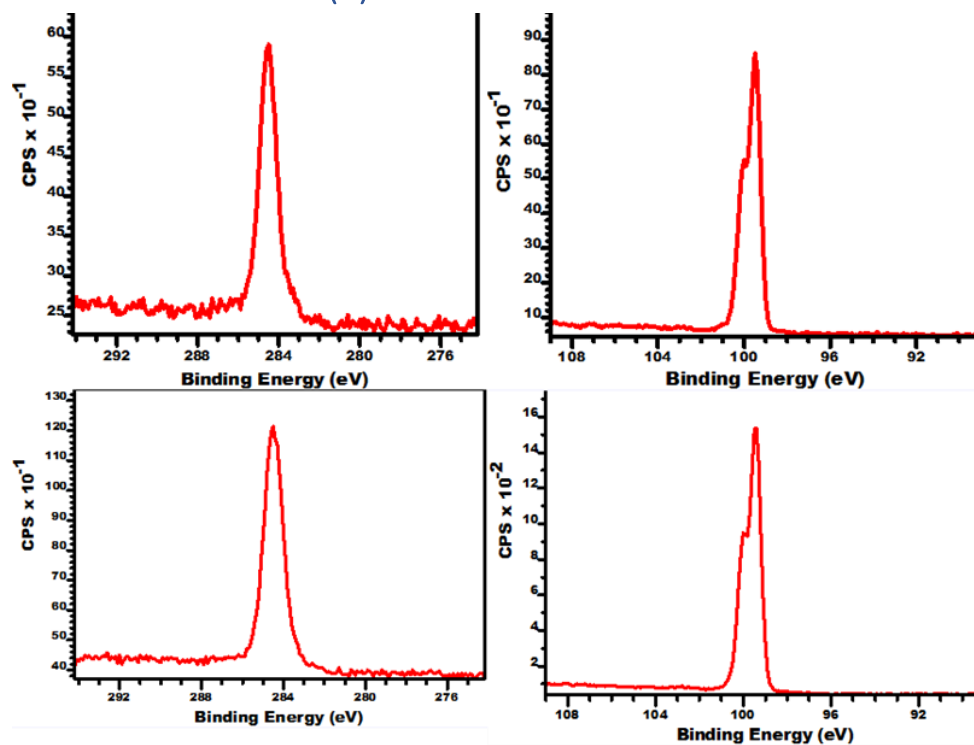


*Figure S. 4* Top row, the carbon and silicon narrow scans of Si-Ph-tetracene (4nm). Bottom row also the carbon and silicon narrow scans but now of Si-Ph-tetracene(35nm)

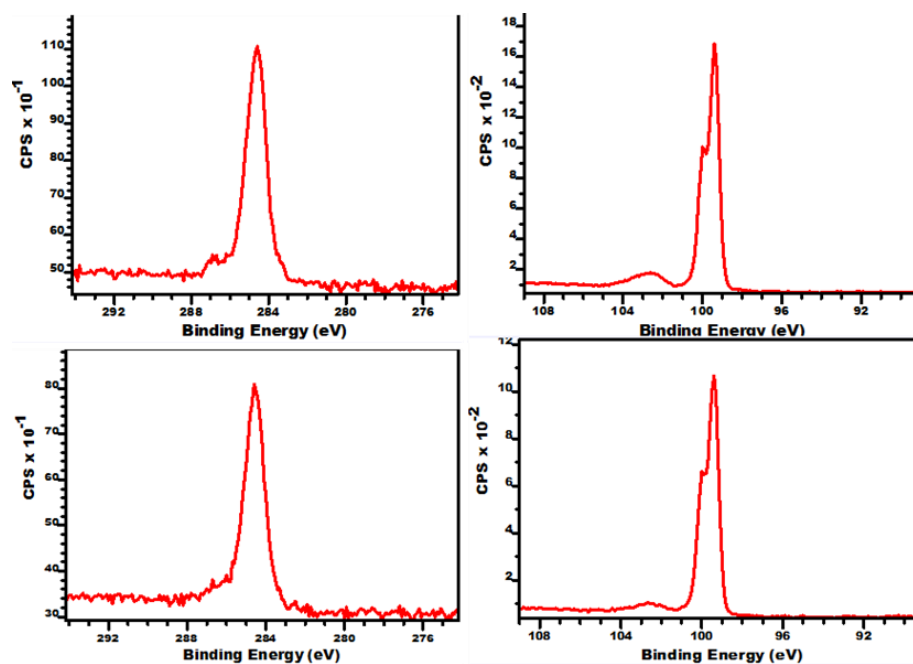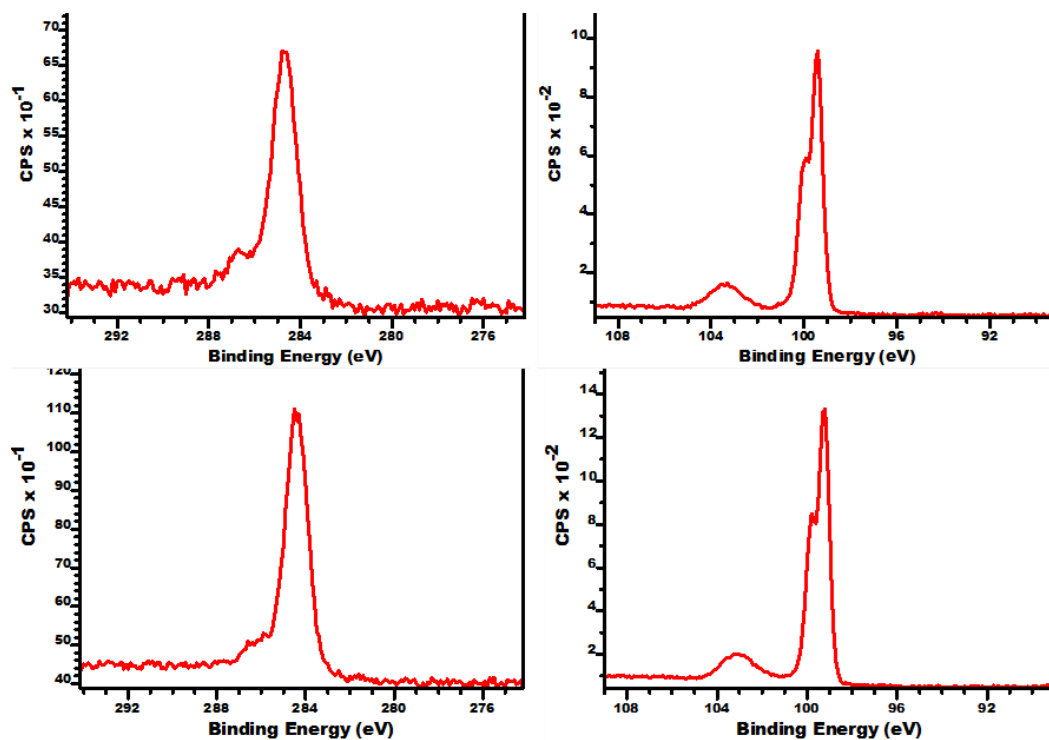Figure S.5. XPS Si-Naph-Tetracene (E)



*Figure S. 5.* The XPS carbon and silicon narrow scans. The top row are the narrow scans of Si-Naph-tetracene (4nm) and the bottom row of Si-Naph-tetracene (35nm)

Figure S.6 XPS Si-Pyr-Tetracene (F)



***Figure S.6.*** *on the left are the carbon narrow scans of Si-Pyr-Tetracene (4nm) and Si-Pyr-tetracene (35nm) top and botto respectively. On the right are the silicon narrow scans of the same surfaces.*

## Figure S.7. Decay Times of Si-Ph/ Si-Naph/ Si-Pyr – Tetracene (G)
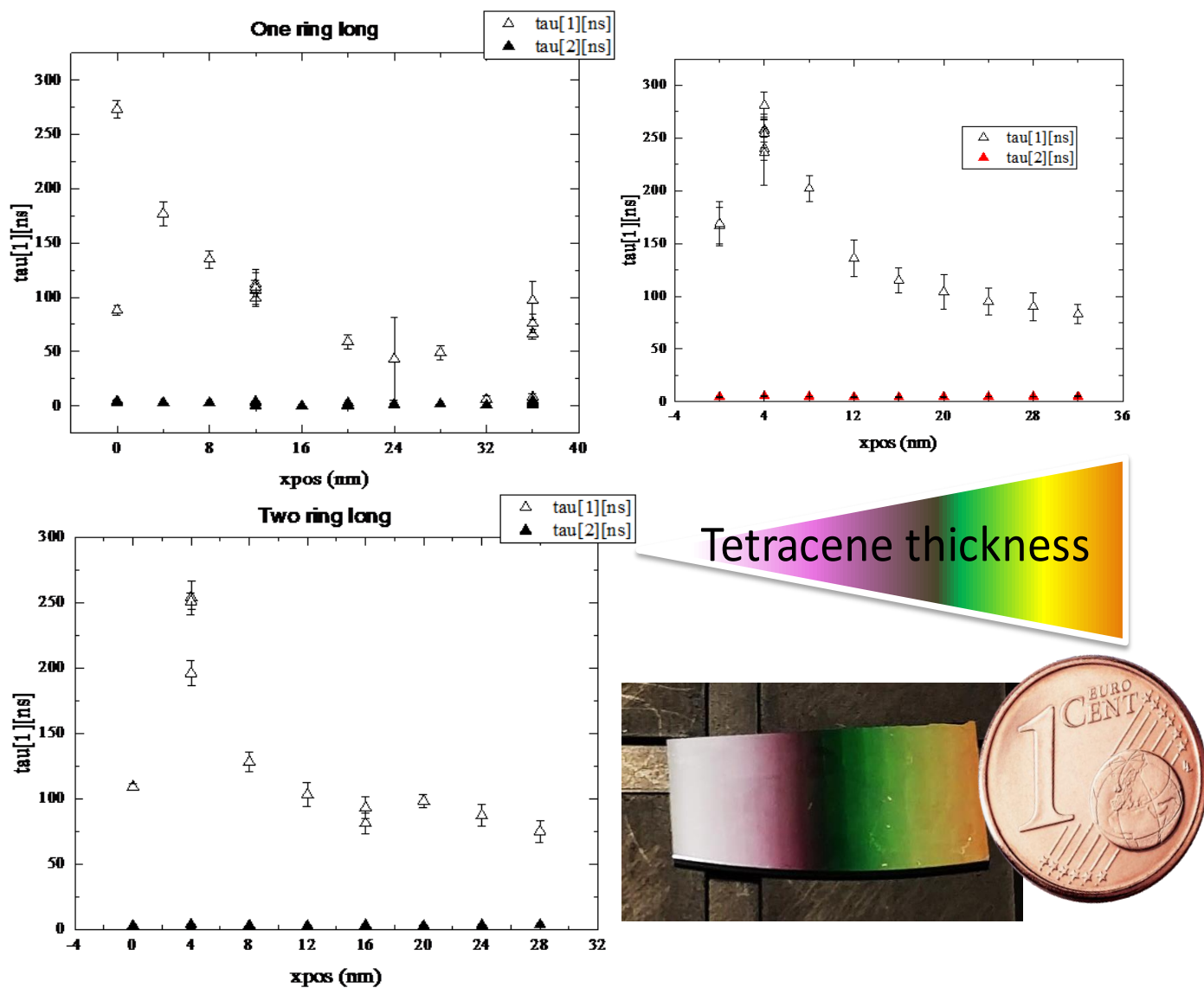


***Figure S.7.*** *Life-time decays plotted as a function of island thickness for Si-Ph-Tetracene (Top-Left), Si-Naph-Tetracene(Bottom-Left),Si-Pyr-Tetracene(Top-Right) and a picture of a Si-Ar surface with varying thicknesses of tetracene deposited on it (Bottom-Right).*

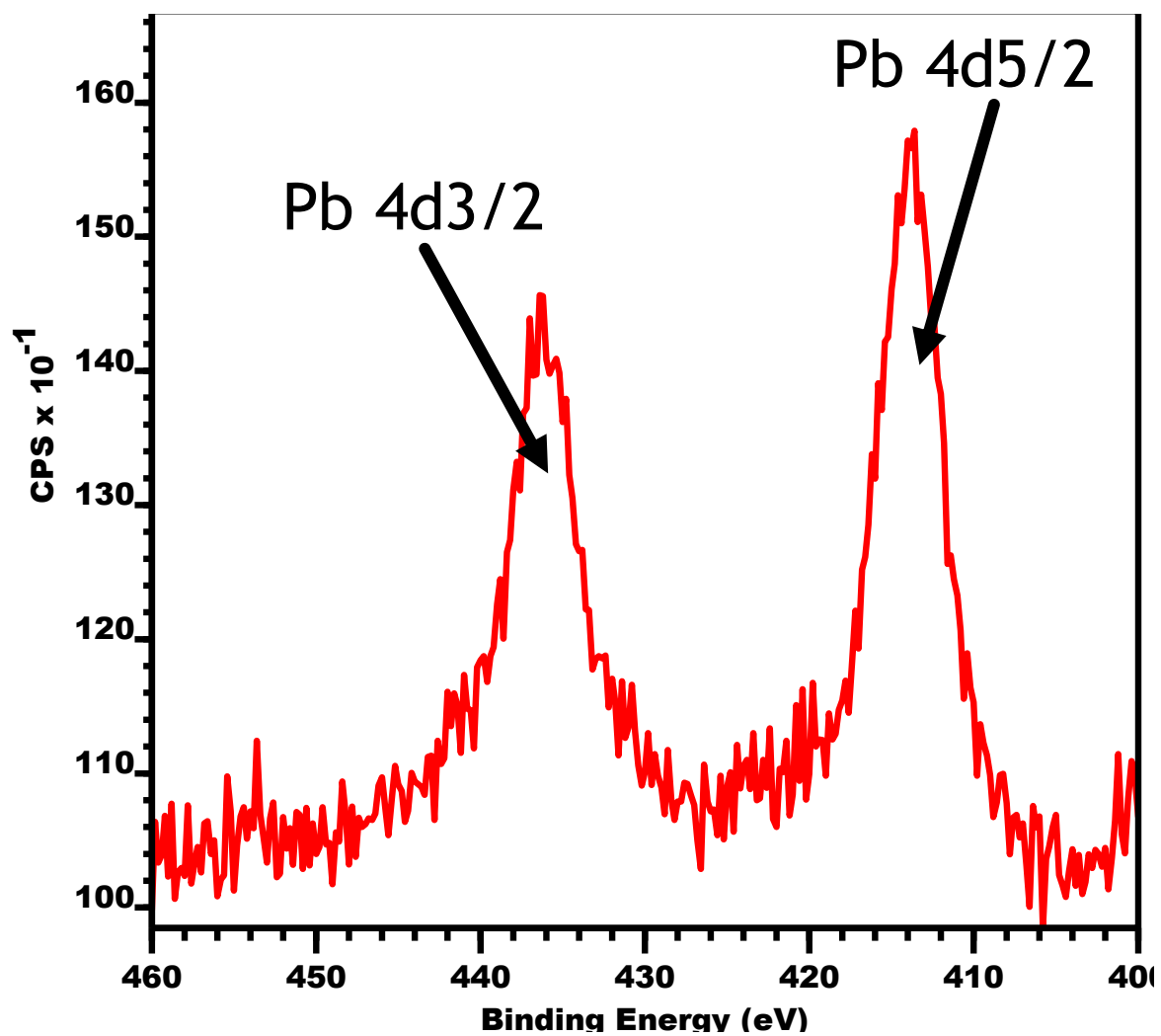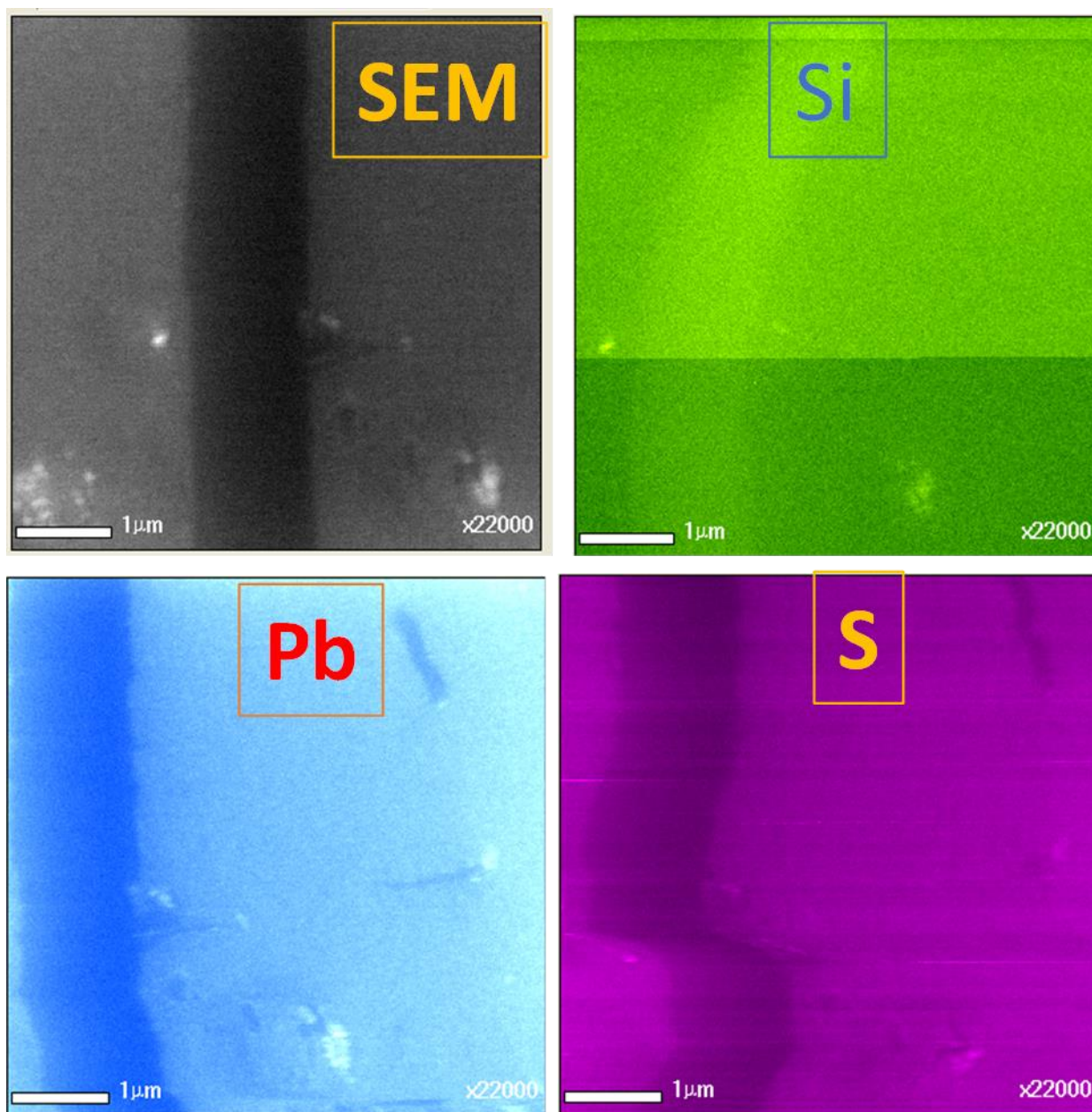Figure S.8. Pb narrow Scan of a Si-Thiol-NP surface (H)



**Figure S.8.** *Pb narrow scan of the Si-Thiol-NP surface with the 4d 3/2 and 4d 5/2 signals*

**Figure S.9. SEM and AES of Si-H-NP- Pentyne (I)**



*Figure S.9*. *SEM and AES images of with their respective elemental intensity. Note that the shift observed in the Si and S AES is due to to the vibrations of the measuring equipment.*

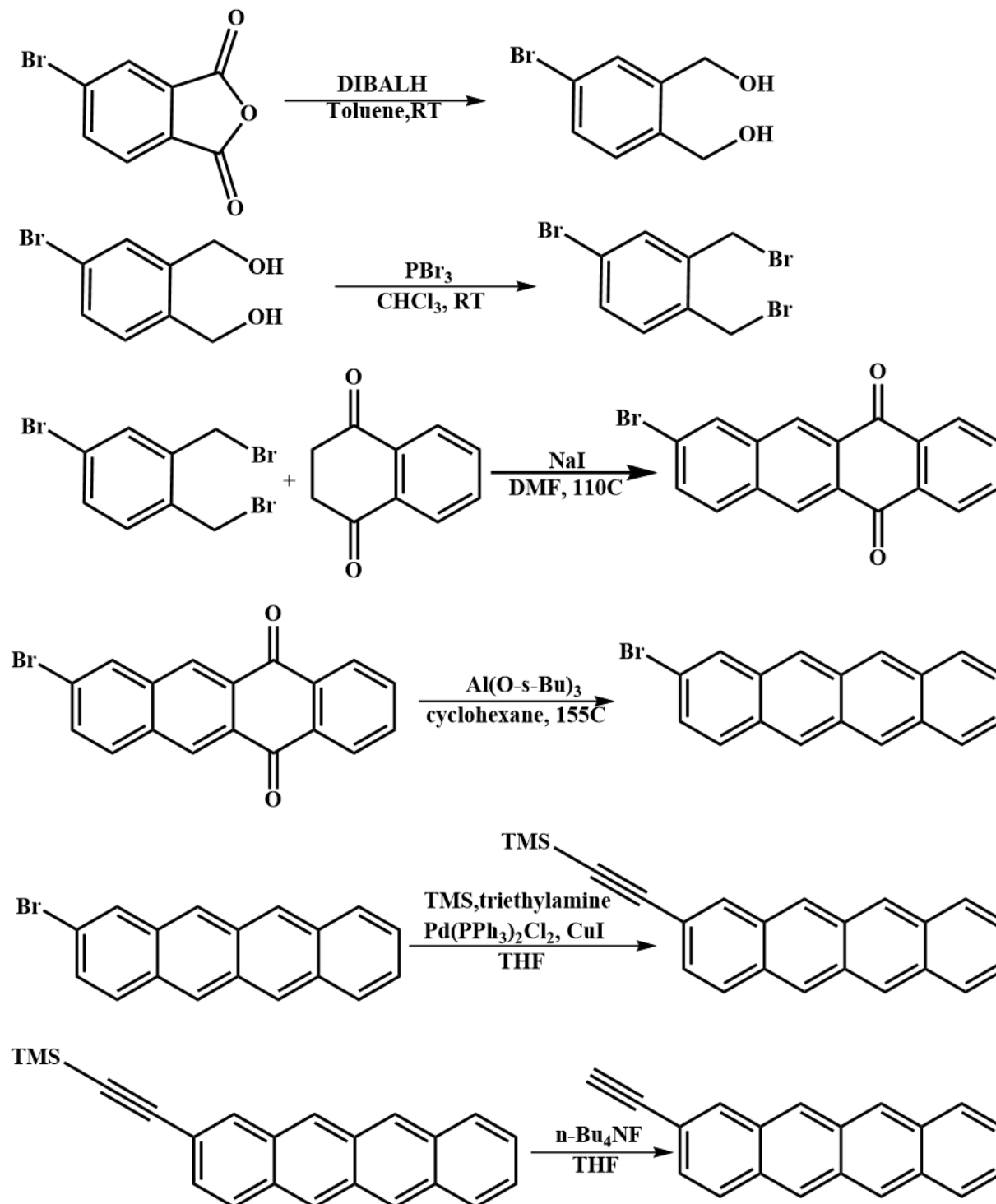## Figure S.10. Synthesis 2-ethynyl tetracene (J)



**Figure S. 10.** *Recommended synthesis for 2-ethynyl-tetracene*

## Synthesis (K)

### Synthesis of 1-butynyl mesylate

A 250 mL round-bottom flask was charged with DCM (150mL) and 1-butynol (9 mL, 116 mmol). Subsequently, the round bottom flask was then cooled to 0 $^0$C and triethylamine (25mL) was added dropwise. Whilst keeping the round bottom flask at 0 $^0$C mesylate chloride (14 mL) was slowly dropped into the solution. Next, the solution was left to stir overnight at room temperature. The following day, the solution was diluted with 2M HCL (100mL) and afterwards washed three times with each: 1M HCL, $NaHCO_3$ and Brine (1:1 v/v ratio). Consequently, the solution was dried with $MgSO_4$, filtered and concentrated under reduced pressure. The resulting solution (8.48g, 49% yield) was used for the synthesis of 1-butynyl thioacetate without further purification. $^1$H NMR (400MHz, Chloroform-$d$) δ 4.29 (t, $J$ = 6.7 Hz, 2H$_c$), 3.65 (s, 1H), 3.03 (s, 3H$_d$), 2.64 (td, $J$ = 6.7, 2.7 Hz, 2H$_b$), 2.04 (t, $J$ = 2.7 Hz, 1H$_a$). $^{13}$C NMR (101 MHz, Chloroform-$d$) δ 78.57(C$_b$), 70.94(C$_a$), 67.01 (C$_d$), 52.55 (Mes-Cl), 37.72 (C$_e$), 19.77 (C$_c$). IR: 3288(C-H alkyne), 3031,2970,2941(CH$_2$/CH$_3$ alkanes), 2124 (C≡C).

### Synthesis of 1-butynyl thioacetate

Butynyl mesylate (8.48g, 148 mmol) was dissolved in 22 mL DMF, a mixture of cesium carbonate (22.3g, 68 mmol), thioacetic acid (4.8 mL,68 mmol) in 45 mL DMF was added dropwise to the butynyl mesylate solution at 0 $^0$C. Note that the solution changed color from a bright orange to a bland green. After having left the combined solutions to stir for 1 hour at room temperature; however, GC-MS revealed unreacted product so the reaction flask was again cooled to 0 $^0$C and more cesium carbonate (15g, 46mmol), thioacetic acid (4mL, 57mmol) and DMF (30mL) was added. Subsequently, the solution was left to stir overnight at room temperature. Next the solution was diluted with DCM, dried with $MgSO_4$ and washed three times with Brine and deionized water. For further surface modification purposes, column chromatography (95:5, heptane: ethyl acetate) was performed. The fractions with the product were combined and the heptane was evaporated under reduced pressure yielding 1.95 g (15mmol, 10% yield). Prior to storage for surface modification, three freeze-pump-thaw cycles were performed to minimize any impurities. $^1$H NMR (400 MHz, Chloroform-$d$) δ 3.06 (td, $J$ = 7.0, 1.3 Hz, 2H$_c$), 2.50 (tdd, $J$ = 7.1, 2.7, 1.2 Hz, 2H$_b$), 2.37 (t, $J$ = 1.1 Hz, 3H$_d$), 2.04 (td, $J$ = 2.6, 0.8 Hz, 1H$_a$). $^{13}$C NMR (101 MHz,

Chloroform-*d*) δ 195.21($C_e$), 82.04($C_b$), 69.59($C_a$), 30.57($C_d$), 28.12($C_f$), 19.50($C_c$). IR: 3292 (C-H,alkyne), 2940 ($CH_2$ alkanes),2837 ($CH_3$ alkanes),2119 (C≡C), 1687(C=O).

## Synthesis of 5-ethynyl-tetracene

A solution of NBS (0.38g,2.19 mmol) in dry DMF (40mL) was prepared in a 100 mL erlenmeyer. Next a solution of tetracene (0.5g,2.19 mmol) in chloroform (200mL) was prepared in a 250 mL three necked round bottom flask and was heated to $55^0$C while stirring. Subsequently, the NBS solution was added at a dropwise rate over the course of 60 minutes and the mixture was then left at $55^0$C and stirring overnight. The following day the mixture was cooled to room temperature and washed twice with 200 mL of Milli-Q-water. The chloroform was then evaporated under reduced pressure and the residue was diluted with 200 mL Milli-Q-water. Afterwards the mixture was fileted, dried and a flash chromatography (DCM) was performed to further purify the acquired brown crystals.

Subsequently, the 5-bromotetracene (0.2g, 0.65 mmol) was placed in a three-necked bottle with a dropping funnel and reflux condenser attached to it. Next 1 mg of CuI and 5 mg of Pd(PPh$_3$)$_4$ in 10 mL fresh THF was added and the mixture was sparged with nitrogen for 10 minutes. Meanwhile a mixture of TMS-acetylene 0.3 mL in 8 mL triethylamine was prepared and sparged with nitrogen for 10 minutes. The mixture of 5-bromotetracene was then heated to $70^0$C; whilst the mixture is refluxing the mixture of TMS-acetylene in triethylamine is added in a dropwise fashion. Once the addition of the two mixtures was complete, the solution was cooled to $60^0$C and was left under nitrogen overflow overnight. No further work up was reported as no new peaks were observed when initial samples were taken for analysis by GC-MS.

Ultimately, once on has successfully isolated 5-TMS-tetracene the next step would be to convert 5-TMS-tetracene into 5-ethynyl tetracene. This would be done by adding 5-TMS-tetracene (0.4g,1.23 mmol) to potassium carbonate (0.6g, 4.52 mmol) and dissolving this in 12 mL THF and 7.5 mL methanol. The solution would then be purged with nitrogen for 15 minutes and left stirring for two hours. After evaporating the solvent under reduced pressure and performing a flash chromatography with DCM this procedure should yield 5-ethynyl-tetracene. The overall schematic of these series of reactions is given in **Figure S.11**.
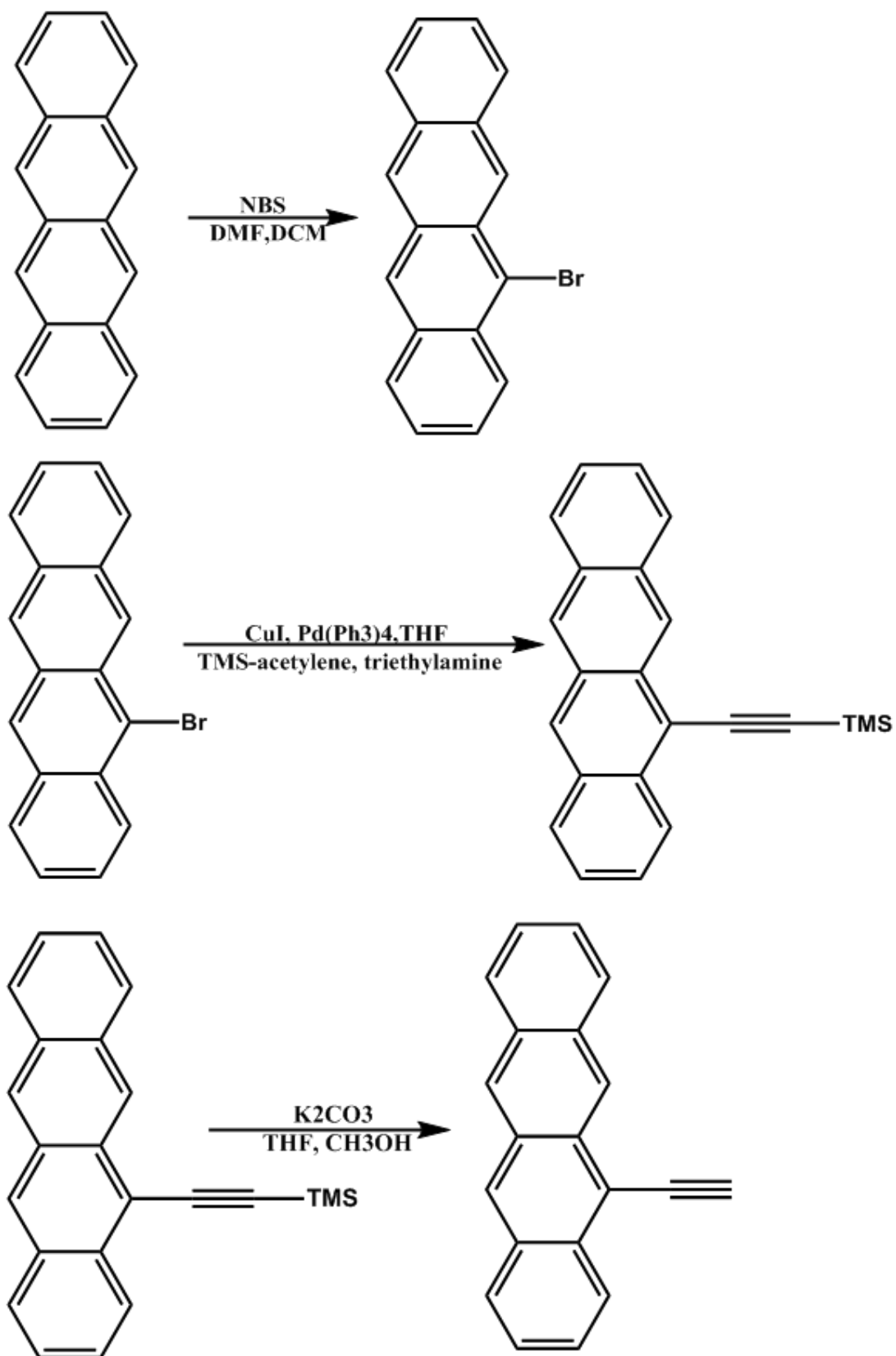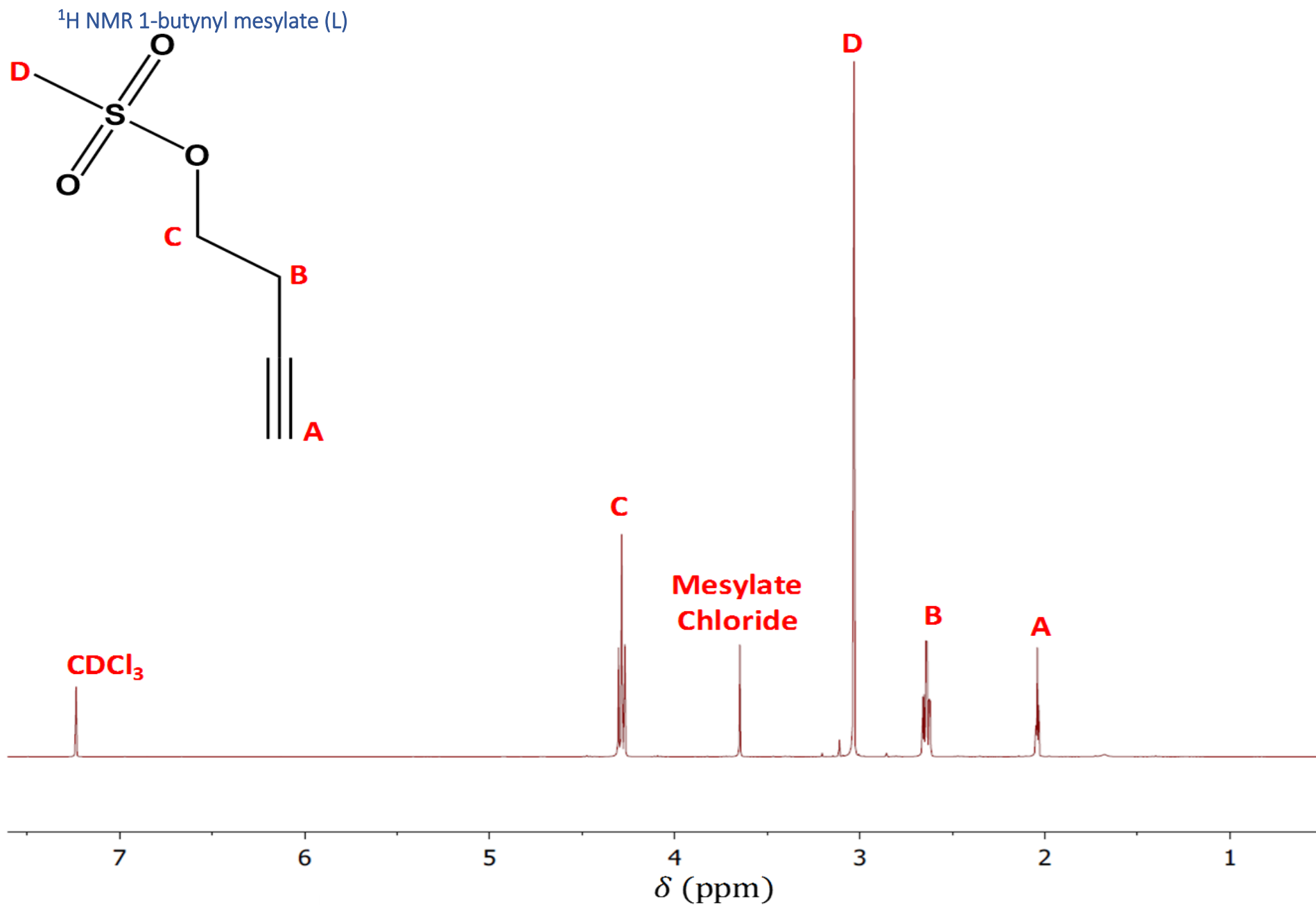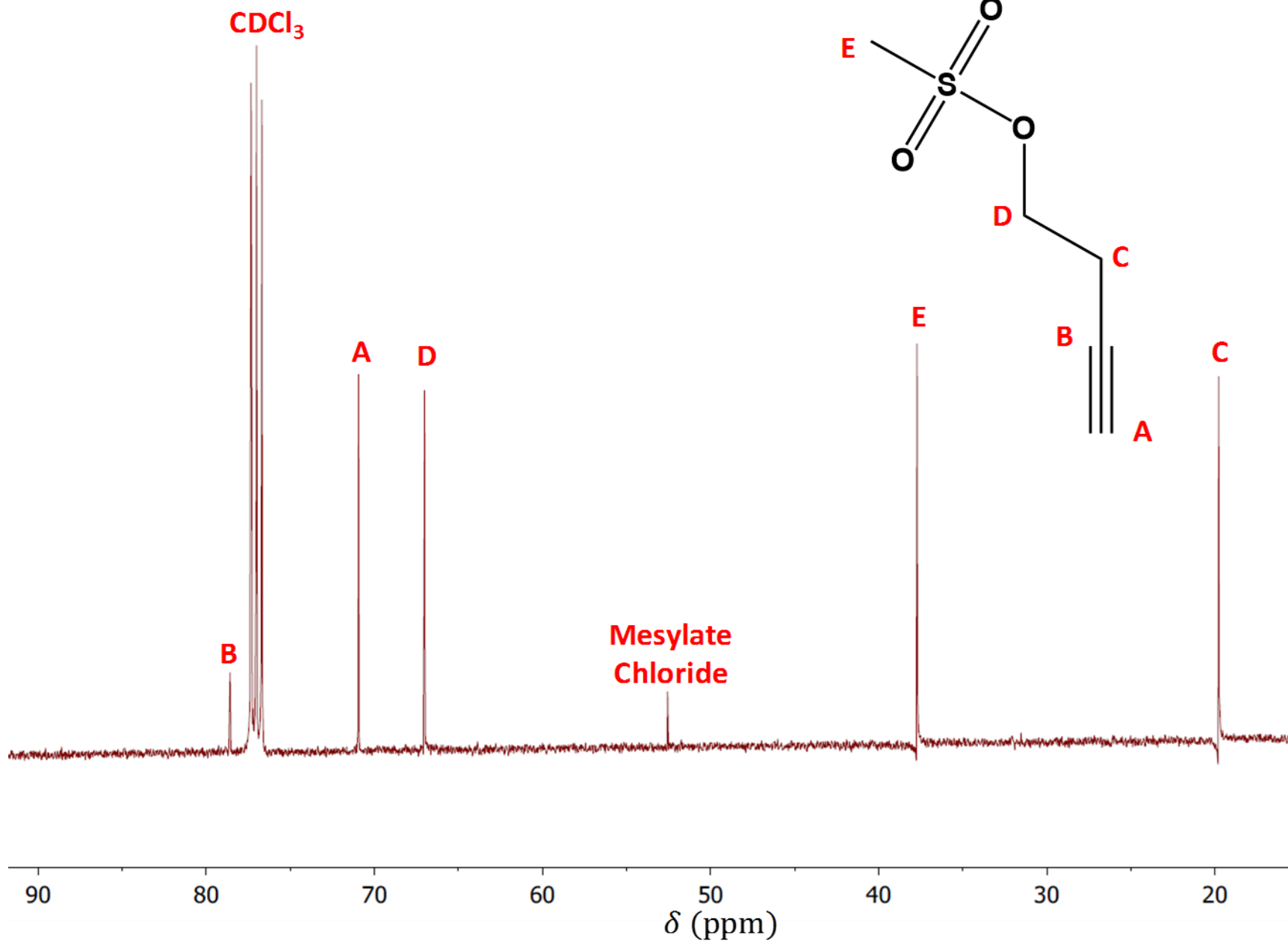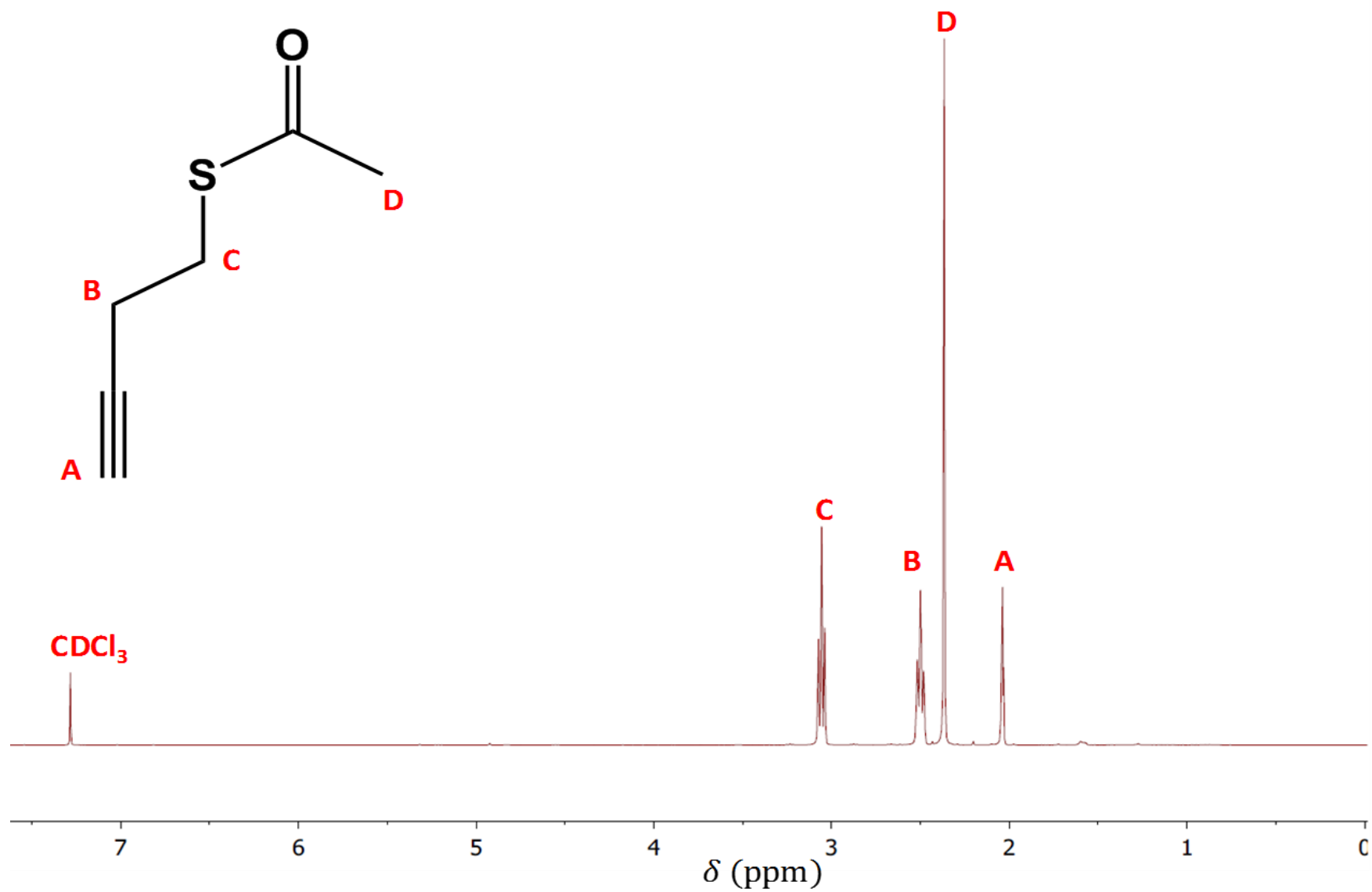
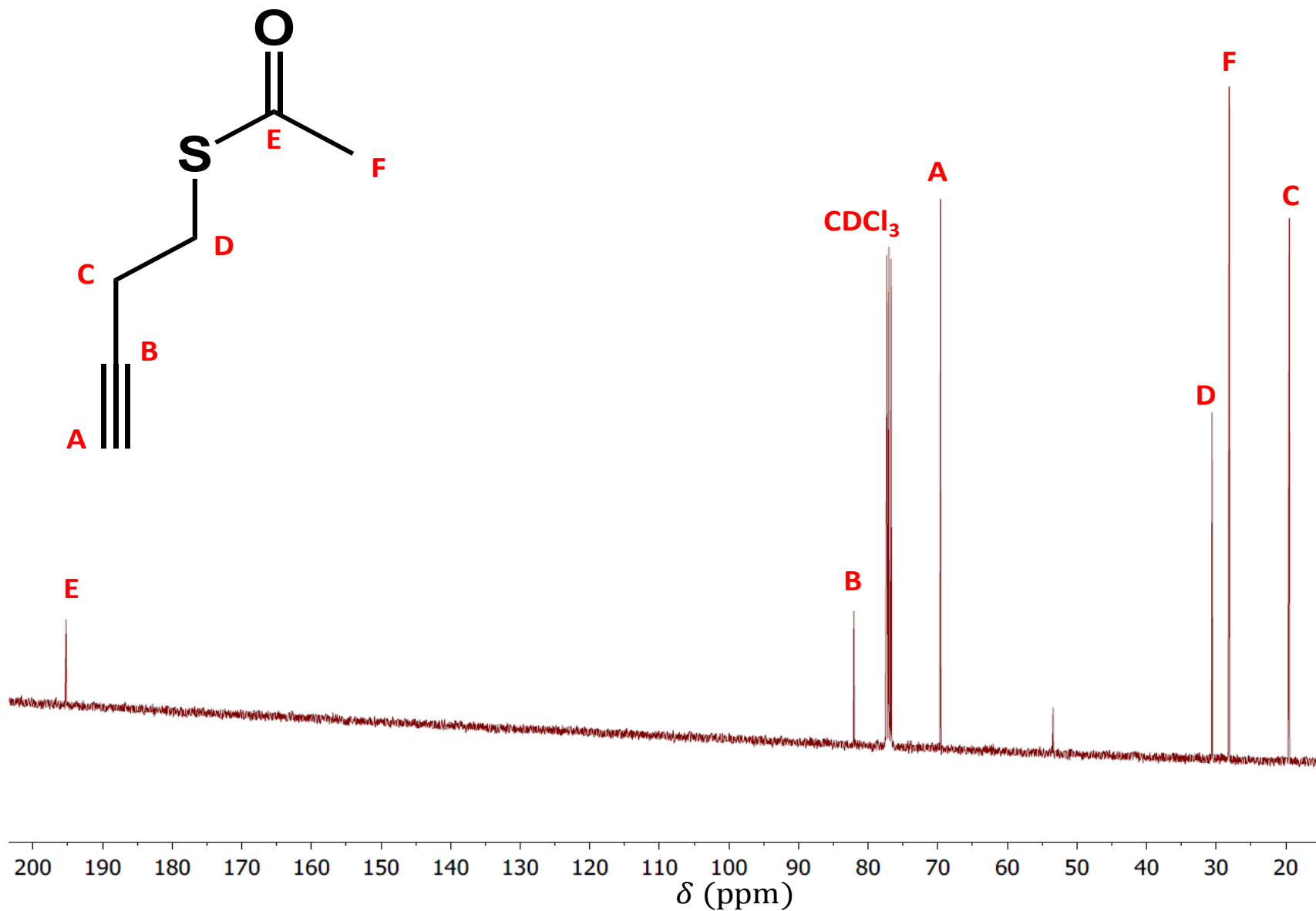*Figure S.11. Series of reactions for the synthesis of 5-ethtnyl-tetracene*

$^1$H NMR 1-butynyl mesylate (L)

## $^1$H NMR 1-butynyl thioacetate (N)

<sup>13</sup>C NMR 1-butynyl thioacetate (O)

## Matlab Scripts (P)

### Molecular Modeling script

```
%% Description/ aim of the script do!
% I)   Input and organizing data correctly
% II)  Plot the data (nicely)
% III) Fit the data and find the minimum
%% Section I: Importing Data
filename= 'Overview Energies.xlsx';
sheetXLS= [1,2,3,4,5];
rangeXLS= 'B2:C10'; %Area in Excel where table is --> Make sure its the same place
A = xlsread(filename,sheetXLS(1),rangeXLS); %Data Phenyl
B = xlsread(filename,sheetXLS(2),rangeXLS); %Data Naphtalene
C = xlsread(filename,sheetXLS(3),rangeXLS); %Data Pyrene
D = xlsread(filename,sheetXLS(4),rangeXLS); %Data Thioacetate
E = xlsread(filename,sheetXLS(5),rangeXLS); %Data Thiol
% A1= xlsread(filename,sheetXLS(7),rangeXLS); %data non conjugate Phenyl
%Alternative way of putting data into a dataset
%data1 = dataset('xlsfile', 'test.xlsx','Range',range,'Sheet',1)%data for Phenyl
%% Section II: Fitting and finding Minimum
fa= fit(A(:,1),A(:,2),'poly2');%,'Weight',[1,1,1,10,1,1,1,1]); %fitting
M= [20:1:90];
fa1=fa(M);
[Emina Posa]=min(fa1);
Pa=[20+Posa Emina]
fb= fit(B(:,1),B(:,2),'poly2');%,'Weight',[1,1,1,10,1,1,1,1]); %fitting
fb1=fb(M);
[Eminb Posb]=min(fb1);
Pb=[20+Posb Eminb]
fc= fit(C(:,1),C(:,2),'poly2');%,'Weight',[1,1,1,10,1,1,1,1]); %fitting
fc1=fc(M);
[Eminc Posc]=min(fc1);
Pc=[20+Posc Eminc]
fd= fit(D(:,1),D(:,2),'poly2'); %fitting
fd1=fd(M);
[Emind Posd]=min(fd1);
Pd=[20+Posd Emind]
fe= fit(E(:,1),E(:,2),'poly2'); %fitting
fe1=fe(M);
[Emine Pose]=min(fe1);
Pe=[20+Pose Emine]
% fa_1= fit(A1(:,1),A1(:,2),'poly2'); %fitting
% fa_12=fa_1(M);
% [Emin1 Pos1]=min(fa_12);
% Pa1=[20+Pos1 Emin1]
%% Section III: Plotting
figure(1)     %Phenylacetylene
plot(A(:,1),A(:,2),'kx',[20:1:90],fa1,'-r','LineWidth',2,'MarkerSize',7);
% graphical features
xticks([25,33,40,50,60,67,75,83]);
yticks([-10,-8,-6,-4,-2,0,2,4,6,8,10]);
axis([20 90 -12 12])
xlabel('Substitution %');
ylabel('Epacking (kcal/mol)');
```

```
title('Packing energies of Phenylacetylene'); shg
legend('Data points for Mol. Studios','Fitted polynominal','Location','southeast')
figure(2)      %Naphtalene
plot(B(:,1),B(:,2),'kx',[20:1:90],fb1,'-r','LineWidth',2,'MarkerSize',7);
% graphical features
xticks([25,33,40,50,60,67,75,83]);
axis([20 90 -25 25])
xlabel('Substitution %');
ylabel('Epacking (kcal/mol)');
title('Packing energies of 2-ethynyl Naphtalene'); shg
legend('Data points for Mol. Studios','Fitted polynominal','Location','southeast')
figure(3)      %Pyrene
plot(C(:,1),C(:,2),'kx',[20:1:90],fc1,'-r','LineWidth',2,'MarkerSize',7);
% graphical features
xticks([25,33,40,50,60,67,75,83]);
axis([20 90 -35 50])
xlabel('Substitution %');
ylabel('Epacking (kcal/mol)');
title('Packing energies of 1-ethynyl Pyrene'); shg
legend('Data points for Mol. Studios','Fitted polynominal','Location','southeast')
figure(4)      %Thioacetate
plot(D(:,1),D(:,2),'kx',[20:1:90],fd1,'-r','LineWidth',2,'MarkerSize',7);
% graphical features
xticks([25,33,40,50,60,67,75,83]);
yticks([-10,-8,-6,-4,-2,0,2,4,6,8,10]);
axis([20 90 -10 10])
xlabel('Substitution %');
ylabel('Epacking (kcal/mol)');
title('Packing energies of Thioacetate'); shg
legend('Data points for Mol. Studios','Fitted polynominal','Location','southeast')
figure(5)      %Thiol
plot(E(:,1),E(:,2),'kx',[20:1:90],fe1,'-r','LineWidth',2,'MarkerSize',7);
% graphical features
xticks([25,33,40,50,60,67,75,83]);
yticks([-10,-8,-6,-4,-2,0,2,4,6,8,10]);
axis([20 90 -15 15])
xlabel('Substitution %');
ylabel('Epacking (kcal/mol)');
title('Packing energies of Thiol'); shg
legend('Data points for Mol. Studios','Fitted polynominal','Location','southeast')
```

## Stability Analysis script

```
 %% Description/ the script!
% I)    Input and organizing data correctly
% II)   Accordingly modify the data
% III)  Plot the data
filename= {'Phenyl Stability Study.xlsx','Naphtalene Stability Study.xlsx','Pyrene Stability Study.xlsx','Pyrene Pentyne Stability
Study.xlsx'};
sheetXLS= [1,2,3,4,5,6];
%% Section I: Importing Data
str= input('What sample would you like to plot? A or B? (default is A)','s');
if str == 'B'
   rangeXLS ='L5:M205'; % For samples B
else
```

```
    rangeXLS= 'B5:C205'; % for samples A & be sure to take the LARGEST range!
end
Title= {'Stability Study of surfaces modified with Phenylacetylene','Stability Study of surfaces modified with
Naphtalene','Stability Study of surfaces modified with Pyrene','Stability Study of surfaces modified with Pyrene backfilled with
Pentyne'};
for i= 1:4
    A = xlsread(char(filename(i)),sheetXLS(1),rangeXLS); %Data Aromatic 0 days
    B = xlsread(char(filename(i)),sheetXLS(2),rangeXLS); %Data Aromatic 2 days
    C = xlsread(char(filename(i)),sheetXLS(3),rangeXLS); %Data Aromatic 6 days
    D = xlsread(char(filename(i)),sheetXLS(4),rangeXLS); %Data Aromatic 10 days
    E = xlsread(char(filename(i)),sheetXLS(5),rangeXLS); %Data Aromatic 20 days
   %F = xlsread(char(filename(i)),sheetXLS(6),rangeXLS); %Data Aromatic 30 days
% Section II: Normalization
    Am = max(A(:,2)); % Maximum y value for normalization
    A(:,3)= A(:,2)/Am; % Accordingly creates a third row which is normalized according to Am
    Bm = max(B(:,2));
    B(:,3)= B(:,2)/Bm;
    Cm = max(C(:,2));
    C(:,3)= C(:,2)/Cm;
    Dm = max(D(:,2));
    D(:,3)= D(:,2)/Dm;
    Em = max(E(:,2));
    E(:,3)= E(:,2)/Em;
% Section III: Plotting
    figure      %Phenylacetylene
    plot(A(:,1),A(:,3),'-r',B(:,1),B(:,3),'-b',C(:,1),C(:,3),'-g',D(:,1),D(:,3),'-k',E(:,1),E(:,3),'-m','LineWidth',2);
    set(gca,'XDir','Reverse')
% graphical features
    xticks([96 98 100 102 104 106]);
    yticks([0 0.2 0.4 0.6 0.8 1 1.2]);
    axis([96 106 0 1.2])
    xlabel('Binding Energy (eV)');
    ylabel('Normalized CPS');
    legend('Day 0','Day 2','Day 6','Day 10,','Day 20','Location','northwest')
    title(char(Title(i)));shg;
end
```

## Curriculum Vitae

Steven Verboom was born on the 24th of May 1994 in Breda. He graduated TTO (bilingual VWO) at Mencia de Mendoza in 2012 and afterwards started his bachelor at University College Roosevelt (UCR). After having graduated in 2015 with a GPA of 2.9 he started his master in Biotechnology at Wageningen University. Missing the aspects of Organic Chemistry in his current studies he decided to start a double master degree in both Biotechnology and Molecular Life Sciences at Wageningen University. He continued to write his first thesis in this group, and the results are described in this thesis. Next will be the start of a second thesis with the Biobased Chemistry & Technology (BCT) chair group in Wageningen focussing on the modelling of a micro plug flow reactor.